Enhancing the photo-Fenton treatment of contaminated water by use of ultrasound and iron-complexing agents

DOCTORAL THESIS

TO BE DEFENDED ON THE 9TH OF OCTOBER 2015

TO THE SCHOOL OF BASIC SCIENCES

DOCTORAL PROGRAM IN CHEMISTRY AND CHEMICAL ENGINEERING

ECOLE POLYTECHNIQUE FEDERALE DE LAUSANNE

FOR OBTAINING THE TITLE OF DOCTOR OF SCIENCE

BY

STEFANOS PAPOUTSAKIS

ABSTRACT

The photo-Fenton process is a promising emerging technology for the treatment of contaminated water streams. It is based on the generation of reactive oxygen species that are capable of destroying recalcitrant contaminants otherwise unaffected by conventional municipal wastewater treatment method. Among its innate advantages are that it can be catalyzed naturally by solar radiation and the main reagents required are iron and hydrogen peroxide, both abundant and relatively cheap. There are however some important limitations. The process functions best at acidic pH, is negatively affected by some inorganic ions present in natural water and the water requires pH neutralization and iron recuperation following the treatment. These limitations inhibit the application of the process at larger-scale.

This work is an attempt to develop new strategies for enhancing the photo-Fenton process for making it a more attractive option for the treatment of municipal or industrial wastewaters. Two main pathways are investigated, the use of ultrasound and the use of iron-complexing agents. Ultrasonic processes have been shown to improve degradation kinetics when applied in combination with photo-Fenton, while at the same time are not as negatively affected by some of the inorganic ions present in water. Iron-complexing agents can maintain iron soluble at a wider operational pH and can also improve process efficiency via pathways discussed at length in the text.

Chapter 2 is focused on the application of ultrasound in combination with photo-Fenton for two very distinct applications: 1) A pilot-scale ultrasound/photo-Fenton system was set-up and evaluated for the treatment of three different contaminants with distinct physicochemical properties and at different concentrations. Synergy was evaluated in terms of degradation kinetics and H_2O_2 consumption efficiency. 2) Ultrasound was applied alone and in combination with photo-Fenton for the treatment of the iodinated contrast agent Iohexol. These agents are injected in patients during radiographic procedures and excreted via urine. This provided an opportunity to examine if ultrasound could improve their treatment in such a complex aquatic medium. Treatment options both in urine (at the source) and in the context of municipal wastewater are discussed.

Chapter 3 is focused on the use of EDDS as an iron-complexing agent for degrading contaminants at near neutral pH across a concentration range usually found in different wastewaters (from µg L^{-1} to mg L^{-1}). EDDS was used both for the treatment of microcontaminants (µg L^{-1}) in municipal wastewater treatment plant effluents as well as for

highly contaminated (several mg L^{-1}) water. The importance of several factors and operational conditions is discussed.

Chapter 4 discusses the possibility of exploiting natural iron-complexing agents (mainly phenolic/polyphenolic compounds) that can be found in some types of wastewater (e.g from natural products processing industries). The concept of reusing polyphenol-rich wastewater in small quantities as an alternative to artificial complexing agents is introduced. As a case study, water containing highly concentrated cork bark extracts (Cork Boiling Wastewater) has been added in natural water spiked with one or several contaminants. Its capacity to maintain Fe^{3+} soluble at near-neutral pH as well as the effect on Fenton/photo-Fenton degradation were observed.

Keywords: Advanced oxidation processes, photo-Fenton, ultrasound, iron-complexing ligands, solar water decontamination, synergy, process control

RESUME

Le procédé photo-Fenton est une technologie émergente et prometteuse pour le traitement des eaux contaminées: C'est basé sur la génération des espèces réactives de l´oxygène qui sont capables de détruire des contaminants récalcitrantes qui ne sont pas affectés par les traitements conventionnels des eaux municipaux. Parmi ses avantages innés, il peut être catalysé naturellement par la radiation solaire et le réactifs principaux requis sont le fer et le peroxyde d oxygène, les deux abondants et relativement peu coûteux. Il y a, cependant, des limitations importantes. Le procédé fonctionne le meilleur en pH acide, il est négativement affecté par des ions inorganiques présents dans l'eau naturelle et depuis le traitement, neutralisation du pH et récupération du fer sont requises. Ces limitations inhibent l´application du procédé à grande échelle.

Cette thèse consiste à un effort de développer des nouvelles stratégies pour améliorer le procédé photo-Fenton, pour qu'il se rende une option plus attractive pour le traitement des eaux usées municipaux ou industrielles Deux voies principales sont investiguées, l'utilisation des ultrasons et des agents chélateurs du fer: Les procédés ultrasoniques ont été démontrées d'améliorer la cinétique de dégradation en s'appliquant en combinaison avec le photo-Fenton, alors qu'en même temps, ne sont pas affectés tant fortement par des ions inorganiques présents dans l'eau: Les agents chélateurs du fer peuvent maintenir le fer soluble sur une gamme de pH plus large et améliorer l'efficacité du procédé par voies longuement discutées dans le texte.

Le chapitre 2 est focalisé dans le couplage des ultrasons avec photo-Fenton pour deux types d'applications distincts: 1) Une système ultrasons/photo-Fenton a l'échelle pilote a été installée et évaluée pour le traitement de trois contaminants avec propriétés physicochimiques distincts et a concentrations différents: La synergie a été évaluée en fonction de cinétiques de dégradation et de la consommation de H_2O_2 2) Ultrasons sont été appliqués seules et en combinaison avec photo-Fenton pour le traitement d'Iohexol, un produit de contraste iodé: Ces produits sont administrées en patients avant du procédures radiographiques et excrété par voie d'urine: Ca fournit une opportunité d'examiner si les ultrasons peuvent améliorer leur traitement dans un milieu aquatique d'une telle complexité. Options de traitement dans l'urine (a la source) et dans le cadre des eaux municipaux sont discutées.

Le chapitre 3 est focalisé sur l'utilisation de l' EDDS comme un agent chélateur du fer pour dégrader des contaminants à pH presque neutre *à* travers d'une gamme de concentrations

habituellement retrouvée dans les eaux usées différents (de µg L^{-1} a mg L^{-1}). EDDS a été utilisé pour le traitement des eaux usées municipaux contenant microcontaminants (µg L^{-1}) aussi bien que pour des eaux fortement contaminés (plusieurs mg L^{-1}). L'importance de plusieurs facteurs et conditions opérationnelles est discutée

Le chapitre 4 discute la possibilité d' exploiter des agents chélateurs du fer naturels (principalement composés phénoliques/polyphénoliques) qu'ils se rencontrent dans certains types d'eaux usées (p.ex. provenant des industries de traitement de produits naturels). Le concept de réutiliser des eaux usées riches en polyphénoles à des petites quantités comme une alternative aux agents chélateurs artificiels est introduit: Comme étude de cas; des eaux contenant de l'extrait de l'écorce de liège fortement concentré ont été ajoutées dans l'eau naturelle contenant un ou plusieurs contaminants: Sa capacité de maintenir du Fe^{3+} soluble en pH presque neutre et les effets sur la dégradation par le Fenton/photo-Fenton ont été observés.

Mots-clés: Procédés d'oxydation avancée, photo-Fenton, ultrason, agents chélateurs du fer; décontamination solaire de l'eau; synergie, contrôle des procédés

TABLE OF CONTENTS

LIST OF FIGURES

Fig.2.16. Zahn Wellens biodegradability test of untreated Iohexol and the solutions acquired following complete elimination by US and pF treatments.

Fig.3.1. Initial degradation rate (a, b, c) and percentage of contaminants removed by the end of the process (d, e, f). Factors kept constant: a), d) $[H_2O_2]$ 65 mg L^{-1}; b), e) pH 6.5; c), f) [Fe:EDDS] 0.1375:0.275 mM.

Fig.3.2. H_2O_2 consumption efficiency (R_p, a,b c) and soluble iron availability by the end of the process (d, e, f). Factors kept constant: a), d) $[H_2O_2]$ 65 mg L-^{1}; b), e) pH 6.5; c), f) [Fe:EDDS] 0.1375:0.275 mM.

Fig.3.3. Cross-scale comparison between the degradation performance on the 1.5 L photo-reactor under simulated solar radiation and using 60 L solar CPC pilot plant.

Fig.3.4. Effect of initial pH, $[H_2O_2]$ and [Fe] on composite desirability (row 1), initial degradation rate (row 2), percentage of contaminants removed (row 3) and H_2O_2 efficiency (row 4).

Fig.3.5. Degradation of 60 mg L^{-1} Imidacloprid and evolution of iron in solution in natural water with and without HCO_3^-/CO_3^{2-} at pH 6.8 and with 0.1:0.2 mM of Fe:EDDS in CPC reactor. The structure of Imidacloprid can be seen in the upper-right corner.

Fig.3.6. Degradation of 60 mg L^{-1} of Imidacloprid in distilled water and evolution of soluble iron at pH 6.8 in presence and absence of O_2 and/ or H_2O_2.

Fig.3.7. Effect of temperature on the degradation of 60 mg L^{-1} of Imidacloprid in natural water containing CO_3^{2-}/HCO_3^- at pH 6.8 with 0.1:0.2 mM of Fe:EDDS.

Fig.3.8. Effect of temperature on the stability of soluble iron in solution during the treatment of 60 mg L^{-1} of Imidacloprid in natural water containing CO_3^{2-}/HCO_3^- at pH 6.8 with 0.1:0.2 mM of Fe:EDDS

Fig.3.9. Comparison of degradation of 60 mg L^{-1} of Imidacloprid treated with conventional photo-Fenton (0.1 mM of Fe, TOC 25 mg L^{-1}, pH 2.8) and Fe:EDDS (0.1:0.2/TOC 50 mg L^{-1}, pH 6.8) in natural water stripped of carbonates.

LIST OF TABLES

CHAPTER 1:

INTRODUCTION AND OVERVIEW

1.1. WATER AND THE ISSUE OF EMERGING ORGANIC CONTAMINANTS

Even though water covers more than 70% of the Earth's surface, only 3% of it is fresh. A large percentage of this freshwater is either in the form of ice-caps or glaciers, in remote areas or impossible to exploit due to seasonal variations (monsoons, floods). Therefore, less than 0.3% of the world's fresh water can be consistently exploited in an ever increasing demand for sanitation, drinking, agriculture and manufacturing. Efficient management of water resources is therefore of vital importance, especially in areas that are heavily urbanized or industrialized. The presence of microcontaminants has been demonstrated in thousands of publications (www.scopus.com) in recent years, giving rise to increasing worries. Sources of micropollutants in the environment are diverse and can be classified either as point sources (municipal wastewater treatment plants, industrial installations, hospitals, livestock farms) or as diffuse (non-point) sources, such as pesticide runoff from agricultural lands or unprotected landfill leachates. Some major categories of micropollutants, along with their main sources, are summarized in table 1.1.The potential risks to human health and the overall environment are not understood in their entirety, but at least some harmful effects have already been clearly demonstrated. They can affect the growth and reproduction patterns of fish and amphibians, damage the nervous systems of a aquatic organisms and inhibit photosynthesis of aquatic flora.

The European Union Water Framework Directive (Directive 2000/60/EC) that has been in effect since 2000 has established a legal framework to protect and restore clean water across Europe and ensure its long-term, sustainable use. The initial aim was the identification of priority substances presenting the highest levels of risk (based on their well-known persistence, bioaccumulation and toxicity). By 2008, a list of 33 priority substances or groups of substances was established at Union level as part of directive 2008/105/EC. Environmental quality standards (EQS) were also introduced, expressed either as annual average value (protecting against longer-term effects) and/or maximum allowable concentrations (protecting against short-term effects). It should be noted however that monitoring of contaminants alone presents a significant challenge, with 40% of EU surface water bodies being of unknown chemical status even in 2015 [1].

Table 1.1. Major categories and sources of microcontaminants (adapted from Luo et al, 2014 [2]**)**

Category	Indicative subclasses	Major sources
Pharmaceuticals	Antibiotics, anticonvulsants, antidepressants, NSAIDs, X-ray contrast agents	•Domestic WW (from excretion) •Hospital effluents • Animal farm run-off
Personal care products	Fragrances, cosmetics, disinfectants	•Domestic WW
Steroids	Estrogens	•Domestic WW •Animal farm run-off
Surfactants	Detergents, non-ionic surfactants	•Domestic WW (bathing, laundry, dishwashing) •Industrial WW (industrial cleaning discharges)
Industrial chemicals	Plasticizers, fire retardants	Domestic WW (from material leaching)
Pesticides	Insecticides, herbicides, fungicides	•Domestic WW (from gardens) •Agricultural run-off

A more recent directive (2013/39/EU) complements the ones of 2000 and 2008 by increasing the number of contaminants to 45. Also, it introduces the principle of 'whoever pollutes, pays', identifies the sources of these contaminants and focuses on the development of new technologies that don't present significantly higher costs. Between these substances (excluding inorganics) are found organochlorine, organophosphates, triazines, phenylureas, piretroides, quinolines, bromates, polyaromatics, phthalates, nonylphenols and solvents. The European Commission also intends to reinforce risk assessment and accordingly revise existing legislative framework. Watch lists of up to 10

substances that are 'under observation' are being established, with the first one published in the Official Journal of the European Union in 24/03/2015 [1].

In Switzerland, the Federal Office for the Environment (FOEN) has launched several projects investigating the problem of micropollutants in recent years. With the adoption of the water protection act in March 2014, the Swiss government decided to implement technical measures on selected MWTPs to reduce microcontaminant load. Much of the scientific basis of the program was gained through Swiss National Research program (NRP) 50 (www.nrp50.ch), conducted between 2002 and 2007. This program identified MWTP effluents as entry points of MCs into the aquatic environment. From 2006 to 2012, the ' Micropoll Strategy' project also quantified loads and toxicities of MCs in effluents, compiling a database of more than 13,000 measurements showing a large number of pollutants in the ng to μg per liter range in Swiss surface waters (Corrosion inhibitors, endocrine disruptors, plant protection products, biocides, pharmaceuticals). Options were then assessed for their removal. A brief overview of conventional wastewater treatment methods, their limitations and current strategies for the elimination of MCs are discussed below.

1.2. CONVENTIONAL WASTEWATER TREATMENT PROCESSES - CURRENT LIMITATIONS AND UPGRADE PLANS
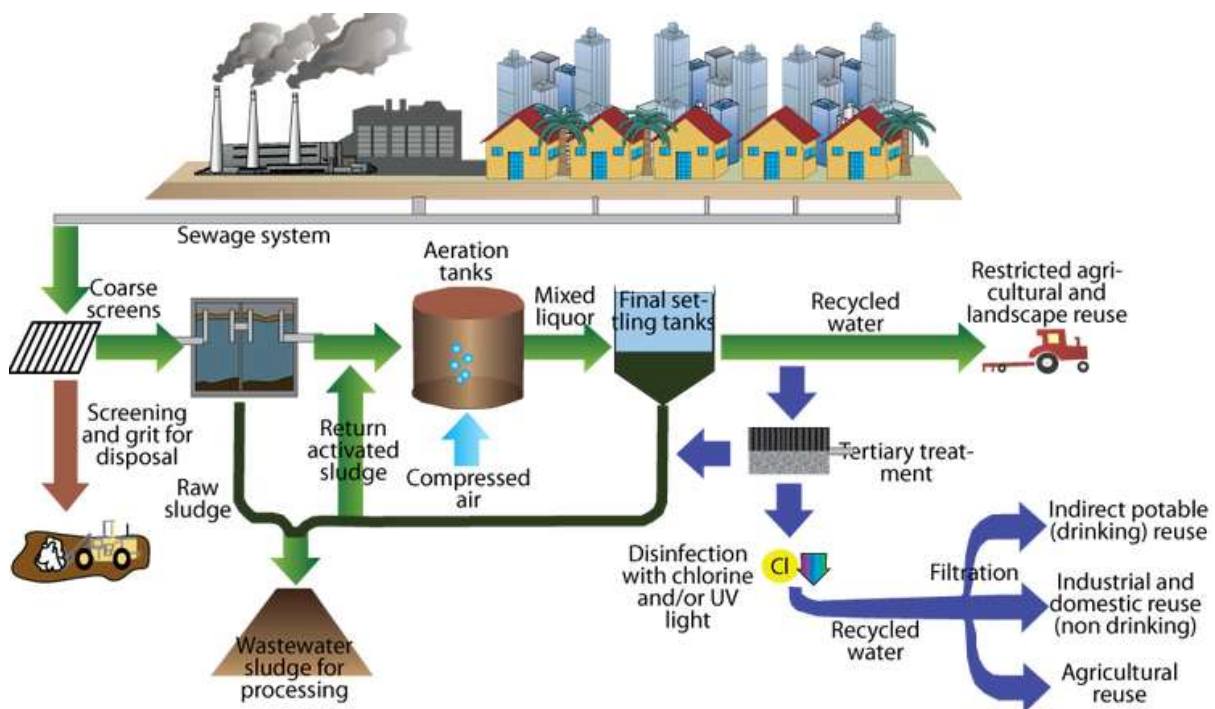
Fig.1.1 Conceptual diagram illustrating a modern urban wastewater treatment treatment plant. **(**from Kruczynski and Fletcher ,2012 [3]**)**

A conceptual diagram outlining the operation of a typical modern wastewater treatment plant is presented in figure 1.1.

- As wastewater enters the treatment facility, it undergoes preliminary treatment. Typically, this consists of screening through a series of progressively finer grates for the removal of large objects and heavy solids.

- Primary treatment consists of holding the sewage in a tank where the heavier solids can settle to the bottom while oils and lighter solids float to the surface. The settled and floating materials are removed while the remaining liquid flows into the next stage, to secondary treatment.

- During secondary treatment, the water is kept in an aeration tank in the presence of a culture of suspended bacteria and other microorganisms (activated sludge) that are able to break down and digest organic matter. The main types of micro-organisms forming the activated sludge, as well as their corresponding role in the process are presented in table 1.2. The aerated mixed liquor is then led to secondary clarifier units (settling tanks) where a part of the biomass is separated and returned to the aeration tanks. Treated water either continues downstream for tertiary treatment, or can be reused as is for agricultural or landscape irrigation.

Table 1.2. Microorganism composition of activated sludge and their main roles in the process

Microorganism	Activity
Bacteria	Mainly responsible for organic matter degradation
Protozoa	Digest free bacteria and suspended particles Improve effluent clarity
Rotifers and nematodes (Metazoa)	Rotifers remove non-flocculated bacteria Nematodes stabilize sludge
Filamentous bacteria	Aid floc formation and BOD reduction In excess, can create operational problems
Fungi	Feed on decaying matter Can indicate problem with pH control or old sludge

- The purpose of tertiary treatment is to further improve effluent quality prior to environmental discharge. Tertiary treatment processes may include control of nitrogen and phosphorus levels (mostly to avoid eutrophication issues), coagulation/sedimentation for removal solids and chlorination/UV radiation for disinfection (always as final step).

Most of the MWTP in operation today however were not designed with the purpose of eliminating these types of micropollutants. The microorganisms of table 1.2 are generally unable to break-down many of these compounds, due both to their recalcitrant nature and their continuous introduction. While some state of the art MWTP can partially remove them, the majority of micropollutants is discharged untreated to the environment. This presents a challenge that calls for modifications to current MWTP infrastructures. An ambitious study evaluating micropollutants from the effluents of 742 MWTP in Switzerland had suggested the need of upgrading at least 100 facilities within the next 20-25 years [4; 5]. The identification of suitable and economically feasible process combinations allowing for their successful removal has therefore become a major focus of environmental research.
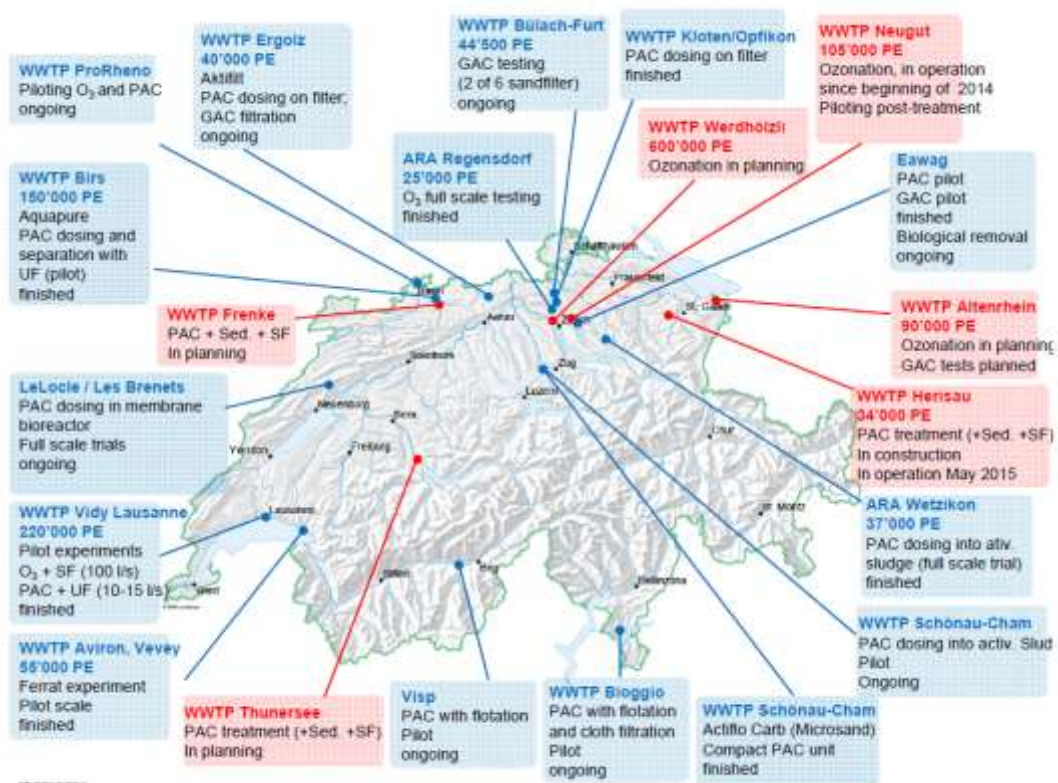
Fig.1.2. Recent and ongoing projects for upgrading Swiss wastewater treatment plants (from Micropollutants: The Swiss Strategy FOEN report [6])

Current strategies are based on two alternative processes that are both technically feasible:

The first is use of powdered activated carbon (PAC) followed by ultrafiltration or sand filtration and the second is oxidation by ozone, followed by sand filtration. Both processes were tested in parallel at pilot scale at the Lausanne MWTP for a period of over a year. Following promising results from both processes, so several plants all over Switzerland are currently in the process of implementing these technologies, as seen in figure 1.2. Costs associated with this upgrade effort estimate a 5-35% increase per MWTP, which at a national level translates to a 12% increase in costs of wastewater treatment.PAC allows for the removal of a broad spectrum of MCs via adsorption to its high specific surface area. However, as organic matter present in WW also competes for adsorption sites, larger amounts of PAC are required. Ozonation belongs to a family of processes called advanced oxidation processes (AOPs), discussed in detail in the following section.

1.3. ADVANCED OXIDATION PROCESSES - POSSIBLE STRATEGIES FOR MICROPOLLUTANT REMOVAL

Oxidation is defined as the transfer of electrons from an electron donor (reductant) to an electron acceptor (oxidant) for which they exhibit higher affinity. These transfers result in the chemical transformation of both oxidant and reductant. The ability of an oxidant to initiate chemical reactions is measured in terms of its redox potential, with table 1.3 showing the redox values of some significant oxidizing species.

Table 1.3. Redox potential of some oxidizing species

Oxidant	E^o (V)
F_2	3.06
$HO^{\bullet}$	2.80
$SO_4^{\bullet-}$	2.60
H_2O_2	1.77
MnO_2	1.68
$HClO_4$	1.63
Cl_2	1.36
$Cr_2O_7^{2-}$	1.33
O_2	1.23
Br_2	1.10

In a broad sense, advanced oxidation processes (AOPs) refer to a set of chemical processes running at ambient temperature and at atmospheric pressure that involve the degradation of organic contaminants in water via the generation of highly reactive radical species, mainly the hydroxyl radical (HO$^•$) [7]. The hydroxyl radical is a powerful non-selective oxidant that reacts rapidly and aggressively with most organic compounds, leading to their gradual decomposition and eventual mineralization. As seen in table 1.3 the redox potential of HO$^•$ is second only to fluorine, suggesting that it can attack most organic compounds. HO$^•$ contributes to contaminant degradation mainly via two types of attacks.

- Hydrogen abstraction (React. 1.1), usually observed when attacking alkanes or alcohols
- addition reactions (React. 1.2.), observed in the case of olefins and aromatics
- electron transfer reactions (React. 1.3.).

HO$^•$ + RH → R$^•$ + H2O   React. 1.1

HO$^•$ + PhX → HOPhX$^•$ + H_2O React. 1.2

HO$^•$ +RH → RH$^{•+}$ + OH$^-$ React. 1.3

Regardless of which of the above three mechanisms is dominant, the degradation pathway generally follows the route shown in react. 1.4:

R + HO$^•$ → Aliphatic acids + HO$^•$ → CO_2 + H_2O + inorganic salts   React. 1.4
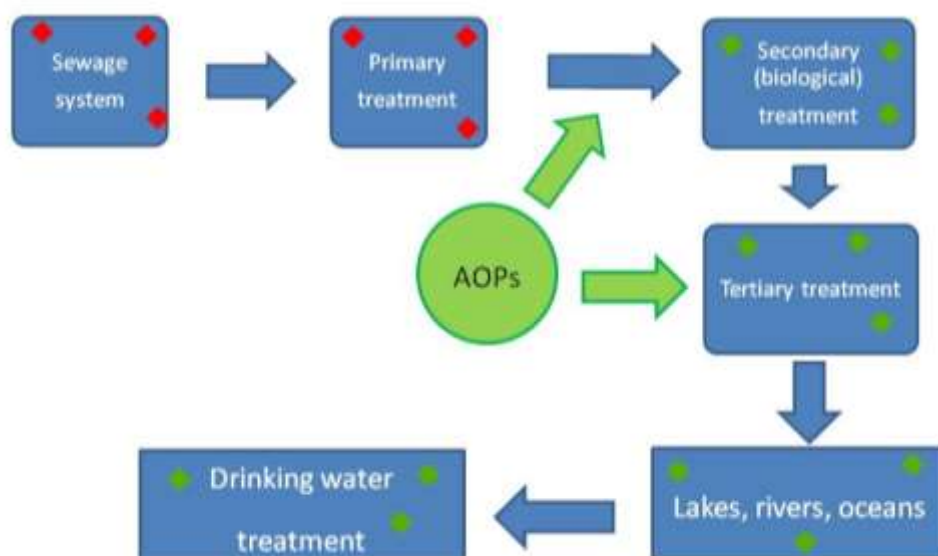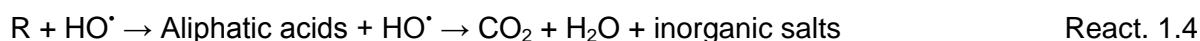
Fig. 1.3. Possible points of AOP application within the context of a municipal wastewater treatment plant

The main problem with the implementation of AOPs is their relative high cost compared to biological treatment. Strategies for optimizing efficiency and operational time thus focus on applying them in combination with biological treatment, either before it (in order to enhance biodegradability), or as part of tertiary treatment (for reducing toxicity), as seen in figure 1.3.

Apart from application in MWTP, AOPs can also be considered for the treatment of point-source contaminated waters, such as industrial (e.g. pharmaceutical, textile, paper mill industries) or hospital wastewaters. Some facilities discharge their effluents directly into water bodies, others treat it themselves before release and others send them directly MWTPs. Hospital wastewater for example is heavily contaminated with pharmaceutical substances, which can also lead to the development of antibiotic resistance mechanisms in any bacteria present in it. Smaller-scale AOP based treatment systems for such effluents could transform any recalcitrant compounds, greatly facilitating their subsequent treatment within MWTPs. AOPs studied in the context of water treatment usually include processes that involve O_3, H_2O_2, UV light, TiO_2 catalysis, cavitation and Fenton's reagent. In addition, combinations of different AOPs are also under investigation with the aim of taking advantage of any synergistic effects that arise from their concurrent application. The operational concepts as well as advantages and disadvantages of some of the most important AOPs are demonstrated in table 1.3.

Table 1.3. Concepts, advantages and disadvantages of some major AOPs

AOP technology	Brief description	Advantages	Disadvantages
General	Oxidation of organic contaminants through reactions with highly reactive radical species (such as HO•). Formation ca**n** occur through several different processes	•Non-specific destructive processes •Also have disinfectant capabilities •Many AOP components already utilized in water community and industry	•Possible accumulation of oxidation by-products •Radical scavenging by natural water components can reduce AOP effectiveness
O_3	O_2 is converted into O_3 by an electric discharge field. Direct oxidative action and $HO^•$, $HO_2^•$ radical generation at high pH via its decomposition in H_2O	•Acts over wide pH range •No chemical addition	•Energy/cost intensive •O_3 extremely toxic, destruction of off-gases necessary to avoid exposure

H_2O_2/O_3	H_2O_2 dissociates to HO_2^- in water, which reacts rapidly with O_3 to form $HO^•$	•Increased $HO^•$ generation than O_3 alone	Same as for O_3
H_2O_2/UV	Dissociation of H_2O_2 to $HO^•$ following irradiation with UV light < 280 nm.	•Among the most well studied and applied AOP systems •H_2O_2 more soluble in water than O_3. Higher amount of $HO^•$ can be generated	•Turbidity interferes with penetration •UV lamp or sleeve failure can lead to mercury contamination
Sonication	Formation of microbubbles in solution that implode after reaching a critical resonance size. HO• formed from dissociation of H_2O or due to extreme cavitation conditions	•Simple design •Less heat transfer relative to UV	•No full-scale application yet •Addition of H_2O_2/O_3 may be required for efficient removal •Significant energy consumption
TiO_2	When TiO_2 is illuminated by UV light, valence band electrons are excited to the conduction band, resulting in formation of positive holes. $HO^•$ formed mainly in holes and other pathways	•Catalytic. •Application at wide pH range . •Can be performed at wavelengths which form part of the solar spectrum	•Separation step required if TiO_2 added as slurry •TiO_2 activity can be easily lost. •Low quantum yield due to rapid charge recombination.
Fenton/ Photo-Fenton	$HO^•$ generation via reaction of Fe^{2+} with H_2O_2/ $HO^•$ generation via activation of Fe^{3+} complex with UV/V is light and Fe^{2+} regeneration	•Catalytic (photo-Fenton) •Not energy intensive •Active at wavelengths which form part of the solar spectrum	•Requires iron removal •Low pH (~3) required to keep the iron in solution •pH adjustment increases operation costs and water salinity

Of the above technologies, O_3, O_3/H_2O_2 and H_2O_2/UV have already seen full-scale applications, with numerous installations worldwide treating groundwater, drinking water as well as municipal and industrial wastewaters [8; 9]. O_3 based processes remain the most

well-developed AOPs, having been applied both for industrial and as part of MWTP effluents. Switzerland's own first full-scale ozonation MWTP has been operating at the Neugut MWTP plant in Dübendorf, near Zurich, since March of 2014. (www.bafu.admin.ch/micropoll). Ozonation remains nevertheless an energy intensive process. Equipment and operational costs are high, and there are significant hazards involved. Ozone is an extremely reactive and toxic gas, so extreme care has to be taken to avoid exposure and minimize risks. First, the choice of construction materials for the ozone reactor has be to be carefully made. In fact, the ozone reactor is encased in reinforced concrete of such high quality that only a single cement plant in Switzerland could provide it. Empirical data on how cement will behave following long-term contact with ozone are scarce, so caution, at least at this stage, is necessary. Additionally, as not all of the supplied ozone reacts with the contaminants, any excess quantity has to be captured and destroyed, introducing additional costs. (www.bafu.admin.ch). It is therefore not surprising that development of other AOPs remains an interesting venture.

The Fenton/photo-Fenton processes remain at an demonstration state, having until now seen few large-scale applications[10] They provide a much cheaper alternative compared to O_3 treatment as they can be applied with low-maintenance, modest equipment and low energy expenditure (also taking advantage of solar radiation). The main limitations arise from the necessity of pH regulation below pH 3 and the accumulation of iron sludge which has to be recuperated. The next section discusses in detail the main mechanisms, advantages and the challenges that need to be addressed for facilitating their large-scale applications.

1.4. THE FENTON AND PHOTO-FENTON PROCESSES

1.4.1. THE FENTON PROCESS

During the Fenton reaction (React. 1.5), the generation of reactive oxygen species is mainly driven by decomposition of H_2O_2 when it reacts with ferrous iron , first reported by H.J.H Fenton in 1894 [11]. Barb et al [12] later proposed the following sequence of reactions (1.6-1.11) that follow decomposition of H_2O_2 in acidic solution in absence of light and other organic compounds.

$$Fe(II) + H_2O_2 \quad \rightarrow Fe(III) + OH^- + HO^{\bullet} \qquad k=53\text{-}76 \ M^{-1} \ s^{-1} \qquad (React. \ 1.5)$$

$$Fe(III) + H_2O_2 \quad \rightarrow Fe(II) + HO_2^{\bullet} + H^+ \qquad k=1\text{-}2 \ 10\text{-}2 \ M^{-1} \ s^{-1} \qquad (React. \ 1.6)$$

$HO^{\bullet} + H_2O_2$	$\rightarrow HO_2^{\bullet} + H_2O$	$k=1.7\text{-}4.5\ 10^7\ M^{-1}\ s^{-1}$	(React. 1.7)
$HO^{\bullet} + Fe(II)$	$\rightarrow Fe(III) + OH^-$	$k=2.6\text{-}5.8\ 10^8\ M^{-1}\ s^{-1}$	(React. 1.8)
$Fe(III) + HO_2^{\bullet}$	$\rightarrow Fe(II) + O_2 + H^+$	$k=0.33\text{-}2.1\ 10^6\ M^{-1}\ s^{-1}$	(React. 1.9)
$Fe(II) + HO_2^{\bullet}$	$\rightarrow Fe(III) + OH^-$	$k=0.75\text{-}1.5\ 10^6\ M^{-1}\ s^{-1}$	(React. 1.10)
$HO_2^{\bullet} + HO_2^{\bullet}$	$\rightarrow H_2O_2 + O_2$	$k= 1.4\ 10^{10}\ M^{-1}\ s^{-1}$	(React. 1.11)
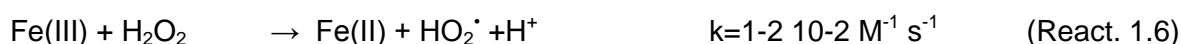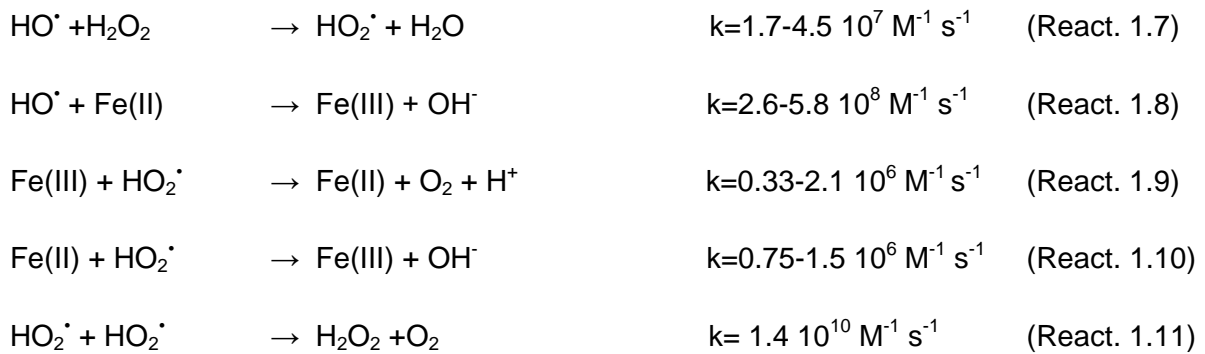
The above reaction sequence is known as the thermal, or classical Fenton process, as it is driven only by thermal and not photochemical energy. The desired hydroxyl radicals are mainly produced via (React. 1.5.), with Fe^{2+} oxidized to Fe^{3+} in the process. As can be seen however (React. 1.6 and 1.9), Fe^{3+} can also be reduced back to Fe^{2+}, albeit at a much slower rate. What tend to complicate matters however is that Fe^{3+} does not remain in its ionic form and tends, in the absence of other complexing substances, to form complexes with water and hydroxyl ligands. The type of ferric-aqua complex that is formed depends on the pH of the medium. The different complexes that are dominant in the 1<pH<5 range are shown in figure 1.3. Among them, $Fe[(H_2O)_5OH]^{2+}$, formed when the pH is within the 2.3<pH< 3.5 range is soluble and exhibits photoactivity in the UV-VIS part of the solar spectrum. From pH 3.5 upwards, insoluble $[Fe(H_2O)_6]^{3+}$ begins to form, leading to iron precipitation. Maintaining pH at acidic values is therefore vital for the Fenton process.
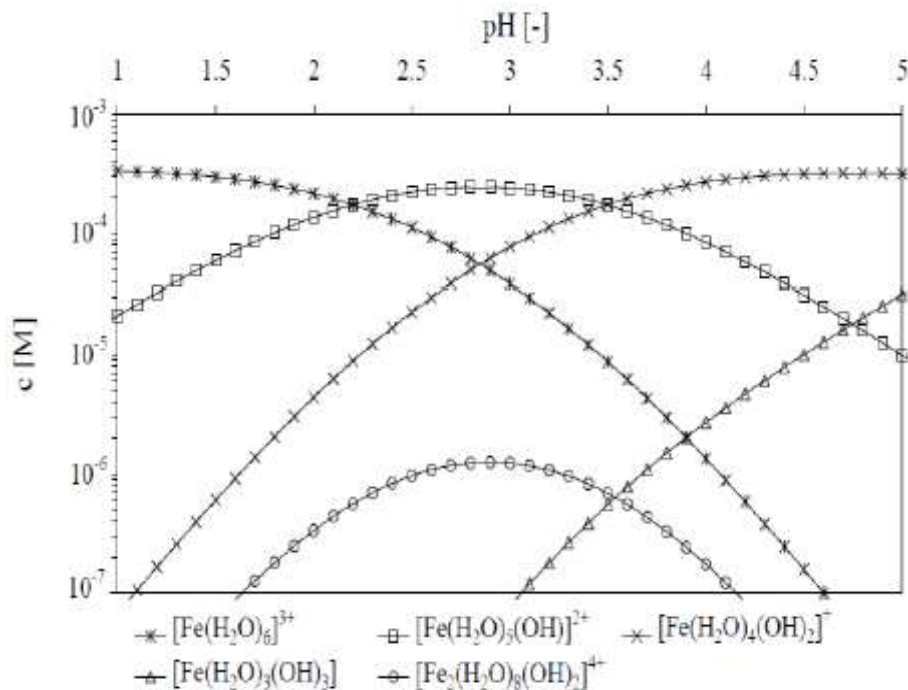
Fig. 1.4. Ferric-aqua complexes formed at the 1-5 pH range in the absence of other competing ligands (from Flynn, 1984 [13])

24

The presence of inorganic salts can also influence the rates of reactions 1.5-1.11. Chloride and sulfate ions can form complexes with Fe^{3+}, markedly decreasing the regeneration of Fe^{2+}, while formation of $Cl_2^{\bullet-}$ and $SO_4^{\bullet-}$ that are less reactive than $HO^\bullet$, decrease the overall system efficiency [14]. Carbonate and phosphate ions have a much stronger effect. Both carbonate and phosphate can scavenge $HO^\bullet$, while phosphate can also precipitate iron via the formation of insoluble iron phosphate salts.

1.4.2. THE PHOTO-FENTON PROCESS

Due to the photochemistry of many Fe^{3+} species, irradiation with UV or UV/Vis light can lead to a series of photochemical reactions that invariably increase reactions rates. In transition metal complexes in general, a change in electron distribution between the metal and a ligand give rise to charge transfer (CT) bands. CT absorptions in the UV/Vis region are intense and selection rule allowed. A charge transfer transition is in itself regarded as an internal redox process. If the ligand molecular orbitals are full, charge transfer may occur from the ligand molecular orbitals to the empty of partially filled metal d-orbitals. The absorptions that arise from this process are called ligand to metal charge transfer bands (LMCT) and result in the reduction of the metal back to. For iron, it means that it can be reduced to its Fe^{2+} state, continuing the Fenton process indefinitely as long as the system remains illuminated (reacting again with H_2O_2 as per reaction 1.5.). This photoreduction process can be described by reaction 1.12.

$$Fe(III)(L)_n + h\nu \rightarrow [Fe(III)\text{-} L]^* \rightarrow Fe(II)(L)_{n-1} + L_{ox}^\bullet \qquad \text{(React. 1.12)}$$

The formed radical can also participate in reactions with oxygen in order to generate is superoxide radicals ($O_2^\bullet$), which can themselves participate in the Fenton reaction system.

$$L_{ox}^\bullet + O_2 \rightarrow O_2^\bullet + L' \qquad \text{(React. 1.13)}$$

In the absence of any organic ligands, Fe^{3+} - hydroxy complexes present in acidic solutions (principally $Fe[(H_2O)_5OH]^{2+}$) are the ones that absorb the most in the UV/Vis region. This allows for the sustainable regeneration of Fe(II), continuing indefinitely as long as the system is illuminated. This variant of the Fenton process is called the photo-Fenton process, with degradation kinetics much higher than dark Fenton [15; 16]. Due to the iron regeneration, and provided the pH remains acidic, the required addition of iron is also much lower, thus minimizing secondary pollution by its precipitates and lowering any costs associated with its removal prior to environmental release.

Fe^{3+} however can form complexes with many organic ligands, especially those acting as polydentate ligands. They typically exhibit higher molar absorption coefficients in the near-UV and visible regions than the aqua complexes, also using a higher fraction of the solar radiation, up to 580 nm [17]. Depending, on the ligand, each complex exhibits different light absorption properties, with different quantum yields at different wavelengths. Polychromatic quantum efficiencies ($<\Phi>$) in the UV/visible can range from about 0.05 to 0.95 [18; 19; 20].

Additionally, they can contribute to maintaining Fe^{3+} soluble at the circumneutral pH of most natural waters allowing for its assimilation by many aquatic organisms for whom it is a dietary requirement. Formation of chelation complexes with organic ligands is thus an essential aspect of iron cycling in nature, regulating iron transport, speciation and availability, especially in sunlit surface waters [21]. In natural waters, these take the form of heterogeneous mixtures of a variety of organic compounds, consisting of aromatic, aliphatic, phenolic and quinolic functional groups with varying molecular sizes and properties.
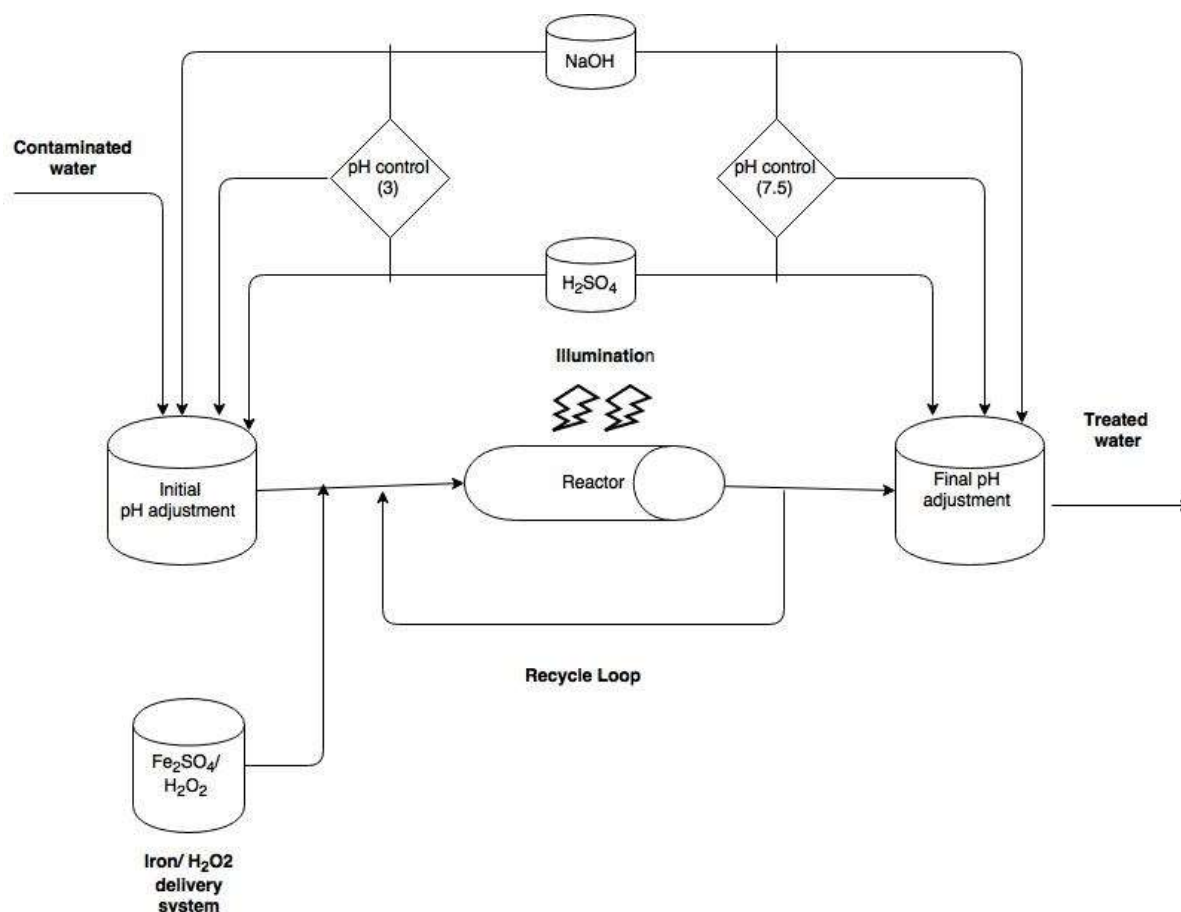
Fig. 1.5. A possible design for a photo-Fenton water treatment system

The fundamentals of photo-Fenton chemistry are therefore well-established. Additionally, efficient designs for solar photochemical reactors such as the Compound Parabolic Collector

(CPC) have been developed [10; 22] . The geometry of the CPC allows for the collection and use of both direct and diffuse radiation, while its modular design makes it ideal for solar-driven large-scale operations. A possible design for a photo-Fenton treatment process can be seen in figure 1.5, which has the potential to be applied either as part of a MWTP or for industrial effluents.

Extensive research on photo-Fenton has established that it can successfully treat a very wide spectrum of contaminants [9; 10; 22; 23]**,** although some of its drawbacks have inhibited its large-scale application. If the following issues could be somehow resolved, then photo-Fenton could become a much more plausible technology.

- Application of this process requires pH control both before (acidification) and after (neutralization) the photo-Fenton stage. This introduces costs associated both with reagents and process control, while also increasing the water's salt , which could account as secondary pollution. Any modifications to the process that would permit operation at natural pH would greatly facilitate the process.
- If addition of iron concentration could be minimized, the costs of recuperating it after the end of the treatment could be significantly reduced.
- Natural waters contain ions (mainly carbonate and phosphate) that can act as radical scavengers and/or contribute to precipitation and subsequent loss of iron.
- Operation costs remain high, so any complementary or synergistic processes that can reduce treatment time and reagent consumption (mainly H_2O_2) can be important.

Some strategies for addressing some of the above issues are discussed in the next section.

1.5. ENHANCING THE PHOTO-FENTON PROCESS

Several authors have suggested the integration of other AOPs such as O_3 [24] or TiO_2 [25] with photo-Fenton as a means of enhancing its performance. Combination with O_3 has proven to be very effective, but it adds significant complexity to the process, especially when considering large-scale applications. Addition of TiO_2 is easily implemented, but achieved reaction rates are not significantly better than the homogeneous process performed at acidic pH. Other authors have suggested the use of inert matrices to fix iron and avoid precipitation. and therefore permitting operation at natural pH; but efficiencies were rather low [26].

This thesis is focused on the evaluation of two distinct strategies for the enhancement of the photo-Fenton process: The use of ultrasound and the use of iron-complexing agents.

1.5.1. ULTRASOUND

Lord Rayleigh [27] had described a mathematical model in which enormous local temperatures and pressures were predicted during the collapse of incompressible liquids. Ten years later, Richards and Loomis [28]reported the first chemical effects of ultrasound. It wasn't until the 1950s and 1960s that interest in ultrasound research would gain enough momentum to finally obtain a relatively good understanding of the processes involved [29].

When ultrasound is applied to a liquid, it creates oscillating regions of positive and negative pressure. Correspondingly, the liquid goes through cycles of compression and expansion. At a certain point, the pressure amplitude can exceed the tensile strength of the liquid, leading to the formation of cavitation bubbles. During subsequent compression cycles, these bubbles collapse implosively, concentrating the diffuse energy of sound and accompanied by extremely rapid heat transfer phenomena. Localized hot spots are formed, reaching temperature and pressure exceeding 5000 K and 500 atm, respectively [30]. According to the temperature profile, three zones of distinct properties have been associated with a cavitation bubble (figure 1.6).

Cavitational bubble

Thermolytic center

State: Gaseous
Collapse temperature: ~5000 K
Collapse pressure: ~500 atm
Thermolysis of water vapor and volatile compounds

$$H_2O\ (g) \longrightarrow H\cdot + \cdot OH$$
$$H\cdot + O_2\ (g) \longrightarrow HO_2\cdot$$

Interfacial region

State: Fluid under extreme conditions
Collapse temperature: ~2000 K
Width: ~200 nm
Lifetime: <2 μs
Vast gradients of temperature and pressure
Oxidation and thermolysis of nonvolatile, hydrophobic, and ionic compounds

Bulk region

State: Liquid
Temperature: Ambient
Accumulation of H_2O_2

Fig. 1.6. The three zones in and around the cavitation bubble and their associated properties (from handbook of applications of ultrasound: sonochemistry and sustainability, 2012 [31])

1) The thermolytic center (bubble core), where the highest temperatures and pressures are found. These extreme conditions result in thermolysis of water, generating radical species such as HO•. Volatile chemical compounds found in this region can be degraded either via thermolysis or via reaction with the generated radicals.

2) The Interface between cavitational bubble and bulk liquid. Vast temperature and pressure gradients are observed in this region, with temperatures around 2000 K measured in this region [32]. Any unreacted HO• from the core is also diffused to this region. Non-volatile and hydrophobic compounds are more concentrated here than at the bulk solution, thus being preferentially attacked by HO• or degraded due to the high temperatures. More hydrophilic compounds remain at the same concentration as in the bulk solution.

3) The bulk region, which retains ambient temperature and pressure. Any HO$^{\bullet}$ unreacted in the previously mentioned regions may either react with hydrophilic compounds or recombine with each other, producing hydrogen peroxide [33].

H_2O +))) → HO$^{\bullet}$ + H$^{\bullet}$ (React. 1.14)

O_2 +))) → 2O$^{\bullet}$ (React. 1.15)

HO$^{\bullet}$ + O$^{\bullet}$ → HOO$^{\bullet}$ (React. 1.16)

2 HO$^{\bullet}$ → H_2O + O$^{\bullet}$ (React. 1.17)

2 HO$^{\bullet}$ → H_2O_2 (React. 1.18)

1.5.1.1. FACTORS AFFECTING CAVITATION

The efficiency of any ultrasonic process for contaminant degradation depends on factors affecting both the cavitation process as well as the behavior of the contaminants within the system. Some of the parameters affecting cavitation and bubble collapse are presented below:

- **Ultrasound Power:** Higher acoustic pressure generally leads to both a greater number of cavitational events, as well as a more violent cavitational collapse [34]. However, optimum power intensity has been suggested to exist with regard to degradation rate. This has been attributed to a "bubble shielding" effect, in which the formation of large numbers of cavitational bubbles around the ultrasonic transducer both scatter and absorb sound waves, leading to effectively lower intensities [35].

- **Ultrasound frequency:** Low-frequency ultrasound has been shown to lead to fewer cavitational events, but also bigger bubble size and more violent collapse. However, increasing frequency leads to the formation of more cavitational bubbles, aiding both HO• production and the diffusion of compounds within the bubble [36].

- **Presence of inorganic salts:** Most natural waters or industrial waters contain significant concentrations of anions such as Cl^-, NO_3^-, SO_4^{--}, CO_3^{--}/HCO_3^-, PO_4^{---}/HPO_4^{--}. Several works exist suggesting that their presence can positively affect sonochemical degradation of organic contaminants in aqueous solutions [37; 38] with higher degradation rates observed in natural than in deionised water. This has been attributed to a "salting out" effect, which pushes organic contaminants towards the bubble-bulk interface. Using Bisphenol A as a model contaminant, it has been shown that presence of bicarbonate, which acts as a scavenger for HO˙ radicals, actually enhances sonochemical degradation more than any other anion [39]. This property of ultrasound could prove a significant advantage in the treatment of complex aquatic media.

- **Contaminant properties:** Volatility and hydrophobicity are the two properties that most affect sonication degradation rate. Volatile compounds can enter the gaseous phase of cavitational bubbles more readily, thus subjected to thermolysis and direct oxidation by generated radicals during the final collapse. A compound's Henry's law constant H (ratio of the partial pressure a compound exerts in gaseous phase over its aqueous concentration) can be used to quantify volatility. Higher H values generally favour sonochemical degradation rate. Hydrophobic compounds also tend to accumulate on the bubble-bulk interface, as they are attracted by the bubble's gaseous phase. Hydrophobicity is approximated by the octanol-water partition coefficient K_{ow} (ratio of a compound's concentration in octanol phase over its concentration in aqueous phase at equilibrium). Compounds with high K_{ow} values tend to be more hydrophobic, accumulating at the interfacial region to be degraded by thermolysis or by HO˙ diffused from the core.

1.5.1.2. COUPLING OF US WITH PHOTO-FENTON

In order for a technology to be sustainable and suitable for application, economical as well as technical feasibility is required. Application of ultrasound alone however is still prohibitively expensive, so options for combining it with different AOPs are being considered. Combination of US with different AOPs was much more attractive economically than US alone. Generally, cost of hybrid US processes is one to two orders of magnitude more than currently established AOPs such as ozonation, O_3/H_2O_2 and UV/H_2O_2 [40]. Specifically for

photo-Fenton, a synergistic effect has been observed in several cases, possibly due to two main reasons: 1) Fe^{2+} can take advantage of any H_2O_2 generated by radical recombination 2) The preferential degradation of some compounds in or near the cavitation bubble, leaving the non-selective photo-Fenton process to focus on the more hydrophilic and leading to synergy with regard to mineralization [41].

While the use of ultrasound has the potential to circumvent some of the problems associated with photo-Fenton in natural waters and enhance degradation kinetics, it doesn't address the issue of required pH adjustment for maintaining iron stability. Especially for large-scale treatment of complex wastewater with high buffering capacity, acidification and neutralization costs can become significant. Therefore, other types of methods have to be investigated for pursuing this particular objective, as applying iron complexing agents to keep iron in solution at circumneutral pH.

1.5.2. IRON COMPLEXING AGENTS

The addition of chelating agents is another means for increasing the optimal operational pH of the photo-Fenton process, while at the same time exhibiting increased quantum yields permitting the use of a wider fraction of the solar spectrum. Carboxylic acids are a special case of chelating agents occurring naturally in photo-Fenton systems, as they are frequent intermediates prior to mineralization during the oxidative treatment of many contaminants. As they accumulate in solution, acceleration of the degradation process is then commonly observed.

Oxalate and citrate are two ligands that have been thoroughly investigated as additives to the photo-Fenton process. The absorption spectrum of ferrioxalate complexes extends further into the visible region, showing increased efficiency for solar photo-Fenton applications. Fe^{3+} has been known to be able to complex from 1:1 to 1:3 Fe:oxalate ratios depending on the pH, with their relative fractions depending on the pH [42]. The working pH can be extended up to 6. Complexes with citrate [43] likewise vary with pH, with Fe-citrate dominant up to a pH near 4, with $Fe(OH)cit^-$ and $Fe(OH)_2(cit)_2^{2-}$ gradually becoming the main species until pH 9, although the optimal pH for $HO^{\bullet}$ production was at 5. A kinetically optimized process with either of these two complexes therefore would still need to operate at acidic pH, necessitating post-treatment neutralization.

Research on other types of complexes that can operate optimally at an even wide pH range remains important. Ethylenediaminetetraacetic acid (EDTA) was under scrutiny for time, as it can form soluble complexes at a wider pH range, but it is not biodegradable and is

considered a persistent pollutant. One of its isomers however, described below, has been gaining attention recently.

1.5.2.1. ETHYLENEDIAMINE-N,N'- DISUCCINIC ACID (EDDS)

Ethylenediamine-N,N'- dissucinic acid (EDDS) is a structural isomer of EDTA and also a strong complexing agent. It is however considered biodegradable and has been reported as safe for environmental applications. The physicochemical properties of the Fe(III)-EDDS have been studied in a recent article by Wu et al [44]. Fe^{3+} is complexed by EDDS with a predominant ratio of 1:1 up to pH 9 (figure 1.7), with hydroxylated forms appearing as the pH further rises. The 1:1 form is also the most photoactive, and can generate $HO^{\bullet}$ when photolyzed.
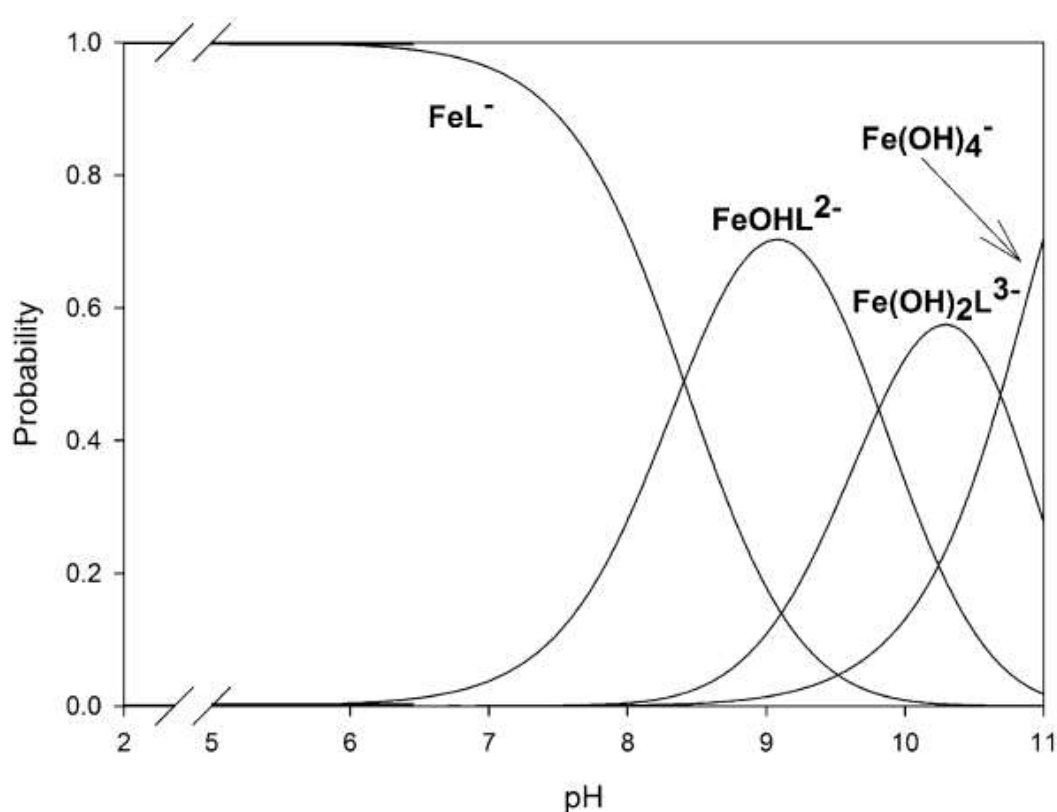
Fig. 1.7. The probabilities of different Fe:EDDS (noted as L) complexes formation as a function of pH (from Wu et al, 2014 [44])

It has proven successful for degrading emerging contaminants in MWTP effluent at neutral pH with low iron and H_2O_2 concentrations [45]. The pH was not lowered by its addition, so no neutralization was necessary, leaving the salinity of the treated water unmodified. Apart from EDDS however, another class of compounds that can exhibit iron binding properties has been of interest within the context of this work.

1.5.2.2. THE POTENTIAL OF POLYPHENOLS AS IRON-COMPLEXING AGENTS.

Polyphenols are a very widely diversified group of compounds, divided into several sub-classes such as catechins, flavonols, flavanols, flavones, anthocyanins, proanthocyanins and phenolic acids. They are amply found in plant materials, and consequently, in many foods and beverages as well. They can be found in green and black teas, coffee, fruits and their juices, vegetables, olive oil, wines and chocolate. They have many different biological activities, mostly related to enzyme regulation and antioxidant behaviour, the latter being their most widely recognized role.
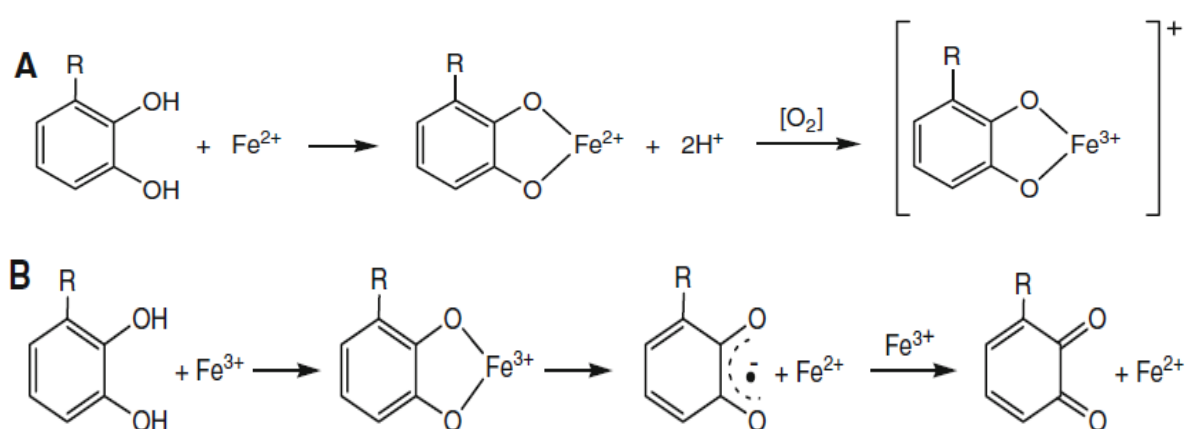
Fig. 1.8. a) Coordination of Fe^{2+} by polyphenols and generation of Fe^{3+}-polyphenol complex in presence of O_2 b) Coordination of Fe^{3+} by polyphenols and subsequent Fe^{3+} reduction and semiquinone / quinone formation (from Perron, 2009 [46]).

Although polyphenolic compounds have been mostly associated with antioxidant activity, several reports have also described prooxidant behavior. This seems to arise from their capacity to bind and reduce Fe^{3+} to Fe^{2+}, allowing it to participate to Fenton-type reactions. Because polyphenol ligands tend to stabilize Fe^{3+}, it is believed that binding of Fe^{2+} to polyphenol lowers the reduction potential of iron and enhances its oxidation rate (figure 1.8. a). In presence of H_2O_2, as oxidation is extremely rapid anyway, this effect may not be particularly important. Once the polyphenol is bound to Fe^{3+}, it can reduce it to Fe^{2+} while it is itself oxidized to a semiquinone [47; 48; 49]. The semiquinone is then capable of reducing another Fe^{3+} equivalent, while oxidized to a quinone (figure 1.8.b). The effect of pH on this process is complex, as different types of complexes can be formed, each either favouring or inhibiting Fe^{3+} reduction. For catacholamines, for example, the process is only favored at low pH values, while at neutral pH formation of stable bis- or tris- complexes prevent any type of

internal electron transfer [50]. Studies with Epigallocatechin gallate (EGCG) and Epitatechin gallate (ECG), both compounds that can be extracted from green tea, have demonstrated that they can each reduce up to four equivalents of Fe^{3+}. DNA damage has also been observed in vitro when Fe^{3+} complexes with gallic acid, EGCG and EGC were added [51; 52]. The importance of iron-binding to the prooxidant activity of polyphenols has also been demonstrated by experiments done in the presence of strong metal chelators such as EDTA and bleomycin [51; 53].

Such type of phenolic/polyphenolic components however can also form a significant fraction of industrial wastewaters originating from the processing of natural products. Cork production industry [54], olive mills [55], wineries [56] and the tea manufacturing industry [57]. The concept of reusing such types of wastewater for stabilizing iron and increasing Fenton/photo-Fenton kinetics is also addressed in this work.

1.6. AIMS AND OUTLINE OF THIS WORK

This work is a broad attempt to evaluate the application of different processes and operational variables for enhancing the photo-Fenton process. The results are organized in 3 main chapters, along with a short final chapter discussing general conclusions and perspectives.

Chapter 2 is focused on the application of ultrasound in combination with photo-Fenton for two very distinct applications:

- A pilot-scale ultrasound/photo-Fenton system was set-up and evaluated for the treatment of three different contaminants with distinct physicochemical properties and at different concentrations. Synergy was evaluated in terms of degradation kinetics and H_2O_2 consumption efficiency.

- As discussed in section 1.5, the use of ultrasound presents some possible advantages when applied in complex aquatic media due to the beneficial effect of anions such as CO_3^-/HCO_3^-. Iodinated contrast media (ICM) are compounds that are injected in patients during radiographic procedures and excreted almost completely unmodified with their urine, a very complex aquatic medium that has been studied very little in the context of AOP research. The possibilities of treating the model ICM Iohexol in the context of municipal wastewater or in urine (at the source) by a process based on ultrasound was evaluated, both by itself and in combination with photo-Fenton.

Chapter 3 focuses on the use of EDDS as an iron-complexing agent for degrading contaminants at near neutral pH across a concentration range from µg L^{-1} to mg L^{-1} covering the different range of concentration usually found in different wastewaters Specifically:

- Treatment of microcontaminants in effluents from municipal wastewater treatment plants. An experimental design was performed in order to determine near-optimal operational parameters such as pH range, Fe:EDDS concentration and required H_2O_2 dosage.

- Treatment of effluents containing contaminants in mg L^{-1} range as in many industrial wastewaters. The importance of carbonates, aeration conditions and temperature were evaluated and some insights regarding the mechanisms of the action of Fe:EDDS were acquired. The alternative process was also compared with classical photo-Fenton in terms of contaminants removal and toxicity.

Chapter 4 discusses the possibility of exploiting natural iron chelating agents (mainly phenolic/polyphenolic compounds) that can be found in some types of wastewater (e.g from natural products processing industries). The concept of reusing polyphenol-rich wastewater in small quantities as an alternative to artificial complexing agents is introduced. As a case study, water containing highly concentrated cork bark extracts (Cork Boiling Wastewater or CBW) has been added in natural water spiked with one or several contaminants. It's capacity to maintain Fe^{3+} soluble at near-neutral pH as well as the effect on degradation and contaminants removal by Fenton and photo-Fenton were observed across a wide pH range.

In chapter 5, some general conclusions are drawn and possible future perspectives for this work are discussed.

CHAPTER 2:

ENHANCEMENT OF PHOTO-FENTON BY USE OF ULTRASOUND

2.1.INTRODUCTION

As discussed in chapter 1, ultrasound, when viewed on its own, is prohibitively expensive for large-scale applications due to high energy expenditure. However, its combination with photo-Fenton could allow for a more cost-effective process due to the presence of possible synergistic effects. Several authors have studied the combined process for different wastewaters, [58; 59; 60], with some of the possible advantages listed below:

I) Take advantage of excess hydrogen peroxide produced from hydroxyl radical recombination during the ultrasonic treatment for promoting Fenton type reactions.

II) Enhance degradation kinetics by the preferential treatment of different types of compounds by each process (hydrophobic and hydrophilic contaminants by US and p-F, respectively).

III) Allow better homogenization of hydrophobic contaminants suspended in water by promoting the formation of smaller droplets, forming emulsions and/or more stable suspensions.

IV) It is not as strongly affected by inorganic ions that are detrimental to photo-Fenton efficiency.

V) Minimize the use of reagents (Fe and H_2O_2) thus limiting secondary pollution.

In order to minimize treatment time, reagent consumption and costs, significant efforts are being made towards the development of hybrid processes. High ultrasound frequencies are widely regarded as more efficient in the destruction of organic pollutants, with several studies pointing towards an optimal frequency region between 300 and 600 KHz [61; 62; 63].

In this chapter, the use of ultrasound is investigated in combination with photo-Fenton for two distinct applications. The first section is dedicated to the evaluation of a hybrid ultrasound/solar photo-Fenton system at pilot scale for the treatment of three contaminants with different physicochemical properties. The second section explores the effect of ultrasound on the treatment of the iodinated contrast agent Iohexol in complex aquatic media (MWTP effluent and in urine).

2.2. COUPLING OF ULTRASOUND WITH SOLAR PHOTO-FENTON AT PILOT SCALE

2.2.1.OBJECTIVES OF THIS SECTION

This part of the work focuses on the application of high frequency ultrasound as a complement to solar photo-Fenton in a 10 L pilot plant reactor system. The objective is to evaluate the extent of synergistic effects between the two processes when treating contaminants of different physicochemical properties and/or at different concentrations. For this purpose, three contaminants were chosen: phenol, bisphenol A (BPA) and diuron

For this purpose, three contaminants were chosen: phenol, bisphenol A (BPA) and diuron. Phenol is a fairly water soluble compound, having a multitude of industrial used in the plastics, herbicide and pharmaceutical industries. It has been used extensively in the study of AOPs as a model compound, even for the development of standardization protocols. Bisphenol is a hydrophobic monomer widely used as a precursor to resin and polymer production. Diuron is the commercial name of DCMU (3-(3,4-dichlorophenyl)-1,1-dimethylurea), a highly hydrophobic photosynthesis inhibitor herbicide. Their structures as well as some of their physicochemical properties are shown in Table 2.1.

2.2.2 MATERIALS AND METHODS

2.2.2.1. REAGENTS

Phenol (99% purity) and bisphenol A (99% purity) were acquired from Sigma Aldrich. Diuron (97% purity) was supplied from Aragonesas Agro, S.A. (Spain). Solutions were prepared with distilled water from the Plataforma Solar de Almeria distillation plant. $FeSO_4.7H_2O$ and H_2O_2 (33% w/v) were obtained from Panreac (Spain). Acetonitrile (ACN) and formic acid (FA) used for liquid chromatography were HPLC-grade and provided by Sigma Aldrich.
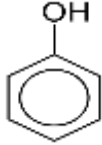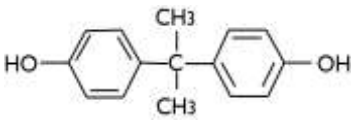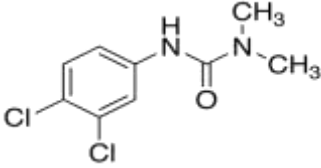
2.2.2.2. ANALYTICAL METHODS

Pollutant concentration measurements were made with an Agilent 1100 series high pressure liquid chromatography (HPLC) equipped with a C18 column (Supelcosil LC-18, 5 μm particle size, length 15 cm, internal diameter 3 mm). Agilent Chemstation LC3D software was used for data analysis. All samples were diluted by a factor of 2 in acetonitrile and filtered through a 0.2 μm syringe-driven filter prior to analysis. The injected volume for all samples was 20 μL. The analytical conditions for the determination of each pollutant can be seen in table 2.1.

Total Organic Carbon was measured by a Shimadzu TOC-VCSN analyzer equipped with an ASI-V automatic sampler.

Hydrogen peroxide concentrations were measured spectrophotometrically following the DIN 38402H15 protocol (5 ml of sample solution were added to 0.5 ml of Titanium (IV) oxysulfate and the absorbance measured at 410 nm). Total iron concentrations were measured following the ISO 6332 protocol (complexation with 1,10 phenanthroline and absorbance measured at 510 nm). All spectrophotometric measurements were made with a UNICAM UV/VIS spectrophotometer controlled with VISION software.

Table 2.1. Structure, physicochemical properties for phenol, BPA and diuron. HPLC parameters for phenol, BPA measurements. Diuron concentrations estimated by chloride release.

	Phenol[a]	*BPA*[b]	*Diuron*[c]
Chemical structure			
Solubility in H_2O (mg L^{-1})	8.2×10^4	ca. 300	42
logKow	1.46	3.4	2.77
P_v (mmHg)	0.46	7.24×10^{-7}	3.1×10^{-6}
Wavelength (nm)	272	280	*Measured by ion chromatography
Eluent composition (v/v)	58:42 (0.5% FA/ACN)	50:50 (0.5 % FA/ACN)	
Eluent flow (mL min^{-1})	0.5	0.5	
Retention time (min)	7	5	

Physicochemical properties acquired from:
a.Sangster, Journal of Physical and Chemical Reference Data
b. Bayer Product Safety Data Sheet on BPA
c.Pesticide information profiles, EXTOXNET(Extension toxicology network)

Chloride (produced from diuron degradation) were determined with a Dionex DX-600 ion chromatography system equipped with an autosampler (Dionex AS40), a quaternary gradient pump (Dionex GP50), a thermostatic column oven (Dionex LC30) and a conductivity detector (Dionex ED50) using a Dionex Ionpac AS11-HC 4x250 mm column. All samples were measured by direct injection after filtration using 0.2 µm syringe-driven filters.

2.2.2.3. EXPERIMENTAL SET-UP

All experiments were carried out in a coupled ultrasonic/solar CPC reactor system set up at the Almeria Solar Platform in Spain (latitude 37°05' N, longitude 2°21' W). The ultrasonic system consisted of a generator (operating at 450 W) and a submersible ultrasonic transducer (400 KHz). The frequency was chosen within the previously mentioned optimal range in order to maximize sonochemical effects. The transducer was provided by Sonosys and comprised of a PZT piezo ceramic array (active area 100x100 mm) encapsulated in a stainless steel casing (outer dimensions 130x100x30 mm). It was fitted to the bottom of a cylindrical stainless steel reactor (d=25 cm, h=25 cm) with circular inlet and outlet. All experiments wre conducted with th ultrasonic reactor filled to 2 liters. The solar reactor consisted of two tubes of a CPC module with an irradiated volume of 7 liters. The 2 reactors were connected by tubing with a volume of 1 L. Total volume of the system was 10 L. Contaminant solution was recirculated in a closed loop through both reactors with the aid of a centrifugal pump under a constant flow rate of 7 L min^{-1}. Following homogenization, initial iron concentrations were tested in the pF and pF/US experiments and an initial concentration of 200 mg L^{-1} of H_2O_2 was added, periodically replenished so as not to fall below 100 mg L^{-1} at any time. The consumption of H_2O_2 was calculated using the acquired data. US experiments were run with the CPC tubes covered so as to avoid solar irradiation. Given the non-constant nature of solar irradiation, solar treatment times are usually normalized over a certain light intensity. However, the concurrent application of ultrasound makes such normalization impossible. Instead, consistency was maintained by performing the experiments in clear days and between hours of similar global irradiation (verified by radiometric measurements). The temperature of the system was controlled via the recirculation of refrigerated water through a cooling coil placed within the ultrasonic reactor and kept around 35°C. Front and rear views of the coupled system can be seen in fig.2.1.
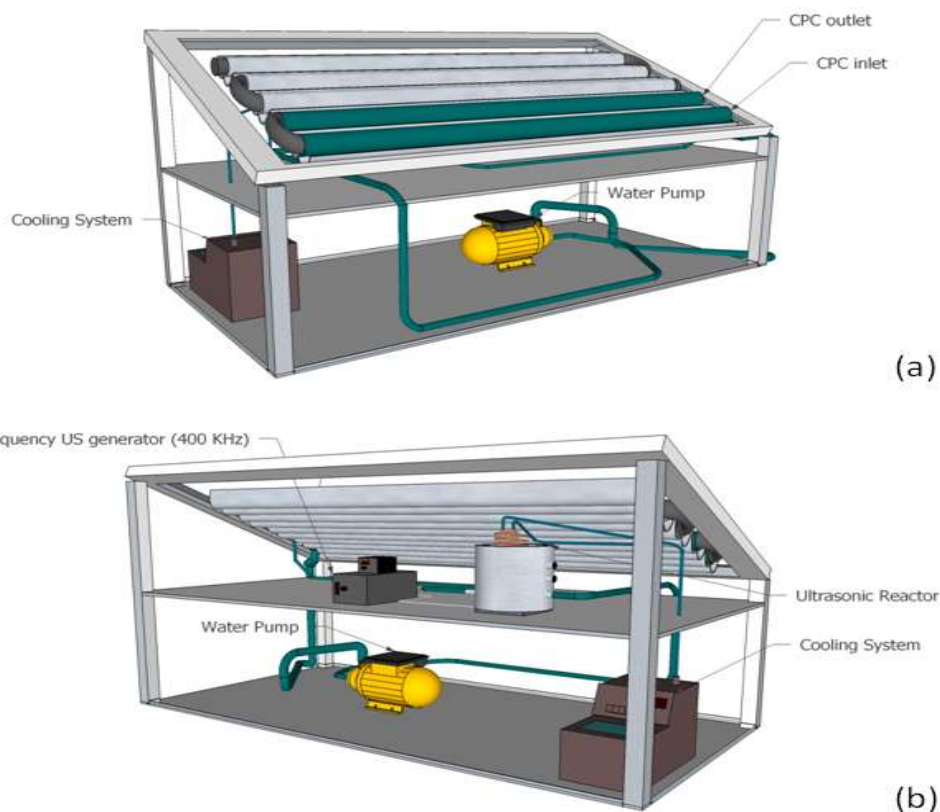
Fig. 2.1. (a) front and (b) rear view of the coupled ultrasonic/ CPC solar photo-Fenton reactor system used.

2.2.3. RESULTS AND DISCUSSION

2.2.3.1. INITIAL CONSIDERATIONS

Initially, the hydrogen peroxide production rate by ultrasound alone in the 10 L system was measured and found to be as low as 1 mg L^{-1} h^{-1}. As this amount was considered negligible for the considered concentrations of contaminants, it was decided to add H_2O_2 to the system instead. An initial concentration of 200 mg L^{-1} of H_2O_2 was decided for all experiments, periodically replenished so as not to fall below 100 mg L^{-1}. This range was chosen from previous experience in solar photo-Fenton in order to avoid having an excess of H_2O_2 which could also lead to HO$^\bullet$ radical scavenging [64]. All contaminants have been found to be stable in the presence of H_2O_2 alone during preliminary experiments, with no degradation observed at all. Degradation rates were calculated by a least-squares fitting between 4 acquired every 10 minutes during the first 30 minutes of the process. Synergy factors for the combined treatment have been consequently estimated by calculating the following ratio for each trio of experiments.

$$S = \frac{r_{combination}}{r_{photo-Fenton} + r_{ultrasound}} \qquad \text{(Eq 2.1)}$$

Lack of synergy would be expressed by S being 1, while values > 1 would suggest a positive synergistic effect.

2.2.3.2. TREATMENT OF PHENOL

A solution of 80 mg L^{-1} of phenol was treated. For photo-Fenton (pF) and coupled (US/pF) experiments, 1 mg L^{-1} of Fe^{2+} was added. 100% degradation was reached in only 40 minutes under US/pF treatment, while significantly longer treatment times of 75 and 210 minutes were required for pF and US, respectively (Fig 2.2.). According to equation 2.1 and the degradation rates calculated in table 2.2, a synergy factor of 1.99 was obtained for 40 minutes of treatment, suggesting a doubling of the reaction rate purely due to the synergy.
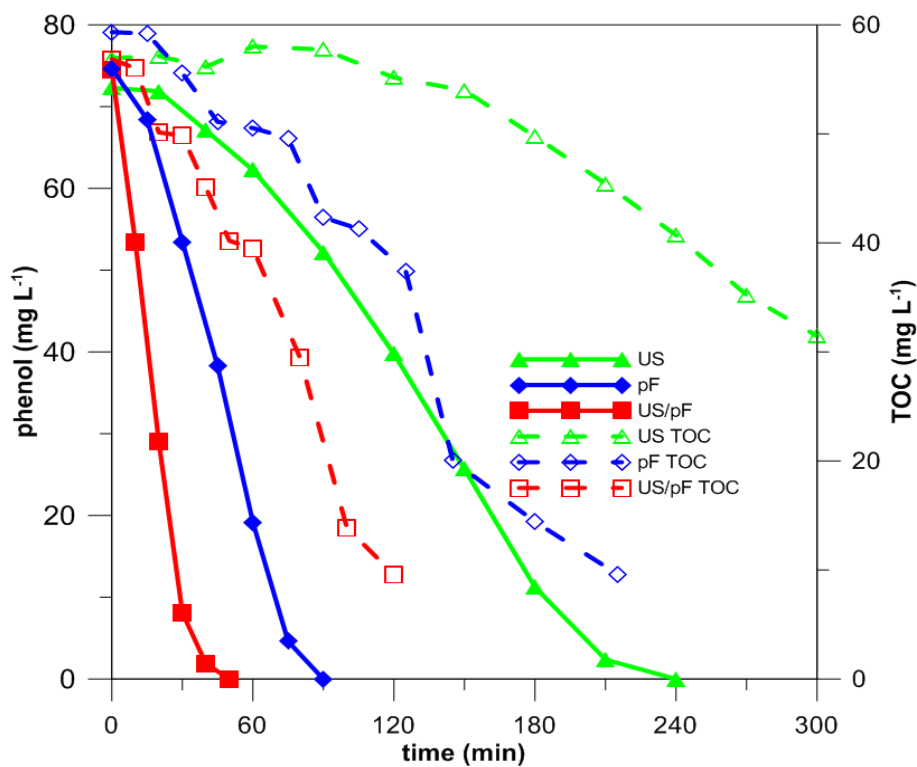
Fig.2.2. Degradation and TOC removal of 80 mg L^{-1} of phenol for each of the three processes.

Table 2.2. Degradation rates (in mg L^{-1} min^{-1}) for all treatments and synergy factors for the combined treatment (calculated via chloride release rate in the case of diuron)

Pollutant	Conc. (mg L^{-1})	[Fe^{2+}] (mg L^{-1})	Time (min)	Degradation rate (mg L^{-1} min^{-1})			Synergy
				Ultrasound	Photo-Fenton	Combination	
Phenol	80	1	40	0.13	0.82	1.90	1.99
Diuron	100	1	90	0.022	0.020	0.041	0.93
	100	5	20	0.02	0.458	1.12	2.93
Bisphenol A	80	1	90	0.57	2.09	2.33	0.88
	400	1	30	0.89	1.21	3.61	1.72

In regard to the removal of TOC (Fig.2.2.), 85% removal was reached by US/pF after 120 minutes. By contrast, the same removal percentage required 215 minutes by pF, while US alone could only remove 50% of TOC even after 300 minutes of treatment. The evolution of the pH also seemed to follow TOC removal, and may also be able to provide some information as to the nature of some of the intermediates. For both pF and US/pF treatment, it dropped from an initial value of 4.8 to 3.2 when TOC was around 50% of the initial (at 100 and 60 minutes, respectively). By the time TOC removal had reached 85%, at 215 and 120 minutes respectively, the pH had increased to a value of 5.2. For the ultrasound experiment (US), it decreased gradually until a value of 4.1 at 300 minutes. The minimum pH most likely corresponds to the time when the highest concentration of aliphatic acid intermediates is accumulated in solution, with the subsequent rise in pH due to their further degradation.

Observing the H_2O_2 consumption curves for each treatment (Fig. 2.3) can also provide some interesting information. Under US, the rate of H_2O_2 consumption, although initially low, sharply increased from the moment phenol was completely removed from the system. This behaviour suggests that phenol is somehow inhibiting the interactions between the cavitation bubbles and H_2O_2. In a study by Bapat [65], phenol's physicochemical properties were used to calculate an estimate of the excess of phenol molecules present at the bubble-liquid interface during ultrasonication of a dilute aqueous solution of 94 mg L^{-1} (similar to the concentration used in this work). The concentration of phenol at the interface was calculated to be 264 times higher than at the bulk liquid, based on the assumption that adsorption equilibrium is reached. The value is most likely an overestimation as such equilibrium is unlikely to be reached at the short timescales of cavitation phenomena.
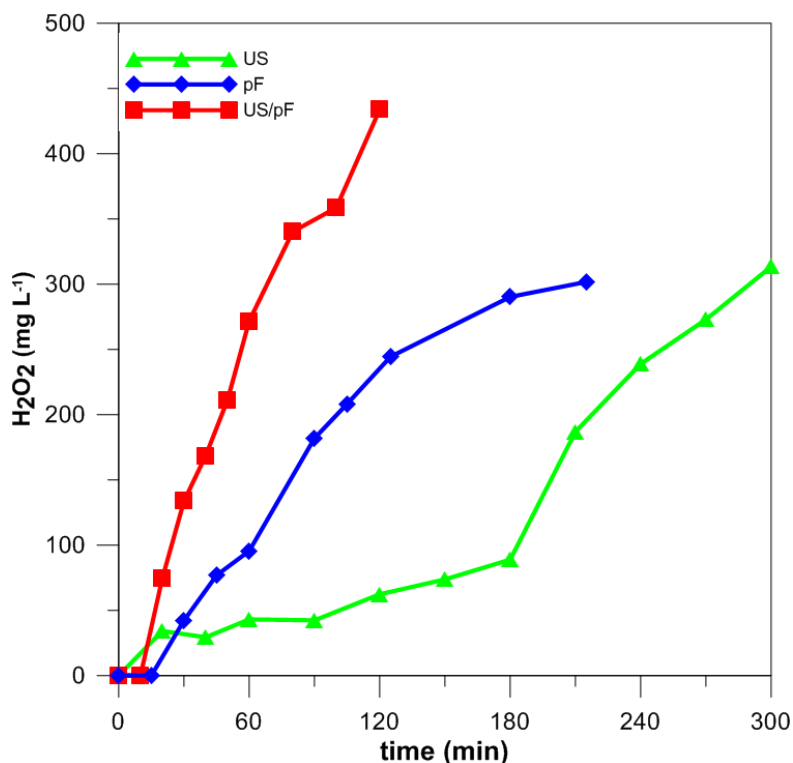
Fig. 2.3. H_2O_2 consumed during treatment of 80 mg L^{-1} of phenol for each of the three processes.

Nevertheless, it clearly illustrates qualitatively the abundance of phenol at the interface. Considering this information along with the observed behaviour, it can be suggested that phenol will be preferentially treated at the interface by $HO^\bullet$ radicals produced via bubble cavitation, as per reactions 2.1 and 2.2.

$$H_2O \rightleftharpoons {}^\bullet H + HO^\bullet \qquad \text{(React. 2.1)}$$

$$O + H_2O \rightleftharpoons 2\,HO^\bullet \qquad \text{(React. 2.2)}$$

This reaction of phenol with $HO^\bullet$ has been suggested to primarily lead to the formation of dihydroxyl cyclohexadienyl radicals and subsequently to catechol, hydroquinone and finally to carboxylic acids [33;34]. The additional $HO^\bullet$ groups increase the polarity of the byproducts, making them more hydrophilic. The formation of acidic intermediates is also suggested, as seen above, by the fall of the pH observed during the process.

Once a significant fraction of phenol has been converted, the more hydrophilic intermediates migrate from the interfacial region to the bulk solution and leave the bubble interface free. From that point onward, H_2O_2 may approach or enter the bubble unhindered, where dissociation may occur, thus introducing a new source of radicals to the system. The

observed high level of synergy under US/pF treatment could possibly be attributed to the participation of the radical species generated from reactions (2.3-2.5).

$$H_2O_2 \rightleftharpoons {}^{\bullet}H + HOO^{\bullet}$$ (React. 2.3)

$$H_2O_2 + O_2 \rightleftharpoons HOO^{\bullet} + HOO^{\bullet}$$ (React. 2.4)

$$H_2O_2 + {}^{\bullet}H \rightleftharpoons H_2O + HO^{\bullet}$$ (React. 2.5)
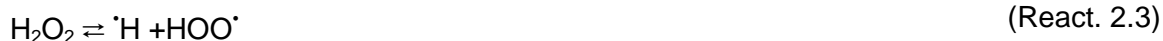
The fact that this behavior has not been observed in the other studied compounds can suggest that it is a result of a specific type of interaction between phenol and the cavitation bubble.

It can also be observed that similar amounts of consumed H_2O_2 do not lead to the same mineralization efficiency for the pF and US processes. This could have two possible interpretations: The first is that even though peroxide is dissociated and radicals are formed, they are nevertheless unable to react as efficiently with the generally more hydrophilic intermediate species. The second is that under US, a larger percentage of hydrogen peroxide wastefully decomposes to water and oxygen due to the extreme local conditions at the bubble vicinity without any significant radical contribution.

Table 2.3. Ratios of mg L^{-1} of H_2O_2 consumed per mg L^{-1} of primary contaminant removed.

Pollutant	Conc. (mg L^{-1})	[Fe^{2+}] (mg L^{-1})	Time (min)	Ratio		
				Ultrasound	Photo-Fenton	Combination
Phenol	80	1	40	5	3.07	2.30
Diuron	100	1	30	10	8.82	3.06
	100	5	30	3.52	1.75	2.31
Bisphenol A	80	1	30	13.25	1.6	1.18
	400	1	40	2	1.33	0.33

The above theoretical considerations aside, it should be stressed out from a practical point of view that the combined process also appears to be favourable in terms of H_2O_2 consumed per mg L^{-1} of phenol removed. As seen in table 2.3, for 40 minutes of treatment this ratio seems to be 2.3 for US/pF, in contrast to 3.07 for pF and 5 for US. Combined with the fact

that the degradation kinetics were enhanced by a factor of 2 due to the synergy, further study of this coupled system could prove beneficial.

2.2.3.3. TREATMENT OF DIURON

This compound was selected due to its low solubility for gaining insight about the behaviour of a partially solubilized hydrophobic substance (as can be found in real industrial wastewater forming emulsions or suspensions) under the applied treatments. 100 mg of diuron were added per liter of water, corresponding to almost the double of the solubility limit (42 mg L^{-1} at 25° C). HPLC measurements could therefore only detect the soluble part, and as the dissolution-degradation processes are concurrently happening, they couldn't provide conclusive information regarding the reaction rate of diuron degradation. TOC could not be followed consistently for the same reasons. The release of chloride anions was monitored instead in order to overcome this limitation. As chloride anions account for 30% of the molecular weight of diuron, chloride release provides a clear indication of diuron degradation, with a release of 30 mg L^{-1} Cl^{-} corresponding to 100% degradation. For the pF and US/pF treatments, experiments were done with two different concentrations of iron (1 and 5 mg L^{-1} of Fe^{2+}).

US treatment alone (Fig. 2.4.a) generally doesn't prove very efficient, with only 20% degradation reached even after 300 minutes of treatment, while at the same time having large H_2O_2 requirements.

With 1 mg L^{-1} of Fe^{2+}, US/pF treatment can lead to 40% degradation after 300 minutes of treatment, while pF behavior is very similar to that of US alone, with 20% degradation reached at the same time (Fig. 2.4.a). No synergy can therefore be observed. The pH during the US experiment decreases from the initial value of 5.5 to stabilize at 4.5 after 4 hours. For the pF and US/pF treatments, the pH decreased from 5.5 to 5 and 4.6 respectively. Total iron at the end of the experiment was 0.76 and 0.9 mg L^{-1} for the pF and US/pF treatments, respectively. This relatively low availability of iron appears to limit the effectiveness of photo-Fenton, leading to the slow kinetics observed. Nevertheless, even though no synergy is present in the kinetics, an important benefit can be observed in terms of H_2O_2 consumption per mg L^{-1} degraded, as seen in Fig. 2.5.a (3.06 for US/pF versus 5.21 for pF for 60 minutes of treatment).
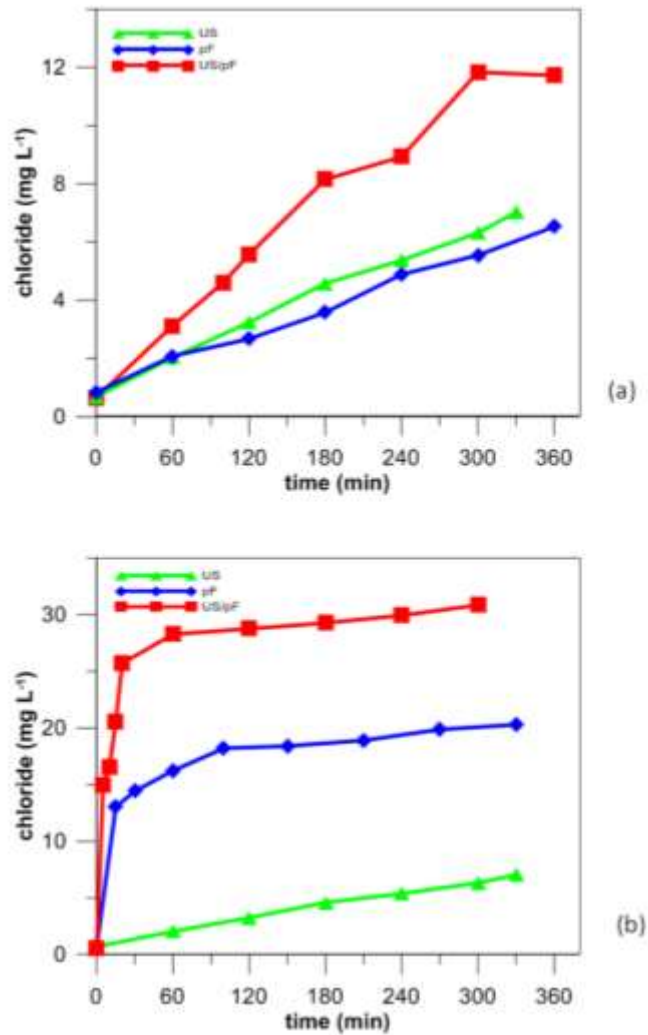
Fig. 2.4. Chloride release during the treatment of 100 mg L^{-1} of diuron with each of the three processes with the addition of (a) 1 mg L^{-1} of Fe^{2+} and (b) 5 mg L^{-1} of Fe^{2+}.

When 5 mg L^{-1} of Fe^{2+} were used however, the results were significantly different (Fig. 2.4.b) Due to the higher availability of iron, pF alone was able to very efficiently remove the dissolved fraction of diuron after 15 minutes (42% removal). However, the rate of chloride accumulation was from that point onwards severely limited, as either the slow kinetics of dissolution dominated the degradation process or some rather stable chlorinated intermediate was formed. With simultaneous application of US however, only 20 minutes were sufficient to remove 85% of the initial compound, with a H$_2$O$_2$ consumption of about 190 mg L^{-1}. Removal until 95% doesn't seem to be cost-effective, as almost the same amount of H$_2$O$_2$ (Fig.2.5.b) and 40 extra minutes of treatment are required. The initial pH was 5.4 in both cases. For pF, it decreased to 3.4 within 30 minutes, and subsequently increased until 4.4 after 2 hours. For US/pF, it reached 3.1 in 15 minutes, increasing until 4.5 after 2 hours. This initial drop in pH also helped maintain a significant fraction of the iron in solution,

reinforcing the action of the photo-Fenton process. Total iron in solution for both cases decreased only slightly until 4.2 mg L^{-1} by the end of the experiment. Despite the higher availability of iron, the action of the ultrasound proved indispensable for the efficient removal of the non-soluble fraction of diuron.
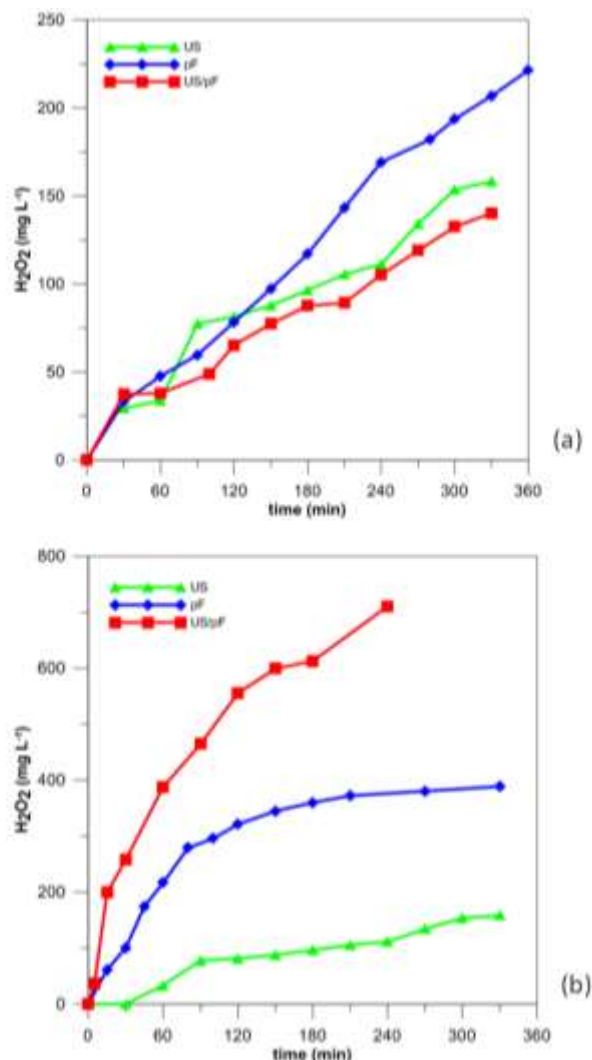
Fig 2.5. H_2O_2 consumed during the treatment of 100 mg L^{-1} of diuron for each of the three processes with the addition of (a) 1 mg L^{-1} of Fe^{2+} and (b) 5 mg L^{-1} of Fe^{2+}.

The synergy factor as calculated for 30 minutes of treatment is 2.39 (table 2.2). This remarkable level of synergy could be attributed to two phenomena which are likely when part of the target contaminant is in the form of particulate matter: 1) Increase in the number of cavitation events due to the presence of additional nucleation sites over the solid surface[66]. 2) The asymmetric collapse of the cavitating bubbles provoked by the local perturbation of the acoustic field near the solid-liquid interface. This deformation could lead to the ejection of a violent liquid microjet towards the solid surface [30], eroding the solid and

47

contributing to a faster dissolution rate. It is possible that this phenomenon is observed in this concentrated heterogeneous solution of diuron. Therefore, as diuron solubilized very quickly, solubilization stopped being the rate-controlling step, and photo-Fenton was able to degrade it faster. Additionally, the fact that these synergies are observed even within minutes of treatment is very encouraging from an application point of view, as minimum costs may be achieved by short treatment times.

2.2.3.4. TREATMENT OF BISPHENOL A

BPA was also chosen due to its relatively low solubility, Experiments with BPA were made at two different initial concentrations, 80 (below solubility limit) and 400 (above solubility limit) mg L^{-1}. Literature sources generally agree that the solubility of BPA should not exceed 300 mg L^{-1} under the studied conditions. Nevertheless, 350 mg L^{-1} were identified in the soluble fraction of the solution. At 80 mg L^{-1}, all of the BPA was solubilised. For US alone, the degradation was slow, requiring more than 200 minutes of treatment for complete removal of BPA. The kinetics for the pF and US/pF treatments were similar, with complete BPA removal reached in both cases after 60 minutes of treatment (Fig. 2.6, left y axis). A synergy factor of 0.88 (table 2.2) suggests that there is no advantage of the combined treatment to the degradation kinetics. Corresponding H_2O_2 consumption can be seen in Fig. 2.7.a.
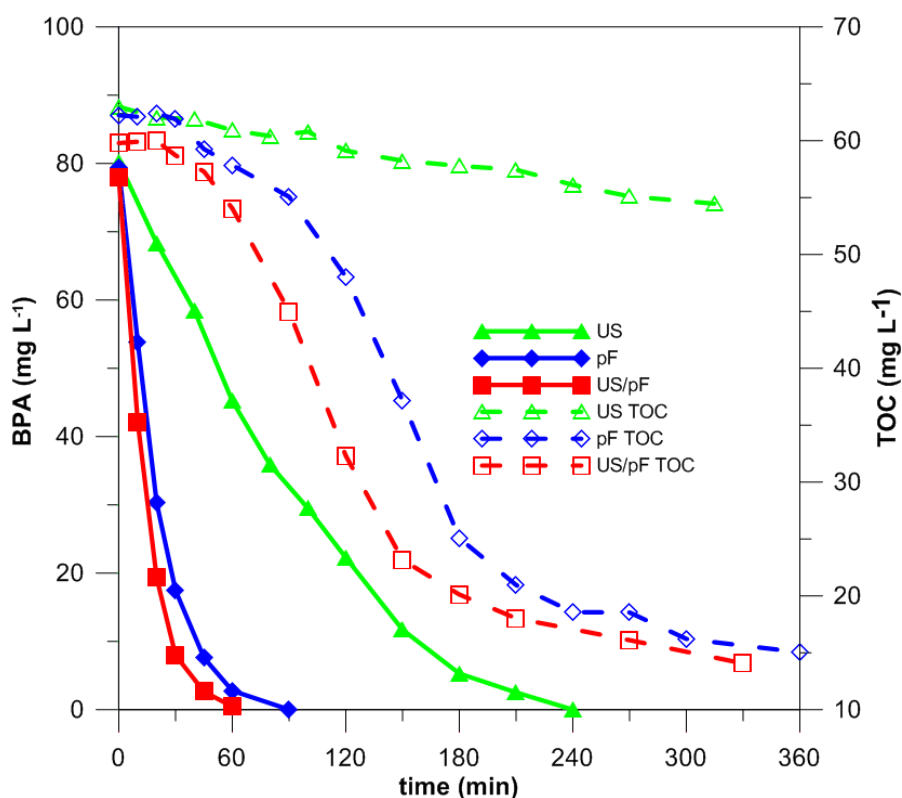
Fig. 2.6. Degradation and TOC removal for 80 mg L^{-1} of BPA for each of the three applied processes.

Regarding TOC removal (Fig. 2.6), US treatment alone was apparently inefficient, with only 8% of TOC removed after 300 minutes of treatment. It has been suggested that the inability of US to effectively remove TOC derived from BPA is due to the formation of hydrophilic aliphatic acids that accumulate in the bulk solution and cannot react with the hydroxyl radicals generated in the bubble[58]. For both processes involving photo-Fenton, 75% removal was achieved after 300 minutes, when a plateau is apparently reached. The decrease of TOC however also begins from the moment BPA is completely degraded, which is in accordance with the literature [58]. Nevertheless, some small benefit can again be observed by a decrease in peroxide consumption per mg L^{-1} of BPA gone with a value of 1.18 for US/pF, compared to 1.63 and 2.58 for the pF and US processes after 30 minutes of treatment (table 2.3).
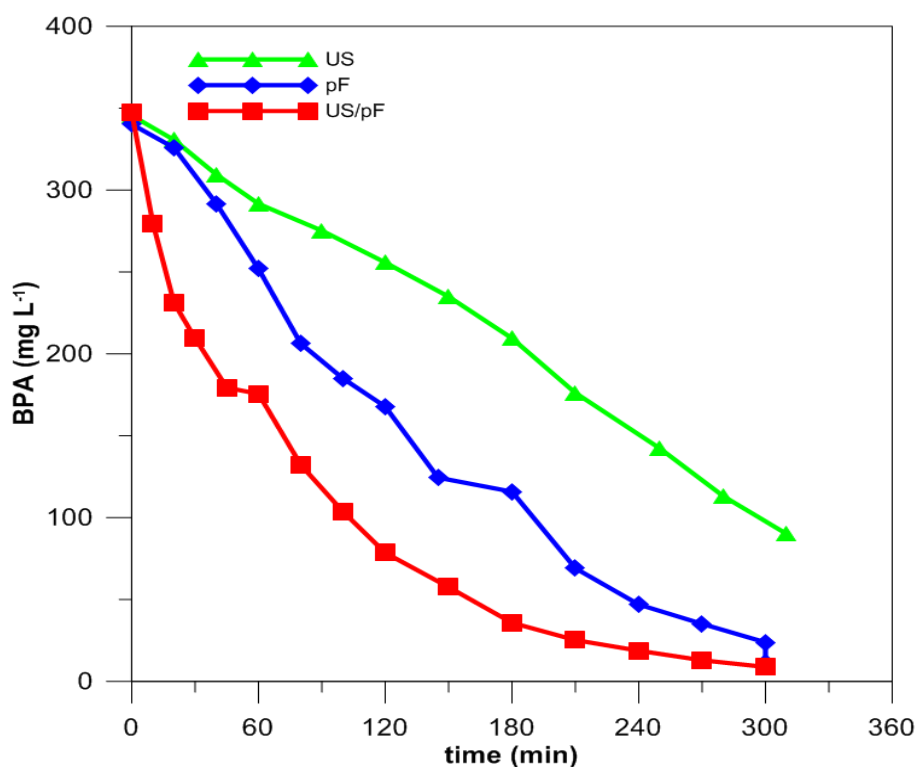
Fig.2.7. Degradation of 400 mg L^{-1} of BPA for each of the three applied processes.

In contrast, when 400 mg L^{-1} of BPA were treated (Fig. 2.7), several differences were observed. Only 350 mg L^{-1} were detected in the initial sample, so it can be assumed that the solution was supersaturated and the remaining 50 mg L^{-1} were not dissolved. The initial pH was 4.5, which was gradually lowered to 3.4 after 120 minutes for pF and 210 minutes for US/pF. Total iron could not be followed in this case as the resulting solution was so dark in colour that the transmitted light was inadequate for an accurate spectrophotometric measurement. As the dissolution kinetics is unknown, it should be noted that a distinction between total and dissolved BPA removal cannot be made. Nevertheless, it is clear that

49

under the US/pF treatment, between 93 and 97% of BPA is removed after 200 minutes, while pF alone required 300 minutes to reach the same state (between 65% and 69% gone in 200 minutes). US treatment alone leads to 45% degradation in 200 minutes. TOC remained unchanged during the course of all the experiments. As complete BPA removal was not reached in any of the them, this persistence is unsurprising.

H_2O_2 consumption (Fig. 2.8.b) is similar for the pF and US/pF treatments, further corroborating the presence of synergy. At 40 minutes of treatment, a consumption of 0.33 mg L^{-1} of H_2O_2 per mg L^{-1} of BPA was also observed for the US/pF treatment, compared to 1.33 and 1.20 for pF and US treatments alone (Table 2.3).
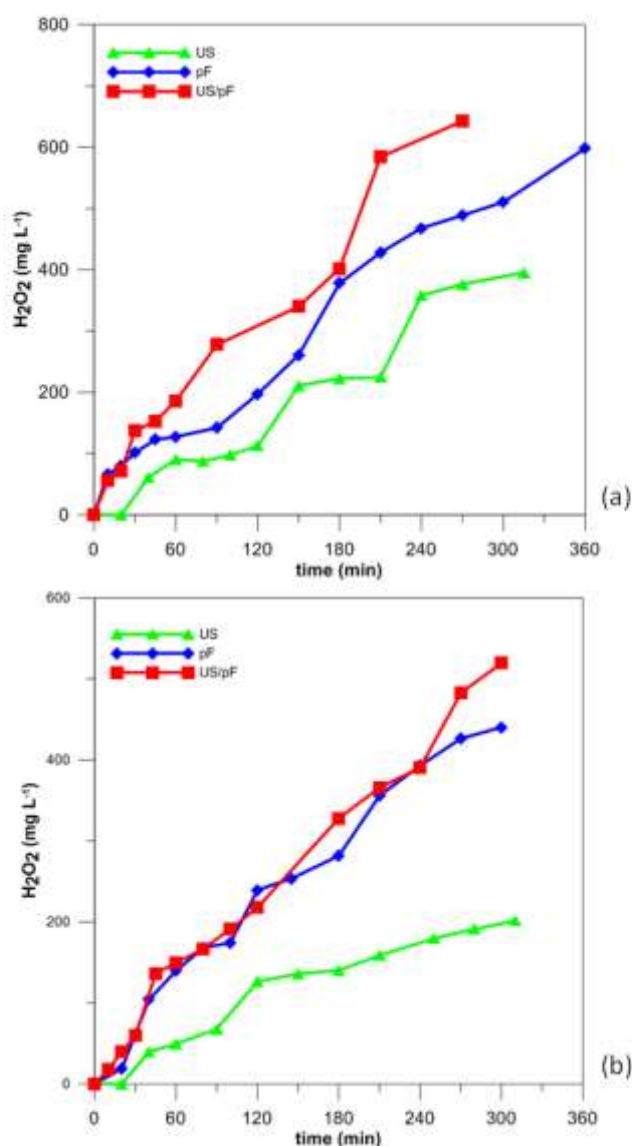
Fig. 2.8. H_2O_2 consumed during the treatment of (a) 80 mg L^{-1} of BPA and (b) 400 mg L^{-1} of BPA for each of the three processes.

2.2.4. CONCLUSIONS

The performance of a combined high frequency ultrasound/solar photo-Fenton treatment was studied, with a primary focus on the identification of synergistic effects and gaining a first estimate for the potential of larger-scale applications. Significant synergy was observed for most cases, although its magnitude appears to be highly dependent on the nature of the contaminant, initial concentrations and, in the case of diuron, the concentration of Fe^{2+}. Combined treatment of contaminants in the saturated state or those forming multiple phase emulsions (as can often be the case for industrial wastewaters) may prove to be particularly effective, even for short US treatment times. Favorable H_2O_2 consumption rates were also obtained for most of the combined treatments. Careful choice and limitation of initial H_2O_2 concentrations and ultrasonication times may therefore allow an ultrasonic system to be an economically viable complement to existing solar decontamination technologies even at larger scales. It seems nevertheless reasonable to assume that any efforts to optimize the operating conditions will have to be made on a case-by-case basis.

2.3. ELIMINATION OF THE IODINATED CONTRAST AGENT IOHEXOL IN WASTEWATER AND URINE MATRICES BY APPLICATION OF ULTRASOUND AND PHOTO-FENTON.

2.3.1. OBJECTIVES OF THIS SECTION

As seen in section 2.2, concurrent application of ultrasound with photo-Fenton can lead to significant synergistic effects, both in terms of degradation rate as well as H_2O_2 consumption. Despite the common assumption that US mainly benefits treatment of hydrophobic compounds, treatment of phenol (highly hydrophilic) was also highly improved by ultrasound. It is therefore preferable to evaluate contaminants on a case-by-case basis.

In this section, the specific case of an Iodinated X-ray contrast media (ICM) compound, Iohexol, is considered. ICM are pharmaceutical compounds widely used for medical imaging applications, with an estimated worldwide consumption of 3.5 x 10^6 kg per year [67]. They are administered to patients prior to X-ray imaging in order to better visualize internal organ structures. They subsequently pass through the body and are excreted, largely unchanged, with the patient's urine. However, they are not effectively degraded by conventional wastewater treatment processes ([68]; [69]; [70]), resulting in µg L^{-1} levels being detected in

urban wastewater. One possible reason is poor adsorption and binding to activated sludge, as demonstrated in the case of diatrizoate and iopromide. ([71; 72]). Although the toxicological impact of ICM and their degradation intermediates is unclear, the low toxicity of the parent compounds do not in any way mean that there is no risk associated with their transformation products [73]. To compensate for the limited biodegradability, advanced oxidation processes (AOPs) have been considered as an alternative. These are processes that are able to generate potent reactive oxygen species (ROS) capable of degrading recalcitrant organic contaminants [74] and have been studied as an option for treating many types of industrial and municipal wastewater [9; 75]. Jeong et al [76] have shown that they can also be efficient for the destruction of ICM. Among the studied processes were ozonation [77], UV/TiO_2 [78; 79] , UV/H_2O_2 [80], sonolysis/O_3/H_2O_2 [81], zero-valent iron [82], BDD electrode oxidation [83]. Different ICM were treated with the aforementioned processes such as iomeprol, iopromide, iohexol and diatrizoate. With varying degrees of success, most of these processes could eliminate the ICM, although mineralization was only partial. This work aims to apply the photo-Fenton and ultrasound AOPs (separately and in combination) for the treatment of the ICM Iohexol. To the best of our knowledge, these processes have never been used for ICM compounds.

Applying photo-Fenton in the context of municipal wastewater is a challenge, as pH adjustment and reagent consumption for such high volumes of water make it economically unfeasible. Additionally, one of the most significant problems when treating real water with photo-Fenton is the presence of inorganic salts (e.g. CO_3^{2-}, HCO_3^{-}, PO_4^{3-}) which act as either radical scavengers on HO• or sequester iron and inhibit degradation. Application of ultrasound, admittedly costly itself, may be able to circumvent some of these problems. As discussed in section 2.2, due to the generation of HO• happening almost exclusively in the vicinity of the gaseous cavitation bubble, it preferentially reacts with hydrophobic compounds that are expected to be found at the bubble-liquid interface, Compounds found in the immediate vicinity may also be subjected to direct pyrolysis. Nevertheless, pH adjustment and iron addition are not necessary, and its partially pyrolytic action occuring at the bubble-liquid interface shouldn't be as strongly affected by the presence of radical scavengers. Additionally, previous research [39] has shown that bicarbonate ions, while detrimental to photo-Fenton, may actually enhance sonochemical degradation due to the generation of carbonate radicals. While CO_3^{-}• have a significantly lower redox potential than HO• (1.78 in comparison with 2.31) [84], they have a half-life of about 3 ms, about 3000 times greater than that of HO• [85]. Application of ultrasound in the context of a bicarbonate-rich medium such as municipal wastewater could therefore improve degradation performance of even hydrophilic compounds like ICM.

However, as the primary source of ICM pollution is hospitals, it is of interest to examine the possibility of treatment before discharging into the urban sewer network. The costs associated with photo-Fenton or US would be comparatively low when applied at this scale. Establishing a protocol for the collection and treatment of patient urine following ICM administration could be feasible, provided the treatment leads to biodegradable byproducts.

The efficiency of ultrasound and/or photo-Fenton treatment options for the elimination of Iohexol has been evaluated in the following media: 1) Distilled water (in order to understand the interactions between Iohexol and the process without complicating factors such as salts or organic matter) 2) Municipal wastewater treatment plant (MWTP) effluent, 3) synthetic urine and 4) real urine

2.3.2. MATERIALS AND METHODS

2.3.2.1. Reagents

Omnipaque Iohexol ($C_{19}H_{26}I_3N_3O_9$) solution (300 mg Iodine mL^{-1}) was acquired from GE Healthcare Inc. Sodium sulfate (Reacto Lab). Hydrogen peroxide 30% (w/v) (Fluka Chemicals). Sodium carbonate (.99.8%, ACROS Organic). 99.5% NaCl acquired from ACROS Organic. $NaNO_3$ from Axon Lab Applichem. KCl from Fluka Chemicals. Urea (98%) from ABCR GmbH & CoKG). Creatinine from ABCR GmbH &CoKG. HPLC gradient grade methanol was from Fisher Scientific. Formic acid (98-100%) was from Merck. Titanium (IV) Oxysulfate and H_2SO_4 for pH control was from Fluka analytical. All the chemicals were used without further purification.

2.3.2.2. Analytical methods

Iohexol concentration was monitored by an Agilent 1100 series HPLC system equiped with a Nucleosil C18 column (28 cm, 4.6 mm , 5 μm particle size). The mobile phase consisted of 5% methanol- 95% deionized water acidified by 0.1% (v/v) formic acid. Flow rate was 0.8 ml min^{-1}. Injection volume was 40 μl. The UV detector was set at a wavelength of 254 nm. Retention time was 15.6 minutes. Total Organic Carbon and Inorganic Carbon weremeasured by a Shimadzu TOC-V$_{CSN}$ analyzer equipped with an ASI-V automatic sampler. pH was measured with a Mettler-Toledo SevenEasy pH meter. Iron was monitored with the ferrozine method. 5 ml of sample were filtered with a 0.2 micrometer nylon filter. 0.2 ml of acetate buffer at pH 4.65, 0.2 ml of hydroxylamine hydrochloride and 0.1 ml of 10 mM ferrozine solution were added. The absorbance of the resulting magenta-colored solution was measured at 562 nm.

H_2O_2 was monitored spectrophotometrically by adding 0.5 ml of Ti(IV) oxysulfate solution to 5 ml of sample and measuring the absorbance at 410 nm (DIN 38402H15). Due to color interference, H_2O_2 in urine experiments was followed by Merck Millipore Peroxide test strips.

2.3.2.3. Water matrices

Distilled water was acquired with use of a Merck Millipore Water purification system. Wastewater was collected from the Lausanne municipal wastewater treatment plant (MWTP), downstream of the secondary biological treatment. Synthetic urine was prepared with the following recipe: 9.7 g L^{-1} urea, 0.67 g L^{-1} creatinine, 1.17 g L^{-1} NaCl, 0.75 g L^{-1} KCl dissolved in distilled water [86]. Urine was provided by volunteers participating in this study. It was collected in a non-transparent container to protect light sensitive components and stored under refrigeration at 4-6°C. All experiments were conducted within one day of collection

2.3.2.4. Experimental set-up

A 400 ml cylindrical water-jacketed ultrasound reactor was used for the ultrasound experiments. US frequency was set at 297 KHz emitted from a piezoelectric disc (d=4 cm) fixed on a Pyrex plate (d=5 cm) at the bottom of the reactor.

The solar simulator used was an Atlas XLS model, providing constant illumination from a Xenon lamp. The lamp has a spectral distribution of about 0.5 % of emitted photons at wavelengths shorter than 300 nm and 7% between 300 and 400 nm. For wavelengths between 400 and 800 nm the emission spectrum simulates solar radiation. 30 W m^{-2} of UV irradiance were used, which is a typical solar UV power during a sunny day. UV radiation was measured with a Kipp & Zonen CUV3 radiometer placed within the solar simulator.

Coupled ultrasound/ photo-Fenton experiments (US/pF) were carried out in a system of the above ultrasound reactor and a series of three 75 ml Pyrex glass vessels placed (225 ml illuminated volume) placed within the solar simulator (Figure 1). Ultrasound was emitted at 297 KHz from a piezoelectric disc (4 cm diameter) fixed on a Pyrex plate (5 cm diameter) at the bottom of the reactor. Taking into account the tubing connecting the system components, the total volume was 700 ml. A peristaltic pump was used to recirculate the solution at a flow rate of 100 ml min^{-1}.
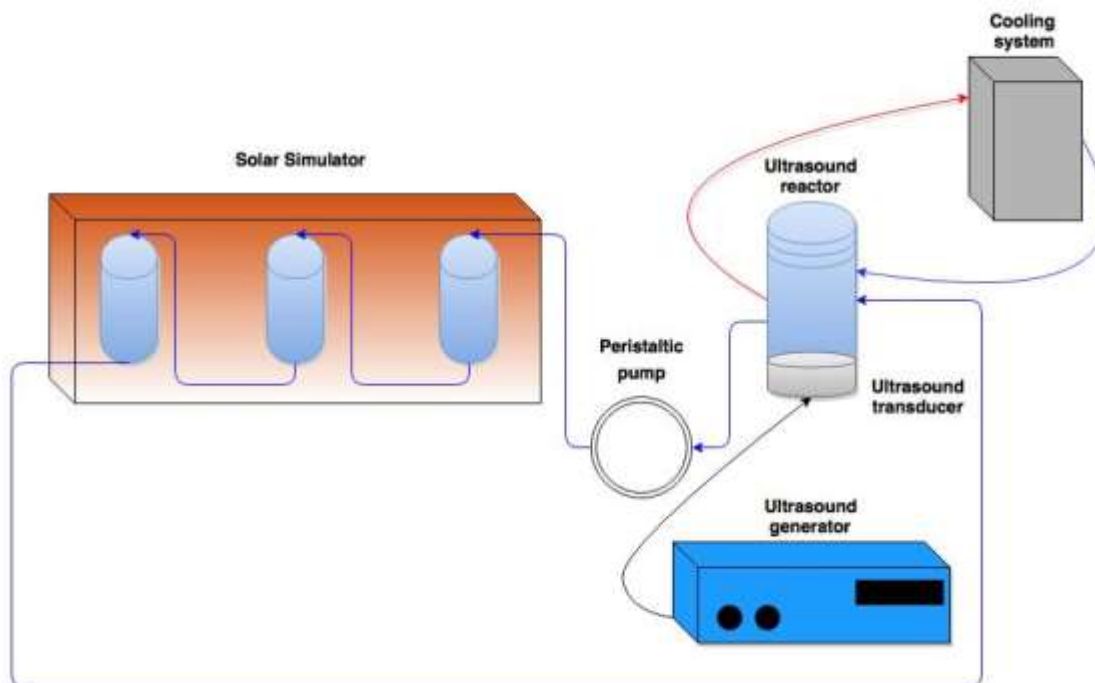
Fig. 2.9. The experimental set-up used for the combined US/pF treatment. The following parts are highlighted: 1) Solar Simulator, 2) Peristaltic pump, 3) Ultrasound generator, 4) Ultrasound reactor, 5) Cooling system.

Zahn-Wellens biodegradability test was conducted following the OPPTS 835.3200 protocol, developed by the Swiss Federal laboratories of Material Science and Technology (EMPA). Activated sludge was acquired from the Lausanne MWTP, stored in a cool place and aerated with an air sparger until used.

2.3.2.5. Design of Experiments (DOE)

A 2_V^{5-1} fractional factorial design has been used for estimating the importance of 5 factors on the ultrasonic degradation of Iohexol. This type of design is ideal for identifying the importance of each individual factor as well as the interactions between them. The chosen factors were: 1) Initial Iohexol concentration, 2) Presence of carbonates, 3) Presence of H_2O_2, 4) Type of liquid medium (distilled water vs municipal wastewater) 5) Ultrasound power level. Each factor was varied between 2 states (table 2.4), with the -1, +1 notation signifying, respectively, the low and high state of each. The chosen response factor was the initial degradation rate r_o (expressed in mg L^{-1} min^{-1}, measured for the first 30 minutes of the process). 16 experiments were conducted. Minitab statistical software was used for analysis of the design and for plotting the main effects and interactions.

Table 2.4. Parameters whose effect on the sonochemical degradation of Iohexol was studied.

	-1	+1
[Iohexol] (mg L^{-1})	20	50
[HCO$_3^-$/CO$_3^{2-}$] (mg L^{-1}, measured as inorganic carbon)	0	50
[H$_2$O$_2$] (mg L^{-1})	0	50
Liquid medium	Distilled water	Wastewater
US power (Watt)	50	80

2.3.3. RESULTS AND DISCUSSION

2.3.3.1. US treatment of Iohexol in distilled water and municipal wastewater: Effect of operational parameters on initial degradation rate.

The performance of ultrasound treatment of Iohexol in distilled water and wastewater has been evaluated by use of experimental design methodology, as described in section 3.2.5. The plots of the main effects and interactions between initial Iohexol concentrations, presence of carbonates, presence of H$_2$O$_2$, type of aquatic medium and the ultrasound power level are shown in Figure 3.2 and Figure 3.3, respectively. The following observations can be made by studying the main effect and interaction plots:

(I) The most important main effect is observed by increasing the initial concentration of the pollutant. This can suggest that the limiting step in the degradation process is the diffusion of Iohexol and not the generation of radical species. Due to its high hydrophilicity, Iohexol does not easily migrate to the ultrasonically active region near the cavitation bubble, and thus not subjected to either the cavitation shock or the radicals generated from the dissociation of water and/or H$_2$O$_2$. The Iohexol concentration/H$_2$O$_2$ interaction plot also shows that addition of H$_2$O$_2$ more positively affects degradation rate when high Iohexol concentrations are treated. As more Iohexol is found in the region around the bubble, HO• generated from H$_2$O$_2$ dissociation has a higher probability of attacking it. Therefore, addition of H$_2$O$_2$ could only benefit the treatment of the primary source of ICM pollution at hospitals (higher concentration) and not at a post-secondary treatment stage, where expected Iohexol concentrations would be expected to be very low (in the region of ng to μg L^{-1}).
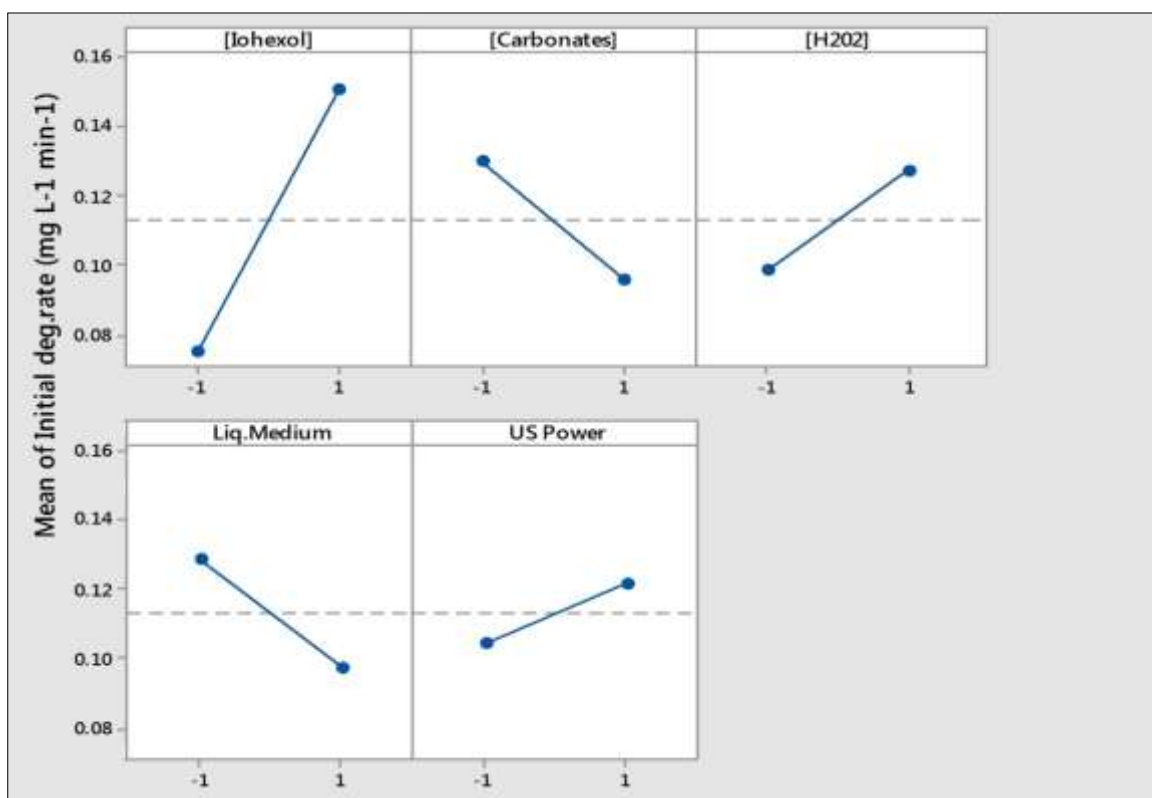
Fig. 2.10. Main effects plot of the parameters (I) Iohexol concentration, (II) Presence of carbonates, (III) Presence of H_2O_2, (IV) Type of liquid medium, (V) US power level on the initial degradation rate of Iohexol (in mg L^{-1} min^{-1}).

(II) In the absence of H_2O_2, increasing US power from 50 to 80 W has a slightly negative effect on the initial degradation rate. However, increasing US power in the presence of H_2O_2 leads to an important 50% increase in initial degradation rate. This suggests that high US power favors the generation of radical species via H_2O_2 dissociation.

(III) Carbonate ions seems to negatively affect the process only when the concentration of the pollutant is high. This is most likely related to observation (I). At high Iohexol concentrations, HO• dominates the degradation kinetics because some of the diffusional limitations are overcome. In this case HO• scavenging, even if there is simultaneous CO_3• generation [39], negatively affects degradation rate. At low concentrations however, where diffusion presents a more significant problem, there is no significant decrease due to carbonate addition. It is possible that the loss of HO• reaction efficiency at low concentrations is at least partly compensated by the longer lifetimes of generated CO_3^-•, so the net effect is limited. When some of the diffusion limitations are overcome by treating higher concentrations, HO• scavenging by carbonate ions becomes a significant problem. In wastewater, where other types of HO• scavengers may also be present, the presence of additional carbonates even appears to mildly increase degradation rate. This could prove to

be an advantage for the treatment of µg L^{-1} levels of ICM, typically found in actual municipal wastewater treatment plant effluents, but not in hospital wastewaters, which is the primary source of ICM.
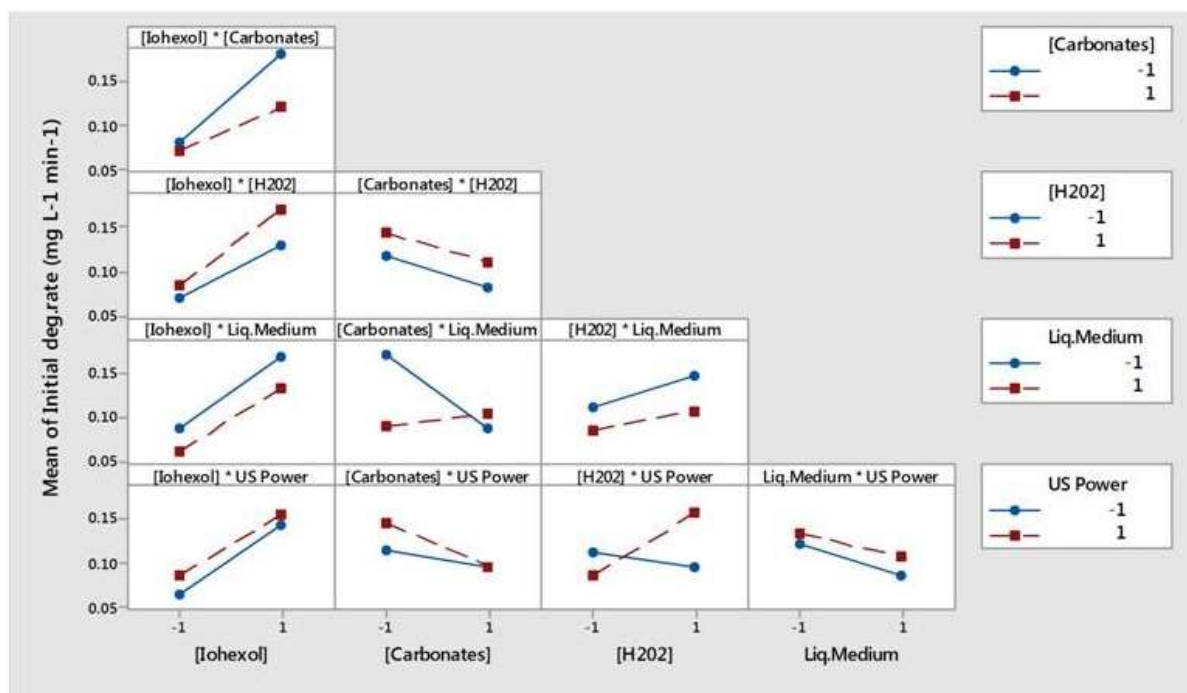
Fig. 2.11. Interactions plot of the parameters (I) Iohexol concentration, (II) presence of carbonates, (III) presence of H$_2$O$_2$, (IV) type of liquid medium, (V) US power level on the initial degradation rate of Iohexol (in mg L^{-1} min^{-1}).

2.3.3.2. Effect of synthetic urine medium on US, pF and combined US/pF treatments of Iohexol.

Despite the potential of ultrasound for treating very small Iohexol concentrations, application of AOPs at the scale of hospital or municipal wastewater plants is undeniably difficult. A more viable alternative could be to treat Iohexol in patients' urine collected in hospitals. A series of experiments were done in a synthetic urine matrix to evaluate how ultrasound, photo-Fenton and combined US/pF treatment options are affected by the synthetic urine medium. The main objective of these preliminary experiments was to identify possible synergistic effects between the two processes. In order to best differentiate between experiments and to have shorter reaction times, a relatively low concentration of 100 mg L^{-1} was chosen. 200 mg L^{-1} of H$_2$O$_2$ were added at the beginning of each experiment.

In figures 2.12a, 2.12b, and 2.13c are presented the degradation curves of 100 mg L^{-1} of Iohexol treated with US, pF and combined US/pF at, respectively, distilled water (DW),

synthetic urine (SU), and synthetic urine matrix diluted 1:1 with distilled water (DSU). US experiments were done at natural pH (6.8 for DW, 7.1 for DSU and 7.4 for SU), while pF and US/pF experiments were done at an initial pH of 3.
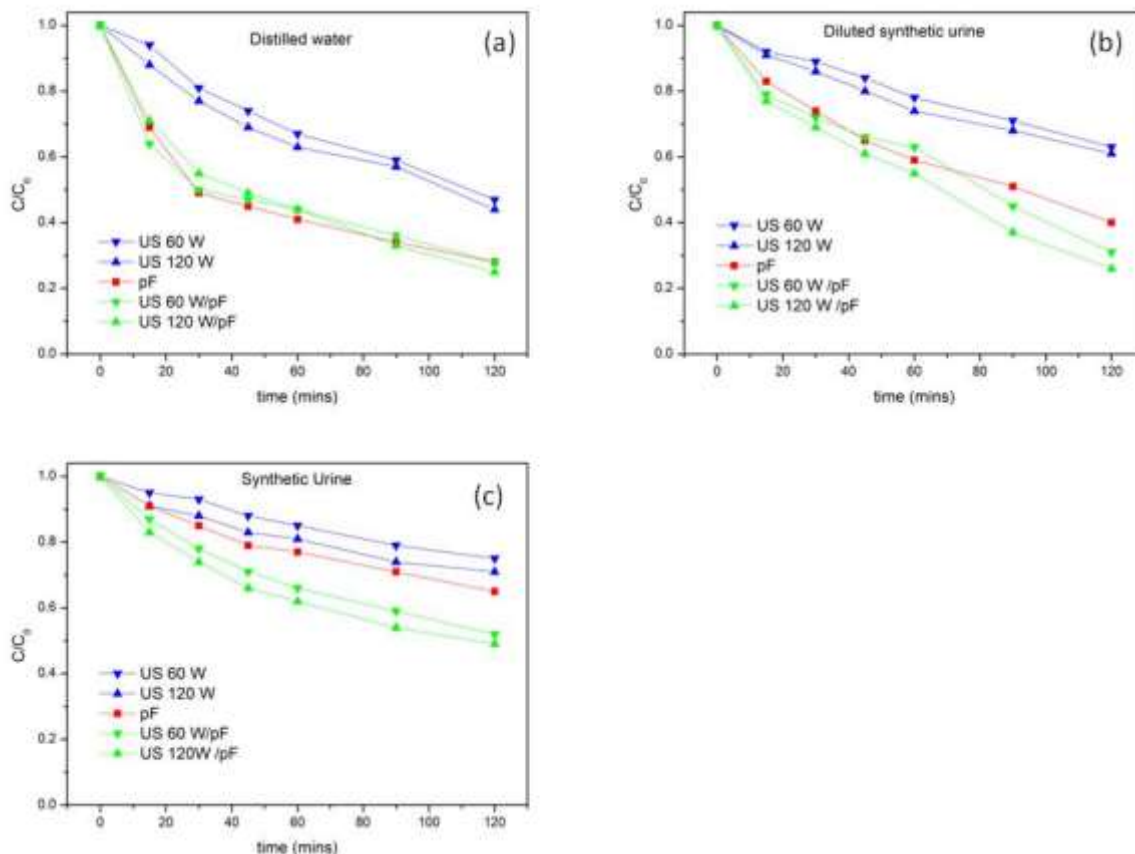
Fig. 2.12. Treatment of 100 mg L^{-1} of Iohexol with US, pF and combined US/pF processes in (a) distilled water, (b) synthetic urine diluted 1:1 with distilled water and (c) synthetic urine.

Increasing sonication power from 60 to 120 W appears to have minimal effect on US degradation, only slightly increasing performance. After 120 minutes of treatment, 55% elimination is achieved in DW, 40% in DSU and 25% in SU. As discussed in section 2.3.3.1, the high hydrophilicity of Iohexol prevents it from efficiently migrating to the bubble-liquid interface. However, both urea and creatinine are significantly more hydrophilic (water solubility around 1000 g L^{-1} and 90 g L^{-1} respectively), so they shouldn´t be expected to compete with Iohexol for placement around it. Nevertheless, as their concentration is in the range of g L^{-1} (almost 2 orders of magnitude higher than Iohexol), they can dominate the interface and inhibit the process.

Following 120 minutes of photo-Fenton treatment, 72% of Iohexol is eliminated in DW, 60% in DSU and 35% in SU. Urea and creatinine have not been reported to have iron binding capacities, thus they are not expected to affect photo-Fenton iron cycling in any way. The

observed decrease in performance can therefore probably be attributed to competing reaction of HO• between Iohexol and these two organic constituents.

Combined use of ultrasound with photo-Fenton is almost identical to photo-Fenton alone in DW. In DSU it performs slightly better than pF, while in SU the increase in performance is significant. To evaluate, however, whether there is a comparative advantage, the synergy between the two processes was estimated. Equation 2.1 has been used for this purpose,

S>1 corresponds to positive synergy, while S<1 suggests that each process acts competitively with the other. S values for the 3 different media and at distinct times within the process are presented in table 2.5.

Table 2.5. Synergy between US and pF at the different media

	US 60/pF	*US 120/pF*
DW 30 min	0.68	0.61
DW 60 min	0.61	0.59
DW 120 min	0.53	0.56
DSU 30 min	0.76	0.72
DSU 60 min	0.67	0.71
DSU 120 min	0.65	0.62
SU 30 min	1	1
SU 60 min	1	1
SU 120 min	0.8	0.77

S is less than 1 in all cases except at the beginning of the process in SU. As seen in figure 3.4, US/pF and pF are identical in distilled water. This can possibly be explained by the dominant photo-Fenton kinetics in the absence of other components. The rapid decrease in Iohexol concentration during the first minutes of the reaction inhibits contribution of US in the process (with US degradation rate lower at more dilute solutions, as seen in section 3.3.1). As pF degradation rate progressively decreases in DSU and SU, US contribution becomes more significant. At best, S has been shown to be equal to 1, clearly demonstrating that combining the two processes offers no comparative advantage. Despite the possible

production of carbonate radicals, as mentioned above, application of US combined with photo-Fenton is not a good option, suggesting that when treating hydrophilic compounds, a proper evaluation of the synergistic effect (Eq.2.1) has to be done.

2.3.3.3. Photo-Fenton treatment of typical dosages of Iohexol in urine.

Photo-Fenton was also applied in an Iohexol solution at the concentrations in which it is likely to be found in a patient's urine. Considering that an average Iodine dosage for typical screening applications is around 2.8 g, it corresponds to an amount of 6.2 g of Iohexol. Assuming normal urinary output (between 800 and 2000 ml per 24 h) and high Iohexol clearance (in excess of 80% in 24 h), its concentration in urine can be roughly approximated between 3 and 6 g L^{-1}. The focus was kept on the highest possible concentration, which accounts to a TOC of about 1600 mg L^{-1}. Experiments were conducted in a 1 L glass beaker under continuous simulated solar light at constant UVA intensity of 30 W/ m^2.

A preliminary experiment in distilled water at pH 2.8 with 10 mg L^{-1} of Fe was conducted to estimate minimum H_2O_2 consumption at an optimal water matrix (Figure 2.13) . The entirety of 6 g L^{-1} of Iohexol were eliminated after 270 minutes of photo-Fenton treatment. 21% of TOC had been mineralized at 270 minutes (340 mg L^{-1}). H_2O_2 consumption was approximately 800 mg L^{-1}.

So the initial concentration of H_2O_2 was chosen at 400 mg L^{-1}, to be replenished whenever it dropped below 100 mg L^{-1} (measured by peroxide test strips). The following treatment scenarios were then tested:

1) Undiluted urine containing the highest theoretically possible Iohexol concentration (6 g L^{-1}).

2) Urine at a 1:10 dilution with distilled water, with a corresponding Iohexol concentration of 0.6 g L^{-1}. The chosen dilution was chosen so as to significantly lower the concentration of urine components, while remaining realistic for a small-scale treatment plant.
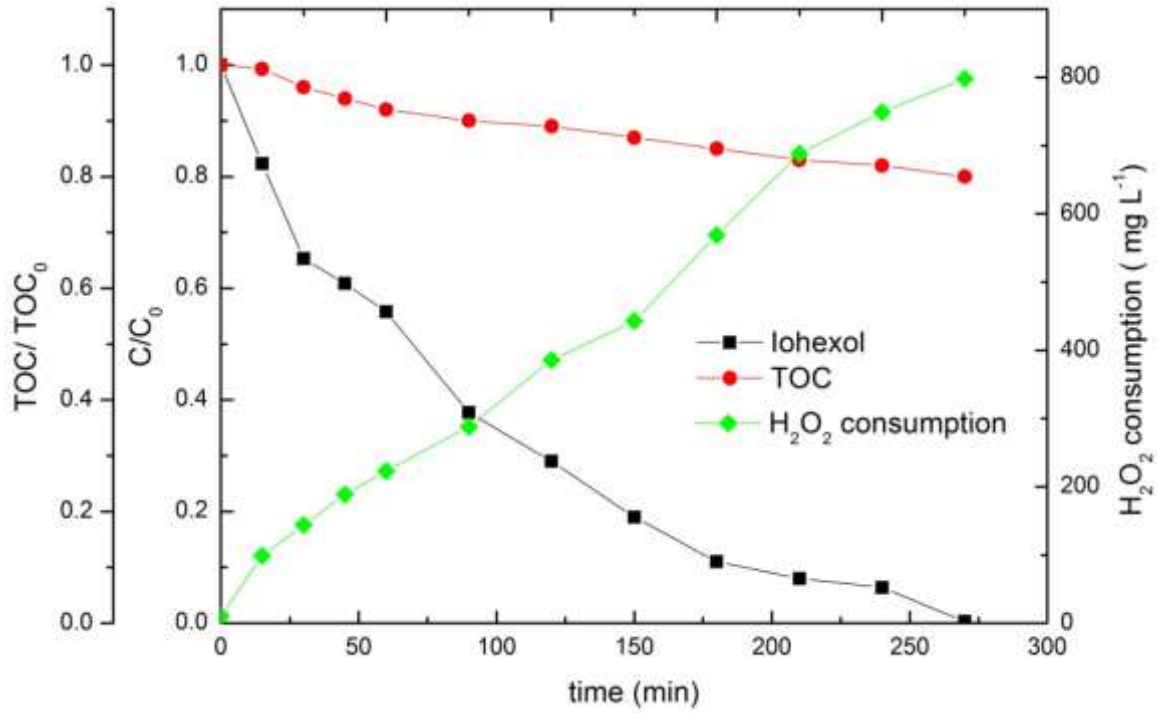
Fig.2.13. Degradation of 6 g L^{-1} of Iohexol in distilled water by photo-Fenton at pH 3, using 10 mg L^{-1} of Fe.
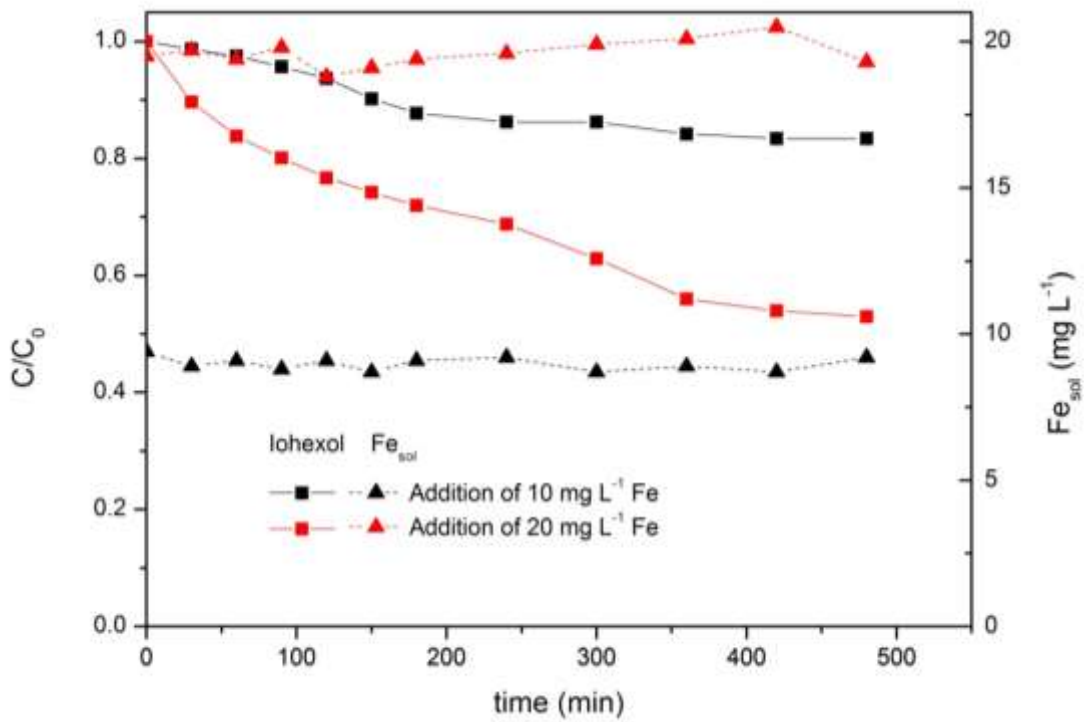
Fig. 2.14. Degradation of Iohexol and evolution of soluble iron during photo-Fenton treatment of 6 g L^{-1} of Iohexol in real urine.

In undiluted urine (Figure 2.14), a plateau was eventually reached after several hours of treatment, after which degradation was completely stopped. With 10 mg L^{-1} of Fe, this plateau was reached at around 200 minutes, with 15% of Iohexol (0.9 g L^{-1}) removed. When adding 20 mg L^{-1} of Fe, this plateau was moved to around 360 minutes, with 48% of Iohexol (2.9 g L^{-1}) removed. TOC was unchanged. The plateau could be attributed to several possible factors : (1) Scavenging of HO• by Iodine ions following the deiodination of Iohexol, (2) Inhibition of Fe^{2+} regeneration due to the presence of iron-binding components in urine, effectively stopping the photo-Fenton cycle, (3) Formation of iron iodide salts [87]. In any case, it is clear that treatment of Iohexol by photo-Fenton in undiluted urine is not possible. Dilution of urine (maybe even with some other type of hospital wastewater) will have to be a necessary part of any treatment design. As seen in figure 2.14, iron measurements appear constant even after the plateau is reached. This suggests that even though iron remains soluble, at some point it becomes unable to participate in the photo-Fenton reaction. During application of the ferrozine method for iron measurement, it was observed that the final magenta color was reached more than 15 minutes after reagent addition. It could be that iron is not available for immediate complexation with ferrozine, so the formation kinetics of the iron-ferrozine complex is negatively affected. Absorption spectra of urine samples at pH 3 with and without iron were also measured in the 250-400 nm range. Addition of 10 mg L^{-1} of iron provokes significant changes in the absorption spectrum of undiluted urine, further strengthening the hypothesis that there is some type of interaction between iron and urine components. When the dilution ratio is high (1:10), the spectra are similar, suggesting that iron is not as strongly affected.

Identifying all possible iron binding components in urine is beyond the scope of this work, yet some of the possibilities merit some discussion. Phosphates and components such as transferin or serum albumin have been known to have iron binding capacities, with stability constants for the Fe^{2+}- transferin complex in particular being very strong (logK around 22 M^{-1} at pH 7) [88]. At the non-physiological, low pH of photo-Fenton, it should be significantly lower, although even loosely bound complexes with other components could negatively affect iron regeneration in a photo-Fenton like process. It can be mentioned that albumin excretion can range from 2 to more than 300 mg per 24h, while transferrin excretion can be as high as 10 mg per 24h [89]

Therefore, it is very probable that the main reason for the inhibiting effect of urine is due to the presence of iron-binding components, not due scavenging of HO• by iodide ions or formation of iron iodide salts. This hypothesis is further strengthened by the fact that this behavior was not observed in the distilled water experiment (Figure 2.13) , despite the even higher concentration of released iodide.
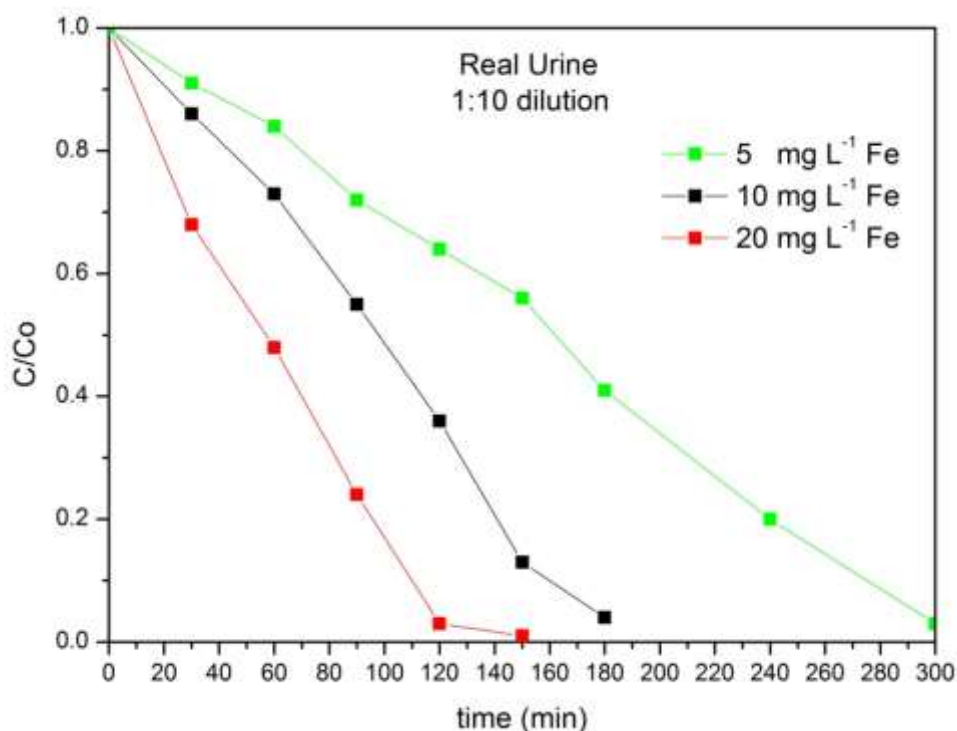
Fig. 2.15. Degradation of 0.6 g L^{-1} of Iohexol in real urine at 1:10 dilution with distilled water.

In 1:10 diluted urine, complete removal of 0.6 g L^{-1} of Iohexol could be achieved (Figure 2.15). 95% removal was observed at 300, 180 and 120 minutes by addition, respectively, of 5, 10 and 20 mg L^{-1} of Fe. It is therefore clear that a relatively reasonable dilution of 1:10 solves this problem and can allows for complete degradation of Iohexol, justifying that iron binding was one of the main reasons for inefficiency of photo-Fenton.

2.3.3.4. Zahn- Wellens biodegradability test of treated Iohexol.

Monitoring mineralization of Iohexol in urine is challenging, as the TOC content of urine interferes with measurement of Iohexol TOC. As seen in section 2.3.3.3 however, even in distilled water, mineralization was very slow. Reaching complete mineralization in urine (whose TOC can be higher than 6 g L^{-1} by itself [86] is not practical, as it would require very large treatment times and be partly wasted on mineralizing the biodegradable organic load of urine.

An attempt has been made to estimate the biodegradability of the photo-Fenton and US treated byproducts at the moment of complete Iohexol elimination. According to the followed protocol, solution TOC has to be at least 50 mg L^{-1} to ensure reliability. For US treatment, 400 mg L^{-1} (TOC=108 mg L^{-1}) of Iohexol were treated in distilled water in the 400 ml US reactor until complete Iohexol elimination. TOC at this stage was unchanged. The solution was subsequently diluted to 1L with 100 mg L^{-1} distilled water and 500 mg L^{-1} mineral

nutrient broth. Final TOC was 54 mg L^{-1}. For the pF treatment, 400 mg L^{-1} of Iohexol (TOC= 108 mg L^{-1}) were treated in distilled water in a 500 ml glass beaker with 2 mg L^{-1} of Fe. H_2O_2 was added in doses of 50 mg L^{-1} as needed until complete Iohexol elimination. A small decrease of TOC could not be nevertheless avoided, so after dilution to 1L with 500 ml of nutrient broth the final TOC was 49 mg L^{-1}. pH was set to 6.5 and activated sludge at the equivalent of 0.5 g of dry mass L^{-1} was added. The mixture was agitated and aerated at 20-25°C under ambient illumination for a period of 28 days. Each collected sample was centrifuged and the supernatant filtered through a 0.45 μm Nylon filter to retain all bacterial matter. TOC was measured each day for 1) The reference compound (Potassium hydrogen phthalate), 2) Untreated Iohexol 3) US treated Iohexol 4) pF treated Iohexol.
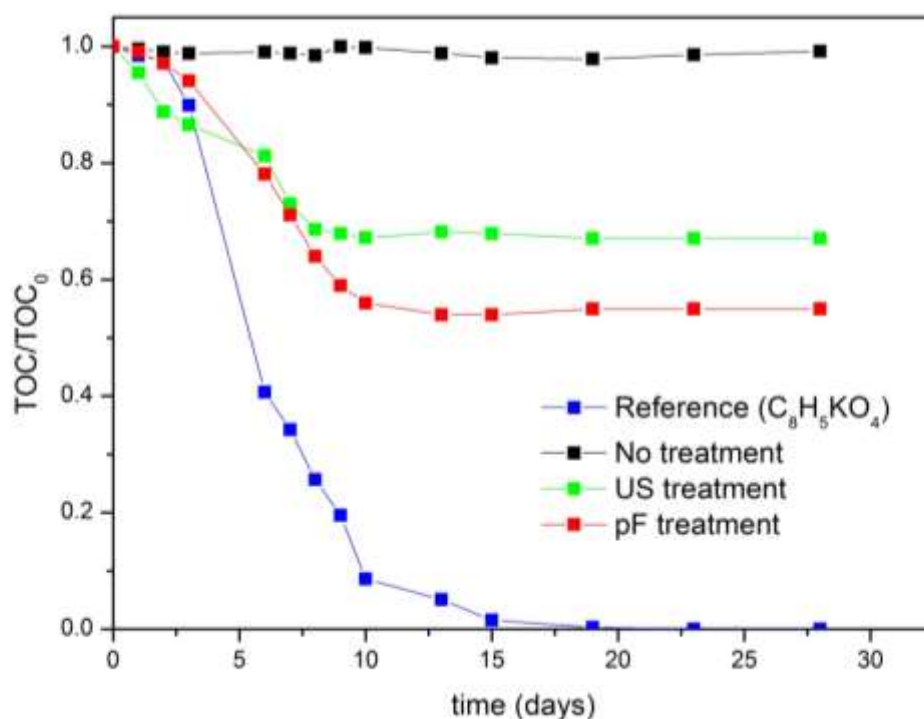
Fig. 2.16. Zahn Wellens biodegradability test of untreated Iohexol and the solutions acquired following complete elimination by US and pF treatments.

Zahn-Wellens results are shown in Figure 2.16. From the reference compound (potassium hydrogen phthalate) we can verify that the bacteria are alive and active. A 33% TOC reduction of the US treated sample has been achieved by day 10, with little progress thereafter. Mineralization of the pF treated sample was higher, at 45%, although a plateau was also reached by day 13. Under both processes however, only partial biodegradability is achieved. This suggests that complete biodegradability is either not possible or it may

require unrealistically long treatment times which may have to be evaluated in the context of cost/time efficiency.

2.3.4. CONCLUSIONS

Several AOP treatment options for the elimination of Iohexol in wastewater and urine have been studied:

- Ultrasound has been shown as inefficient for Iohexol treatment, as its low hydrophobicity prevents efficient migration in the cavitational bubble region. Addition of H_2O_2 and high ultrasound operational power present no additional benefits when treating the low concentrations found in WW.

- A plateau was observed during photo-Fenton treatment of 6 g L^{-1} of Iohexol in urine. Given the availability of soluble iron, H_2O_2 and light, it has been attributed to the formation of soluble iron complexes (not photoactive) with some of the components found in urine.

- Complete Iohexol elimination could be achieved after proper dilution of urine, avoiding the formation of soluble iron complexes.

- Zahn-Wellens tests have shown that the intermediates acquired at the moment of complete Iohexol elimination are only partially biodegradable. This result is encouraging as generation of biodegradable transformation products of Iohexol is possible, but further investigations in diluted urine are however necessary to establish pF optimal treatment times for achieving complete biodegradability.

CHAPTER 3:

ENHANCEMENT OF PHOTO-FENTON BY USE OF EDDS IRON-COMPLEXING AGENT EDDS

3.1. INTRODUCTION

Chapter 2 explored the application of ultrasound in different scenarios for improving the efficiency of photo-Fenton. Although different degrees of success were observed in terms of kinetics improvement, the associated benefits do not address one of the most important limitations of photo-Fenton, the necessity of acidification and subsequent neutralization before release to the environment.

An alternative to acidification would be the use of complexing agents that are able to form photoactive Fe^{3+}-Ligand species able to maintain iron in solution at a wider pH range. Among such compounds are oxalic acid [90; 91], citric acid [92; 93] and the complex fraction of natural organic matter known as humic acids [94; 95]. Although they are able to maintain iron soluble at neutral pH, the optimal behavior of Fe(III)-citrate and Fe(III)-oxalate photochemical processes are still under slightly acidic pH(5.0 for Fe(III)-citrate and 4.3 for Fe(III)-oxalate) [42; 43]. Treatment of heavily contaminated industrial wastewater has been shown to be efficient at neutral pH with the addition of humic acids [96]. However, for treating contaminants at the µg L^{-1} level in neutral pH MWTP effluent, degradation rate was slow and the residual pH acidic [97]

Of particular interest are aminopolycarboxylic acids (APCAs), which can form stable water-soluble complexes over a wide pH range. Ethylenediaminetetraacetic acid (EDTA) has been extended in industrial applications due to its ability to solubilize and inactivate metal ions. However, due to its high biorecalcitrance, it has been classified as a persistent pollutant [98; 99]. An alternative APCA, ethylenediamine- N,N'- disuccinic acid (EDDS) has metal complexing properties similar to EDTA, but is biodegradable and considered environmentally safe [100; 101]. Due to these favorable characteristics, the use of EDDS could present an attractive option for application in municipal wastewater tertiary treatments.

Most of the work published with EDDS has been for the treatment of contaminant concentrations between the range of a few ng L^{-1} to a few mg L^{-1} in distilled water [102],[100],[103],[104].

This chapter aims to provide some insight on how EDDS can affect the photo-Fenton process in two different scenarios: 1) for removing microcontaminants in real MWTP effluents (section 3.2) and 2) for removing relatively high concentrations contaminant concentrations, as would be the case for agricultural or industrial wastewater (section 3.3).

3.2. TREATMENT OF MICROCONTAMINANTS IN MWTP EFFLUENTS

3.2.1 OBJECTIVES OF THIS SECTION

Previous work with EDDS in real MWTP effluents has been promising, demonstrating that the use of Fe:EDDS at 0.1:0.2 mM concentration ratio can efficiently degrade emerging contaminants at neutral pH [45; 105]. However, a systematic study focusing on the effect of the common parameters affecting the photo-Fenton process applied at neutral pH and in the presence of EDDS has never been done before.

The aim of this section is to better understand the effect of pH, H_2O_2 and Fe:EDDS concentrations on various aspects of an EDDS-assisted photo-Fenton treatment of five micro-contaminants by performing a central composite experimental design (CCD). Phenol, bisphenol A, sulfamethoxazole, carbamazepine and pyrimethanil were chosen so as to be representative of the spectrum of different classes of chemicals commonly found in municipal wastewater. Actual MWTP effluents have been spiked with 100 µg L^{-1} of each of the five pollutants. The ranges of the three studied variables were: pH between 5 and 8, [Fe^{3+}] between 0.025 mM and 0.25 mM and [H_2O_2] between 30 and 100 mg L^{-1}. Response surfaces were constructed for initial degradation rate, percentage of contaminants degraded, H_2O_2 efficiency and stability of soluble iron. Lab-scale and pilot-scale systems were compared and an approach for determining operability regions of near-optimal performance was carried out.

3.2.2. MATERIALS AND METHODS

3.2.2.1. REAGENTS

Iron source $Fe_2(SO_4)_3 \cdot H_2O$ (75% purity) and (S,S)-ethylenediamine-N,N'-disuccinic acid trisodium salt solution (35% w/v) were both provided by Sigma Aldrich. Hydrogen peroxide (30% w/v) was purchased from Pancreac. Sulfuric acid (96%) and sodium hydroxide were obtained from J.T.Baker. Carbamazepine and bisphenol A were obtained from Sigma Aldrich. Sulfamethoxazole from Fluka, phenol from Pancreac and pyrimethanil from Agrevo. Acetonitrile (ACN) for the UPLC mobile phase was HPLC-grade and provided by Sigma-Aldrich. Millex PVDF 0.45 µm filters were used for the preparation of the UPLC samples. For

dissolved organic carbon, dissolved iron and H_2O_2 analyses, Millipore Nylon 0.20 µm were used.

3.2.2.2. MUNICIPAL WASTEWATER TREATMENT PLANT EFFLUENT

All experiments were conducted in actual wastewater collected from the El Ejido (Almería, Spain) municipal wastewater treatment plant (MWTP), downstream of the secondary biological treatment.

Table 3.1. Composition of the MWTP effluents used in this work.

Main parameters	Range
Ions (mg L^{-1})	
Cl^-	440-687
NO_2^-	3.5-4.0
Br^-	3.0-3.5
NO_3^-	3.0-4.5
SO_4^{2-}	148-174
Na^+	276-358
NH_4^+	19-50
K^+	26-35
Mg^{2+}	63-89
Ca^{2+}	78-114
Turbidity (NTU)	8.5-9.0
Conductivity (mS cm^{-1})	1.9-2.1
pH	7.6-7.8
COD (mg L^{-1})	60-62
IC (mg L^{-1})	80-102
DOC (mg L^{-1})	11-15

H_2SO_4 was used to strip HCO_3^-/CO_3^{2-} (measured as inorganic carbon (IC)), until the final IC load was below 5 mg L^{-1} in order to avoid scavenger effect on hydroxyl radicals. Care was taken to not significantly modify the natural water pH. Wastewater collected from the experimental design was stored under refrigeration (4-6ºC) and used within 10 days. Treated effluent collected from the pilot-scale experiments was used within 3 days. Some important physicochemical characteristics have been measured and can be seen in Table 3.1.

3.2.2.3. ANALYTICAL SETUP

An analytical method for Ultra Performance Liquid Chromatography (UPLC) has been developed. A Zorbax XDB-C18 column (4.6x50 mm, particle size 1.8 Micron) was used. A linear gradient of 25 mM formic acid/ACN solutions was used, progressing from 80/20 to 0/100 in 8 minutes. Post time for subsequent equilibration was 4 minutes. The flow rate was 1 mL min^{-1}. UPLC samples were prepared by filtering 8 mL of solution through a 0.45 μm PVDF syringe-driven filter, subsequently washed with 2 mL of ACN to verify total elution of the contaminants. The injected volume for all samples was 100 μL. The UV signal for each compound was recorded at the wavelength of maximum absorption (213 for phenol, 269 for carbamazepine, sulfamethoxazole and pyrimethanil, 280 for bisphenol A). Limits of detection (LOD) ranged from 1 to 7 μg L^{-1}, while limits of quantification (LOQ) ranged from 1.5 to 15 μg L^{-1}, depending on the contaminant. Concentrations were calculated using a 5-point calibration curve (5, 10, 25, 50 and 100 μg L^{-1}). Fe:EDDS complexes were prepared daily prior to the experiments by adding $Fe_2(SO_4)_3$ in 50 mL distilled water acidified at pH 3 and adding EDDS solution. Dissolved organic carbon (DOC), H_2O_2 and soluble iron were measured with the same methods as described in section 2.2.2

3.2.2.4. EXPERIMENTAL SET-UP AND PROCEDURE

Experimental design was conducted in an Atlas XLS suntest solar simulator under constant illumination from a Xenon Lamp with an average UV irradiance of 30 W m^{-2} (typical solar UV power during a sunny day). The mixture of contaminants was prepared and stored in pure methanol, at a concentration of 1500 mg L^{-1} each as the parent solution. When the contaminants were added to the effluent, a small amount of DOC from methanol (20 mg L^{-1}) was also introduced. A cylindrical Pyrex glass vessel (height 8.5 cm, diameter 19 cm, wall thickness 3.2 mm) was filled with the MWTP effluent containing 100 μg L^{-1} of each of the five contaminants (500 μg L^{-1} of contaminants total) and the Fe:EDDS solution to a final volume of 1.5 L. This volume corresponds to a height of 5 cm in this vessel, deliberately chosen so as to be the same as the diameter of a CPC tube. The sides of the pyrex vessel were covered so that light could only penetrate to the upper surface (0.025 m^2 of illuminated

area). UV radiation was monitored throughout the process with a SOLARLIGHT PMA2100 radiometer placed within the simulator. The pH was fixed to the desired level with 0.1 M solutions of NaOH or H_2SO_4. H_2O_2 was added and the simulator was sealed. Samples were taken every 5 minutes without disrupting the operation via a tube fixed to the vessel walls. The duration of each experiment was 60 minutes. pH was followed with a portable CRISON pH meter. Temperature was measured with a HANNA portable water resistant thermometer. All experiments were conducted at initial solution temperatures of 22^oC. Application of air cooling kept it below 29^oC during the course of the experiments.

Pilot scale experiments were conducted in a mobile CPC plant. The photocatalytic reactor was comprised of 20 borosilicate tubes (50 mm internal diameter, 1.5 m length, 2.5 mm thickness) and CPC mirrors of anodized aluminum. The plant was tilted 37°, equal to the local latitude (Tabernas, Almeria, Spain). Volume of each batch was 60 L, with an illuminated volume of 45 L and a total illuminated area of 4.5 m^2. Temperature and pH were monitored by probes inserted in the pipes. In all experiments the temperature never deviated from the 24- 28^oC range, so its effect is assumed negligible. Wastewater was introduced into a recirculation tank then pumped into the tubes with a flow of 29 L min^{-1} by using a centrifugal pump. Contaminants and Fe:EDDS were added and the pH was fixed with 2M solutions of H_2SO_4/NaOH. H_2O_2 was then added and the system was left to recirculate. Solar photo-Fenton was initiated by uncovering the tubes and samples were taken every 5 minutes.

Accumulated energy (eq. 3.1) was used instead of treatment time in order to have a normalized value for comparing the efficiency between the two reactors of different size and geometry, including variations of solar irradiation during scaling-up experiments in the CPC pilot plant.

$$Q_{UV,n+1} = Q_{UV} + \Delta t_n \cdot \overline{UV}_{G,n+1} \cdot \frac{A_i}{V_T};$$ Eq. 3.1

$$\Delta t_n = t_{n+1} - t_n;$$

Where Q_{UV} (kJ L^{-1}) is the accumulated UV energy per unit of volume, $\overline{UV}_{G,n+1}$ (W m^{-2}) is the average solar ultraviolet radiation (λ< 400 nm) measured between t_{n+1} and t_n and A_i is the illuminated area (m^2). V_T (L) is the total volume of the reactor.

3.2.2.5. CENTRAL COMPOSITE DESIGN

Response Surface Methodology (RSM) is a set of mathematical and statistical techniques widely used for analyzing engineering problems dependent on several variables. Central

composite designs are among the most popular RSM methods, allowing for estimation of curvature along the response surface via the inclusion of quadratic terms.

Table 3.2. Experimental design matrix with each of the acquired responses. (R^2 >0.990 for the initial degradation rates used for the calculation of y_1).

Standard Order	Run Order	pH	Fe	H_2O_2	y1	y2	y3	y4
1	17	5.0	0.0250	30	195	31	4.2	22
2	4	8.0	0.0250	30	106	19	2.6	6
3	6	5.0	0.2500	100	1561	95	14.4	93
4	20	8.0	0.2500	30	610	67	8.1	91
5	14	5.0	0.0250	100	320	39	9.7	40
6	15	8.0	0.0250	100	118	17	2.0	5
7	18	5.0	0.2500	30	1283	80	11	90
8	3	8.0	0.2500	100	1230	93	6.6	75
9	8	5.0	0.1375	65	929	85	8.9	34
10	10	8.0	0.1375	65	464	70	4.8	40
11	7	6.5	0.0250	65	208	25	4.8	7
12	9	6.5	0.2500	65	804	90	7.2	92
13	11	6.5	0.1375	30	811	73	11.4	52
14	13	6.5	0.1375	100	826	92	9.6	30
15	2	6.5	0.1375	65	770	81	10.2	47
16	1	6.5	0.1375	65	801	79	9.9	49
17	5	6.5	0.1375	65	829	80	10.2	51
18	16	6.5	0.1375	65	814	80	11.4	48
19	12	6.5	0.1375	65	799	81	11.2	45
20	19	6.5	0.1375	65	819	82	10.4	48

In this work, the chosen region of interest for each variable selected was between 0.025 and 0.25 mM for [Fe^{3+}] (Fe:EDDS always maintained at 1:2 ratio), [H_2O_2] between 30 and 100 mg L^{-1} and pH between 5 and 8. Previous work has shown that 0.1:0.2 mM of Fe:EDDS has been sufficient for treating concentrations from 60 to 1500 µg L^{-1} of total contaminants in MWTP effluent with a H_2O_2 consumptions between 30 and 90 mg L^{-1} [106]. The range of

concentrations was chosen on the basis of these results. The choice of maintaining the molar ratio at 1:2 was made because it has been demonstrated to be favorable to 1:1 in terms of degradation rate and H_2O_2 consumption for the treatment of pharmaceuticals in MWTP effluent[105; 106]. Higher ratios were not used in order to limit the increase of DOC due to the addition of EDDS. A rotatable central composite design with an alpha value of 1.682 would require experimentation at inadmissible negative values of Fe^{3+} concentration and pH values well beyond the typical ones found in real wastewater. In light of this limitation, a face-centered central composite design (FCD) was used instead, which is advisable whenever the regions of interest and operability coincide [107].

The experimental matrix found in Table 3.2 summarizes the performed runs. Minitab statistical software was used for analysis of the design and plotting of the response surfaces. Depiction of the response surfaces was made by holding one of the variables constant at the center point (5 for pH, 0.1375 mM for $[Fe^{3+}]$ and 65 mg L^{-1} for $[H_2O_2]$) and plotting the response as a function of the other two. A set of three graphs was generated for each response. Different responses have been selected in this study as it is explained below.

3.2.3. RESULTS AND DISCUSSION

When conducting an experimental design for an applied engineering problem, it can be worthwhile to explore multiple response factors. In this way, the effect of the operational variables on several aspects of the process can be evaluated. In this work, the following response factors have been studied, presented here along with their corresponding model equations (Eq.3.2- Eq. 3.5). Corresponding ANOVA tables for each model equation are presented in table 3.3. Only the terms with $p<0.1$ (90% level of significance) have been used for the construction of the model equations.

1) Initial degradation rate (in terms of µg L^{-1} of contaminant removed per kJ of UV radiation received $R^2=0.9521$, F value of model =43.49):

$$y_1 = -279 + 163\, pH + 13096\, Fe - 6.86\, H_2O_2 - 17304\, (Fe)^2 \qquad \text{Eq. 3.2}$$

$$+0.08\, (H_2O_2)^2 - 830\, pH * Fe$$

2) Percentage of the sum of micro contaminants removed by the time the degradation process slows down ($R^2=0.9852$, F value of model=136.51):

$$y_2 = -10.60 + 13.51\, pH + 598.54\, Fe - 0.14\, H_2O_2 - 1850(Fe)^2 \qquad \text{Eq. 3.3}$$

$$-14.8\, pH * Fe + 1.1\, Fe * H_2O_2$$

73

3) Efficiency of hydrogen peroxide consumption (in terms of µg L^{-1} of contaminant eliminated per mg L^{-1} of H$_2$O$_2$ consumed, R^2=0.9054, F value of model =11.89):

$$y_3 = -26.21 + 11\,pH + 90.2\,Fe - 0.93(pH)^2 - 231.10\,(Fe)^2 - 0.36\,Fe * H_2O_2 \qquad \text{Eq. 3.4}$$

4) Percentage of total dissolved iron in solution by the end of the process (R^2=0.9686, F value of model=33.64):

$$y_4 = -40.52 + 19.80\,pH + 78\,Fe + 0.18\,H_2O_2 + 593\,(Fe)^2 \qquad \text{Eq. 3.5}$$

Table 3.3. ANOVA tables for the linear, quadratic and interaction terms of each of the four model equations y$_1$ (a), y$_2$ (b), y$_3$ (c) and y$_4$ (d).

a)

	DF	Adj SS	Adj MS	F-value	P-Value
Model	9	2583051	287006	42.5	0.000
Linear	3	2220177	740059	110	0.000
pH	1	469589	469589	69.5	0.000
Fe	1	1709244	1709244	253	0.000
H2O2	1	41345	41345	6.1	0.033
Square	3	186448	62149	9.2	0.003
pH*pH	1	2259	2259	0.3	0.576
Fe*Fe	1	131904	131904	19.5	0.001
H2O2*H2O2	1	23959	23959	3.6	0.089
2-way interactions	3	176425	58808	8.7	0.004
pH*Fe	1	156800	156800	23.2	0.001
pH*H2O2	1	3961	3961	0.59	0.462
Fe*H2O2	1	15664	15664	2.32	0.159

b)

	DF	Adj SS	Adj MS	F-value	P-Value
Model	9	12676.2	1408.5	136.1	0.000
Linear	3	9430.7	3143.6	303.6	0.000
pH	1	396.9	396.9	38.3	0.000
Fe	1	8584.9	8585.9	829.2	0.000
H2O2	1	448.9	449.9	43.4	0.000
Square	3	3033.5	1011.2	97.7	0.000
pH*pH	1	32.0	32.0	3.1	0.109
Fe*Fe	1	150.0	1507.0	145.6	0.000
H2O2*H2O2	1	7.0	7.0	0.7	0.431
2-way interactions	3	212.0	70.7	6.8	0.009
pH*Fe	1	50.0	50.0	4.8	0.053
pH*H2O2	1	0.0	0.0	0.0	1.000
Fe*H2O2	1	162.0	162.0	15.6	0.003

c)

	DF	Adj SS	Adj MS	F-value	P-Value
Model	9	162.0	18	7.5	0.002
Linear	3	79.3	26	11	0.002
pH	1	39.5	39	16.6	0.002
Fe	1	39.1	39	16.4	0.002
H2O2	1	0.6	0.6	0.3	0.627
Square	3	66.2	22.1	9.2	0.003
pH*pH	1	11.9	11.9	5	0.049
Fe*Fe	1	23.5	23.5	9.8	0.011
H2O2*H2O2	1	6.8	6.8	2.9	0.122
2-way interactions	3	16.5	5.5	2.3	0.139
pH*Fe	1	0.9	0.9	0.4	0.555
pH*H2O2	1	1.6	1.6	0.6	0.438
Fe*H2O2	1	14.1	14.1	5.9	0.036

d)

	DF	Adj SS	Adj MS	F-value	P-Value
Model	9	13929.4	1547.7	33.6	0.000
Linear	3	13569.8	4523.3	98.1	0.000
pH	1	152.1	152.1	3.3	0.099
Fe	1	13249.6	13249.6	287.3	0.000
H2O2	1	168.1	168.1	3.6	0.085
Square	3	181.3	60.4	1.3	0.325
pH*pH	1	44.0	44.0	0.9	0.352
Fe*Fe	1	154.7	154.7	3.3	0.097
H2O2*H2O2	1	0.0	0.0	0.0	1.000
2-way interactions	3	178.4	59.5	1.3	0.331
pH*Fe	1	91.1	91.1	2.0	0.190
pH*H2O2	1	21.1	21.1	0.5	0.514
Fe*H2O2	1	66.1	66.1	1.4	0.259

3.2.3.1. INITIAL DEGRADATION RATE (r$_o$) AND PERCENTAGE OF DEGRADATION ACHIEVED

In Figure 3.1 the response surfaces obtained for the two first response factors (y$_1$ and y$_2$) considered in this work are shown.
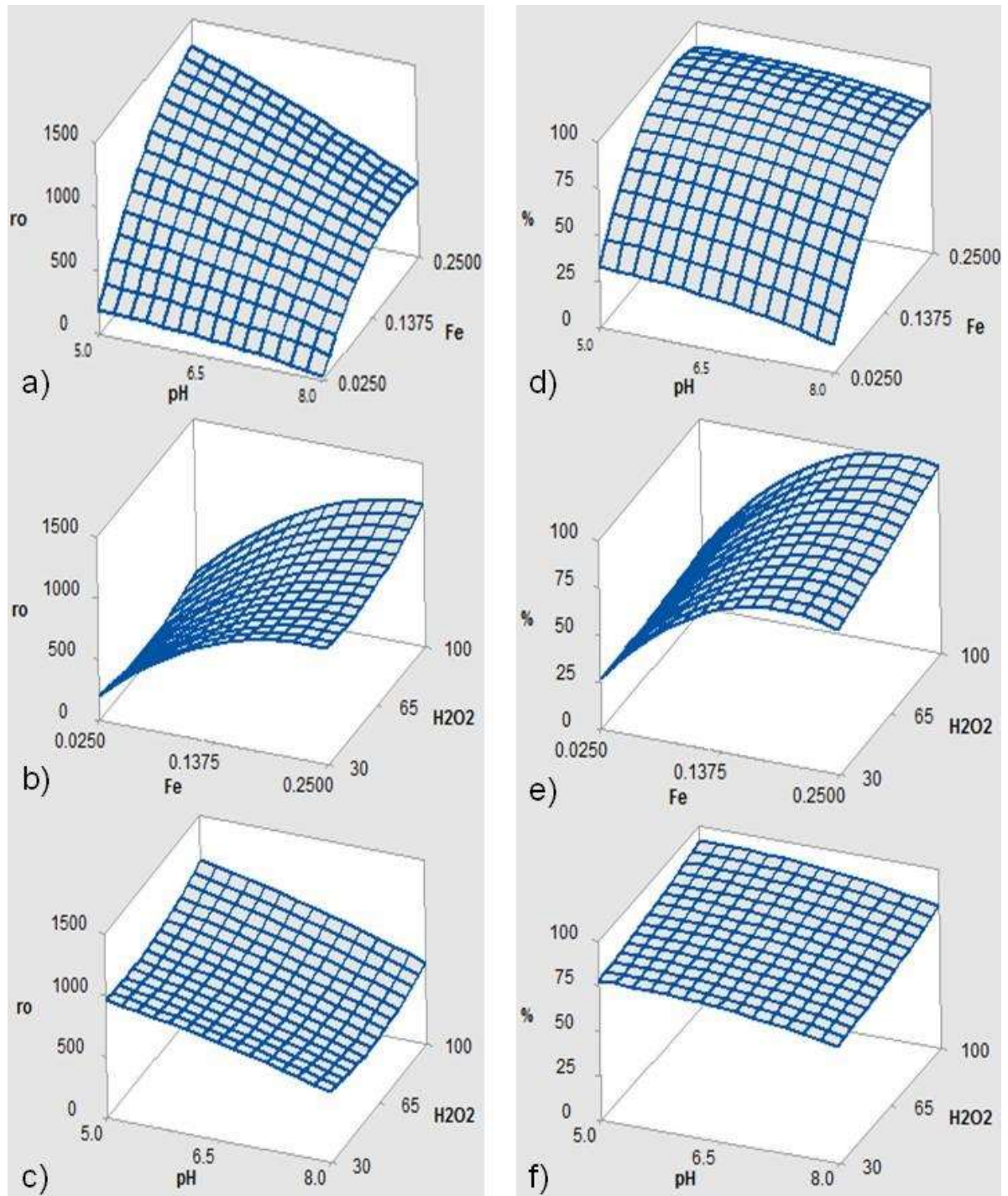
Fig. 3.1. Initial degradation rate (a, b, c) and percentage of contaminants removed by the end of the process (d, e, f). Factors kept constant: a), d) [H$_2$O$_2$] 65 mg L^{-1}; b), e) pH 6.5; c), f) [Fe:EDDS] 0.1375:0.275 mM.

The Fe(III)-EDDS complex, if kept in the dark, is stable in the entirety of the 5-8 pH region. Due to the stability of the complex, iron is not initially available for participating in homogeneous Fenton reactions. No contaminant degradation was therefore observed in the dark.it was not available for participation in homogeneous Fenton reactions. Under illumination, the complex is rapidly photodegraded and the iron consequently liberated. Complete photodegradation of 0.1 mM of Fe(III)-EDDS has been reported to occur within only 12 minutes of UV-visible light (300 nm $<\lambda<$ 500 nm) irradiation [44]. The low degradation efficiency observed when 0.025:0.05 mM of Fe:EDDS were used is indicative of the loss of iron from the solution. Higher Fe:EDDS concentrations would be more successful.

Initial degradation rate exhibits a downward trend between pH 5 and 8, regardless of H_2O_2 concentration. This behavior appears contrary to what has appeared in the literature (in demineralized water), where higher pH leads to higher initial rates when EDDS complex agent is used [103]. There are several effects which can occur within this pH range: First, at higher pH, superoxide radical anion ($O_2^{\bullet-}$) is present in higher quantities and contributes to the direction of the Fe(II)/Fe(III) equilibrium towards Fe(II) formation. Second, starting from pH 7 upwards, the speciation of Fe(III)/EDDS complexes begins to differ, with the form FeL^- decreasing and $FeOHL^{2-}$ becoming more dominant. At pH 8, it is suggested [44] that the two species are present in almost equal concentrations. As the $FeOHL^{2-}$ form is suggested to be less photochemically efficient [44], it could contribute to the decrease in degradation rate. Third, the quantum yield of $HO^{\bullet}$ formation from the photolysis of Fe(III)-EDDS increases at higher pH [103] (contrary to what happens with citrate, oxalate and Fe(III) aquacomplexes, whose quantum yield becomes negligible around pH 7 [108]). Fourth, the iron released once the Fe(III)-EDDS complex begins to photolyse would be expected to precipitate faster at higher pH, hindering the degradation. The fact that the initial rate is lower with increasing pH may mean that the equilibrium of these different elements in MWTP effluent is different than in demineralised water.

In addition, independently of the other two variables, there is not a significant influence of hydrogen peroxide on the initial degradation rate. As the entire range of H_2O_2 concentrations studied was about 2 orders of magnitude greater than of the contaminants, this result is not unexpected, especially given the complexity of the effluent.

Regarding the percentage of contaminants eliminated at the end of the process, it can be seen that at the lowest iron concentration (0.025 mM), removal percentage is lower than 40%, regardless of the combination of the other two variables. It could be argued however that the limiting step is the rapid photodegradation of the Fe(III):EDDS complex. The

relatively low concentration of excess EDDS (0.05 mM total) recomplexed the iron in solution, but is depleted before complete degradation can be achieved. Studies conducted with varying ratios of Fe to EDDS have shown [104] that iron concentrations as low as 0.01 mM can be maintained in solution and contribute to contaminant degradation, provided EDDS is found in abundance (0.25 mM).

The influence of the pH on the percentage of contaminants degraded is relatively minimal throughout the whole region of interest. High pH may negatively affect the kinetics of the degradation, but the end-point nevertheless remains the same. This observed stability could be attributed, as mentioned above, to the competing tendencies at higher pH between faster iron precipitation and higher quantum yield. Even though 30 mg L^{-1} of H_2O_2 are successful in removing about 70- 75% of contaminants under all conditions, removal of 90% and above requires addition of H_2O_2 concentrations above 65 mg L^{-1}.

3.2.3.2. H_2O_2 CONSUMPTION EFFICIENCY (R_p) AND IRON AVAILABILITY

In Figure 3.2 the response surfaces obtained for the third and fourth response factors (y_3 and y_4) are shown.

H_2O_2 consumption efficiency (R_p = µg contaminant/mg H_2O_2 consumed) is exceptionally low at the lowest iron concentrations (Figure 3.2, a) and b)). As the concentration of EDDS is also low, its complete photodegradation occurs within a few minutes. The medium is almost immediately deprived of the decomplexed iron due to its fast precipitation (faster at higher pH values, Figure 2 a)). In the absence of iron, it is probable that H_2O_2 is being consumed while reacting with the less recalcitrant natural organic compounds present in the wastewater. Higher iron concentration allows for better H_2O_2 consumption, regardless of initial H_2O_2 concentration, and near-optimal values are clearly observed around 0.1375 mM.

Maintaining iron in solution is one of the most significant challenges when working at neutral pH. Therefore, it was of interest to observe its stability in the studied region. Figure 3.2 d), e) and f), displays the response surfaces of the percentage of iron remaining in solution after 60 minutes of simulated solar irradiation. Given the constant lamp radiation of 30 W m^{-2} of UVA, this corresponds to an accumulated UVA energy of 2.04 kJ L^{-1}. As seen in figure 2 d) and e), almost all of the iron was lost at the lowest concentrations. The percentage of iron remaining in solution increased with higher initial Fe:EDDS concentrations, with almost no losses observed at the highest concentrations.
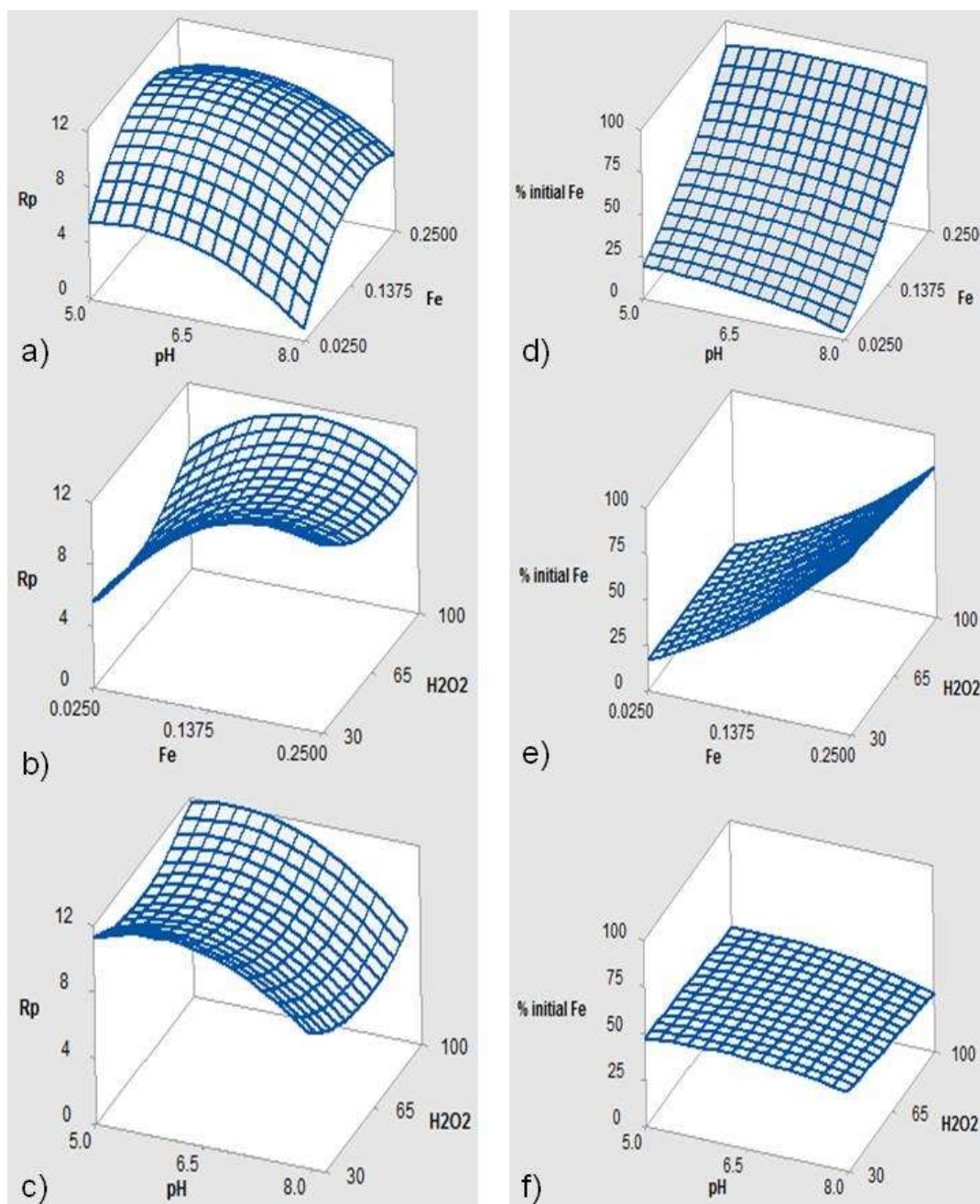
Fig. 3.2. H_2O_2 consumption efficiency (R_p, a,b c) and soluble iron availability by the end of the process (d, e, f). Factors kept constant: a), d) $[H_2O_2]$ 65 mg L-[1]; b), e) pH 6.5; c), f) [Fe:EDDS] 0.1375:0.275 mM.

It is mentioned in the literature that the ratio between Fe(III) and EDDS in Fe(III)-EDDS species prevalent between pH 5 and 8 is always 1:1 [44]. Additionally, Metsarinne et al [109] mentioned that while Fe(III)-EDDS is rapidly photodegraded, EDDS alone can be stable for days in both distilled and more complex lake water. Uncomplexed EDDS can thus be expected to remain stable for the duration of the experiment. Following the initial photochemical reaction, oxidation of Fe(II) and complexation has been suggested to be

possible when EDDS is found in excess [104], according to the following reactions (React. 3.6-3.7).

$$Fe(III)\text{-}EDDS \xrightarrow{h\nu} [Fe(III)\text{-}EDDS]^* \rightarrow Fe(II) + EDDS^{\cdot}$$
React. 3.6

$$Fe(II) + EDDS \xrightarrow{O_2, H_2O_2} Fe(III)\text{-}EDDS$$
React. 3.7

It should be mentioned that the observed loss of iron was not gradual from the beginning of the experiment but would happen rapidly from the moment a certain amount of radiation had been received by the system. At the highest concentrations (around 0.25:0.5 mM of Fe:EDDS), no loss of iron was observed at all during the 60 minutes of the experiment. Given that Fe(III)-EDDS photolysis begins almost immediately and that any free iron would be expected to precipitate rapidly in the 5 to 8 pH range, this delay seems to suggest that React. 3.7 does indeed happen. The persistence of iron in solution at the highest Fe:EDDS concentrations also suggests that the complexation of free iron with excess EDDS was faster than its precipitation. In the case of medium concentrations, the observed behavior means that only part of the excess EDDS was photodegraded within the time of the experiment and was available for complexing more iron through React. 3.7.

Effects of pH and H_2O_2 on the percentage of iron retained in solution are minimal, although the curvature observed around pH 6.5 seems to be in accordance with Metsarinne et al [109], who have observed higher stability of Fe(III)-EDDS at pH 6.5 both in distilled and lake water.

3.2.3.3. SCALING UP TO A CPC SOLAR PHOTO-REACTOR AT PILOT PLANT SCALE

In order to verify the general applicability of the results obtained in the solar simulator, a set of three conditions has been tested in a 60 L CPC photo-reactor under solar light.

The rate of energy accumulation in the CPC tubes was higher than in the solar simulated system considering an average radiation of 30 W m^{-2} (about 0.17 kJ min^{-1} L^{-1} in the CPC compared to 0.03 kJ min^{-1} L^{-1} in the simulator), so the process was significantly faster. 90% degradation was reached in 35 minutes in the simulated system, while the same percentage was reached in the CPC in less than 10 minutes. As can be seen in figure 3.3, there is a good degree of correlation between the two systems despite the different timeframes. At low concentrations of Fe:EDDS the correlation was not adequate as it was seriously affected by the iron lost.
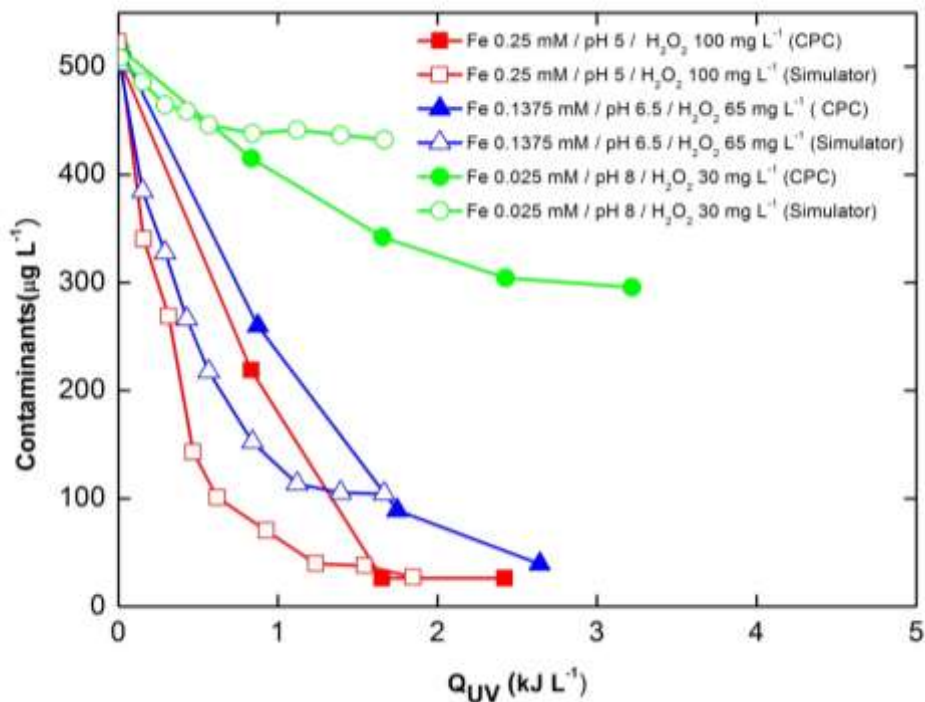
Fig. 3.3. Cross-scale comparison between the degradation performance on the 1.5 L photo-reactor under simulated solar radiation and using 60 L solar CPC pilot plant.

As commented before, Fe (III)-EDDS photolysis begins almost immediately and any free iron would be expected to precipitate rapidly in the 5 to 8 pH range. In the solar simulator (where experiments were longer as incident radiation per minute and litre was lower) the precipitation of iron had a more serious effect than in the CPC. This reinforces the idea that solar photo-reactors should be designed to profit the most of solar irradiation absorbance, maximizing illuminated volume/total volume ratio.

3.2.3.4. DESIRABILITY FUNCTION APPROACH FOR MULTIPLE RESPONSE PROCESS OPTIMIZATION

When discussing optimization, it should be preferable to take into account more than one aspect of the process, seeking instead a compromise for achieving efficiency across multiple responses. This approach can help in defining regions of near-optimal performance. As there is a high degree of correlation in terms of accumulated Q_{UV} between the two systems, the experimental design results could be applied even in the context of multiple-module CPC reactor systems. In this case, the objective should be a set of condition achieving high initial degradation rate (y_1), complete contaminants removal (y_2) and high H_2O_2 consumption efficiency (y_3). A common strategy used within the response surface framework is the desirability function approach, consisting of converting the multiple responses into a single composite function [110]. For each of the three responses y_1, y_2, y_3, individual desirability

functions (d_i) are defined according to Eq. 3.8. It can obtain values between 0 and 1, with maximum desirability obtained at the maximum response.

$$d_i = \begin{cases} 0 & y \leq y_{min} \\ \left(\dfrac{y - y_{min}}{y_{max} - y_{min}}\right)^{W_i} \\ 1 & y \geq y_{max} \end{cases}$$

Eq. 3.8

The parameter W_i represents a weight which defines the shape of the function. Large weights signify a sharp increase in d_i only when y_i is close to y_{max}. Consequently, if one of the responses has higher importance for a given optimization objective, setting a high W_i limits the acceptable range to a region very near the maximum. As reaching complete contaminant removal is the most important objective, the corresponding W_2 has been set higher than both W_1 and W_3. W_1 and W_3 have been set to 1, while W_2 has been set to 2. An aggregate composite desirability function D is constructed by calculating the weighted geometric mean of the three individual desirabilities.

$$D = \sqrt[3]{d_1^{W_1} * d_2^{W_2} * d_3^{W_3}}$$

Eq. 3.9

Each column of the plot shown in figure 3.4 displays the influence of each factor on the composite desirability D (row 1) and on each of the chosen responses (rows 2-4). Highlighted areas in Figure 3.4 demonstrate acceptable operability conditions. In terms of process control, it could be said that pH would only have to be regulated when it strongly deviates towards high values. [Fe] should be around 0.2 mM, while [H_2O_2] should be above 65-70 mg L^{-1} for maximum removal. The chosen weights are indicative, as this approach allows for flexible optimization objectives, depending on individual priorities.
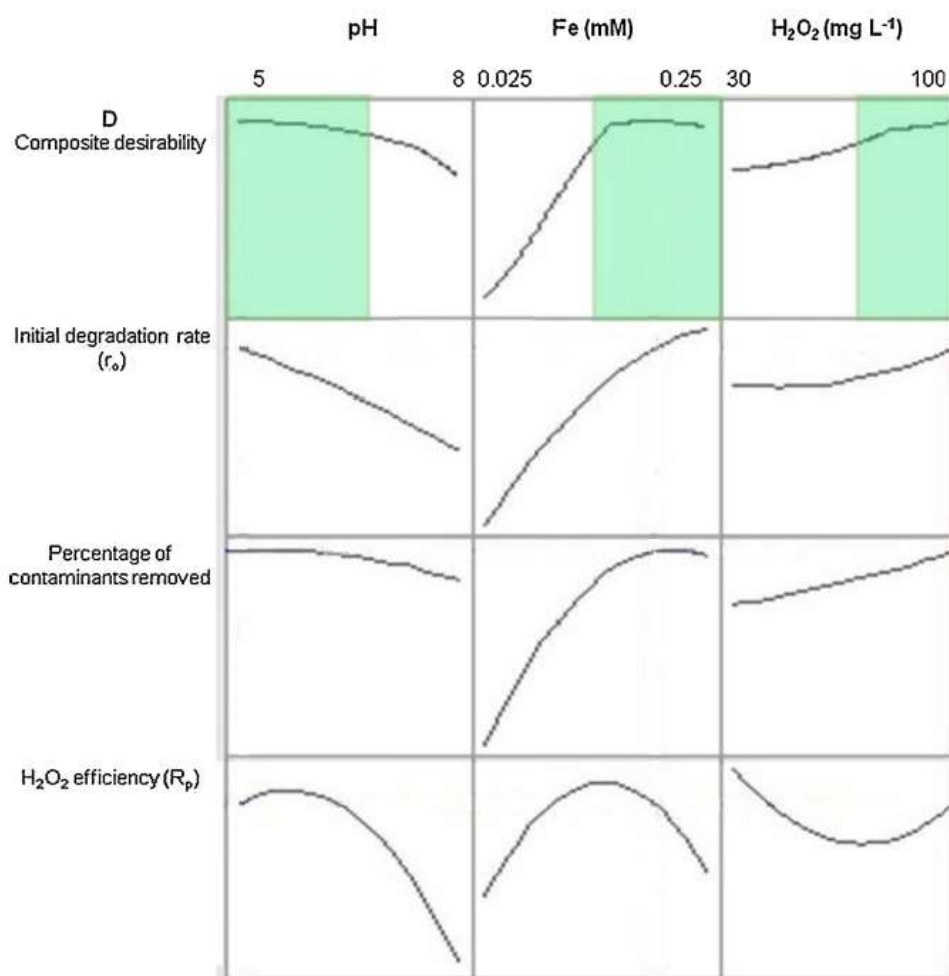
Fig. 3.4. Effect of initial pH, [H_2O_2] and [Fe] on composite desirability (row 1), initial degradation rate (row 2), percentage of contaminants removed (row 3) and H_2O_2 efficiency (row 4).

3.2.4. CONCLUSIONS

This work has verified that treatment of micro-contaminants with the use of EDDS as an iron-complexing agent is possible in real wastewater effluent at a pH range between 5 and 8. Initial degradation rate decreases at higher pH, but complete degradation is nevertheless achieved in the presence of sufficient Fe:EDDS concentrations. The fact that the contaminants are eliminated in the presence of relatively high DOC values (about 2 orders of magnitude greater) is especially promising.

The results obtained from the solar simulator provide a very good estimate of the behavior of the pilot-scale CPC solar photo-reactor in terms of Q_{UV}. Due to the limited irradiated area of the reactor in the solar simulator, the process was significantly longer. In the CPC however,

82

the amount of radiation necessary for achieving complete degradation was reached within just a few minutes.

A correlation has also been made between iron precipitation and accumulated UV radiation. Further research is definitely required but it could allow for an empirical estimation of optimal Fe:EDDS ratios with respect to different applications.

3.3. USE OF EDDS FOR THE TREATMENT OF HIGHLY CONTAMINATED WATER

3.3.1. OBJECTIVES OF THIS SECTION

The use of EDDS in the context of microcontaminant degradation in WMTP effluent was evaluated above. While undoubtedly successful, it raises the question whether such treatment could also be viable when considering higher contaminant concentrations. While treatment of highly contaminated water (such as agricultural or industrial wastewater) with classical photo-Fenton has been studied extensively [75], the comparative use of Fe(III)-EDDS at neutral pH for high contaminant concentrations has never been evaluated. This section aims to provide a critical view towards the benefits and limitations of substituting the classical photo-Fenton process at acidic pH with Fe (III)-EDDS at near-neutral pH, under realistic conditions and using natural water.

The major objectives of this study are: 1) Determine the possibility of using Fe(III)-EDDS in waters containing significant levels of carbonate/bicarbonate 2) Explore the oxidative potential of Fe(III)-EDDS assisted treatment in different aeration conditions 3) Determine how temperature affects the photolysis of the Fe(III)-EDDS complex and whether it could prove detrimental for solar-driven treatments 4) Comparative kinetics between classical photo-Fenton at pH 2.8 and Fe(III)-EDDS assisted treatment, while estimating differences in acute toxicity during and following the treatment. All experiments were done with high concentrations of the contaminant (in the range of 60 mg L^{-1}), which have not been tested before with Fe(III)-EDDS and at near-neutral pH.

Imidacloprid, a neonicotinoid systemic insecticide has been used as a model compound for this study. It is among the most widely used insecticides in the world and has been classified by the European Food Safety Authority as presenting a high acute risk to several animal species, especially to honeybee populations. While persistent in soils, it is subjected to aqueous photolysis [111] (half life in surface water of 4 hours, but minimal in the timeframe

of current experiments) and is soluble enough in water to attain the desired high concentrations.

3.3.2. MATERIALS AND METHODS

3.3.2.1. REAGENTS

Iron source $Fe_2(SO_4)_3 \cdot H_2O$ (75% purity) and (S,S)- ethylenediamine- N,N´dissucinic acid trisodium salt solution (35%) were both provided by Sigma Aldrich. Hydrogen peroxide (30% w/v) was purchased from Pancreac. Sulfuric acid (96%) and sodium hydroxide were obtained from J.T.Baker. Imidacloprid of 97% purity was provided by Bayer Hispania S.A. (Barcelona, Spain). Acetonitrile (ACN) for the HPLC mobile phase was HPLC-grade and provided by Sigma-Aldrich. Millipore Nylon 0.2 μm filters were used for the preparation of samples for HPLC, dissolved organic carbon, dissolved iron and H_2O_2 analyses.

3.3.2.2. ANALYTICAL METHODS

Imidacloprid concentrations were monitored with an Agilent 1100 series High Pressure Liquid Chromatography (HPLC) equipped with a C18 column (Supelcosil LC-18, 5 μm particle size, length 15 cm, i.d. 3 mm). A mobile phase of 25 mM formic acid/acetonitrile was used at 80/20 ratio. Flow rate was 0.5 ml min^{-1}. The UV signal was recorded at 270 nm. All samples were prepared by diluting 8 ml of sample with 2 ml of acetonitrile.and filtered through a 0.2 μm syringe-driven filter prior to analysis. The introduced acetonitrile was sufficient to interrupt any Fenton or Fenton-like reactions (checked against a standard). The injected volume for all samples was 20 μL.

Acute toxicity was followed by measuring the inhibition of bioluminescence intensity of the microorganism *Vibrio fischeri*. A commercial BioFix Lumi Luminescent kit was used. Hydrogen peroxide present in the samples was removed prior to analysis by using catalase (2500 U mg^{-1} bovine liver; 50 mg L^{-1}) acquired from Fluka Chemie AG (Buchs, Switzerland). The pH of all samples was adjusted to between 6 and 8, and the salinity to 2% NaCl. The change in bioluminescence was measured after 5, 15 and 30 minutes and compared against an Imidacloprid-free control (2% NaCl solution). The toxicity results shown in this work are from the inhibition observed at 30 minutes.

Total organic carbon, hydrogen peroxide and iron concentrations were monitored with the same procedure as described in section 2.2.2.

3.3.2.3. COMPOSITION OF NATURAL WATER

Experiments in natural water were conducted by using tap water from the groundwater well of Plataforma Solar de Almeria. CO_3^{2-}/HCO_3^- were measured as inorganic carbon load (IC). For stripping the water of carbonates, H2SO4 was added until IC was lower than 5 mg L^{-1}.The pH was not significantly modified in the process. Some important physicochemical characteristics of the water can be seen in Table 3.4.

Table 3.4.. Ion composition and properties of the water matrix used in the experiments.

Ions (mg L^{-1})	Tap water	Tap water
Mg^{2+}	21	21
Ca^{2+}	25	24
K^+	4	5
Na^+	203	179
Cl^-	136	120
NO_3^-	4	4
SO_4^{2-}	75	320
pH	7.15	6.88
Conductivity	0.9	1.0
TOC (mg L$^-$	1.5	1.5
IC (mg L^{-1})	98	3

3.3.2.4. EXPERIMENTAL SET-UP AND PROCEDURE

Experiments in both CPC and in the solar simulator were conducted in the same systems as described in section 3.2.2.4. Normalization of accumulated energy was done in all experiments with the use of eq. 3.1.

3.3.3. RESULTS AND DISCUSSION

The concentration of Imidacloprid for all experiments was 60 mg L^{-1}. This choice was made so as to evaluate the viability of this process for treating wastewater containing high concentrations of contaminants. In this way, the TOC of the contaminant is equal to the TOC introduced to the water by the addition of 0.2 mM of EDDS (25 mg L^{-1} each, for a total of 50 mg L^{-1}).

3.3.3.1. EFFECT OF CARBONATES

As demonstrated in previous work [106], the presence of HCO_3^-/CO_3^{2-} had little detrimental effect during the EDDS modified Fenton-like treatment of a MWTP effluent containing a mixture of 15 contaminants at 5 µg L^{-1} each (75 µg L^{-1} in total). This has been attributed to the main action of $HO_2\cdot/O_2\cdot^-$ radicals formed during the photodegradation of Fe (III)-EDDS via reactions 3.10-3.12.

$$Fe(III)\text{-}EDDS + hv \rightarrow Fe^{2+} + EDDS^\bullet \qquad\qquad \text{React. 3.10}$$

$$EDDS^\bullet + O_2 \rightarrow product + O_2^{\bullet-} \qquad\qquad \text{React. 3.11}$$

$$HO_2^\bullet \leftarrow\rightarrow H^+ + O_2^{\bullet-} \qquad\qquad \text{React. 3.12}$$

As the reactivity of both $HO_2\cdot/O_2\cdot^-$ radicals with bicarbonate is much lower compared to that of $HO^\bullet$, the scavenging effect is expected to be minimal [99],[112].

The degradation of Imidacloprid as well as the iron kept in solution are presented in figure 5.1. With the intention of demonstrating the importance of React 3.10-React. 3.12 in the overall process, experiments were repeated with and without H_2O_2 (effectively with and without $HO^\bullet$). The Fenton-like process (H_2O_2 addition) was able to remove more than 90% of Imidacloprid in the absence of HCO_3^-/CO_3^{2-}, with an accumulated UV energy of about 2 kJ L^{-1}. In the presence of carbonates however, only 30% removal was reached. Total Fe precipitation occurred within a few minutes of illumination almost simultaneously in both cases. All tests were done at near-neutral pH.

Without addition of H_2O_2 the degradation efficiency was also between around 30%, independently of the presence of HCO_3^-/CO_3^{2-}. Fe was maintained in solution for longer in the absence of carbonates. This is in accordance with the behavior observed by Miralles et al [113] in which carbonates have been shown to have a destabilizing effect on the soluble iron. Degradation performance was not affected, as is expected when Fenton type reactions do not occur.

Considering the similarities in performance between $Fe(III)\text{-}EDDS/H_2O_2/HCO_3^-$ and $Fe(III)\text{-}EDDS/no\ H_2O_2/\ no\ HCO_3^-$ (only dissolved oxygen), it appears that adding H_2O_2 has no benefits in carbonated water. This verifies the scavenging of all generated $HO^\bullet$, making the contribution of the classical Fenton reaction (React. 1.5) practically negligible.

However, as about 18 mg L^{-1} of imidacloprid are degraded in all cases, alternative degradation mechanisms via $EDDS^\bullet$ and $O_2^{\bullet-}$ radical are most likely not affected (React 3.11 and React. 3.12). This is important because it suggests that the action of Fe(III)-EDDS in

natural water containing carbonates is not related to Fenton chemistry at all, and that addition of H_2O_2 is wasteful, generating $HO^•$ that will be immediately scavenged. It should be noted that the oxidation potential of $O_2^{•-}$ is significantly lower that of $HO•$ (0.94 compared to 2.31 V) [114] so only weaker bonds can be successfully oxidized. In the case of Imidacloprid, this can due to dissociation of the C-Cl or N-NO_2 bonds, both with relatively low dissociation energies of 3.4 eV [115] and 1.9 eV [116]. While Cl^- release could not be followed due to interference by the chloride naturally present in the water, the dechlorination of Imidacloprid has been shown in previous work to be very rapid [117]. In the same work, no transformation products containing the N-NO_2 bond were found. Additionally, dechlorination of pentachlorophenol [118] and carbon tetrachloride [119] has also been observed by the action of superoxide radicals alone. Although the achieved degradation percentage is limited, it could prove sufficient for removal of relatively low concentrations of contaminants without requiring pretreatment or H_2O_2 addition. Therefore, previous results obtained by other authors in which Fe(III)-EDDS/H_2O_2/HCO_3^- efficiently removed a few hundred µg L^{-1} of contaminants at neutral pH could be mainly attributed to $HO_2•$/$O_2•^-$ radicals (React 3.11 and React 3.12) and not to the photo-Fenton process. However, Fe(III)-EDDS/H_2O_2/HCO_3^- is not efficient for removal of contaminants in the tens of mg L^{-1} range.
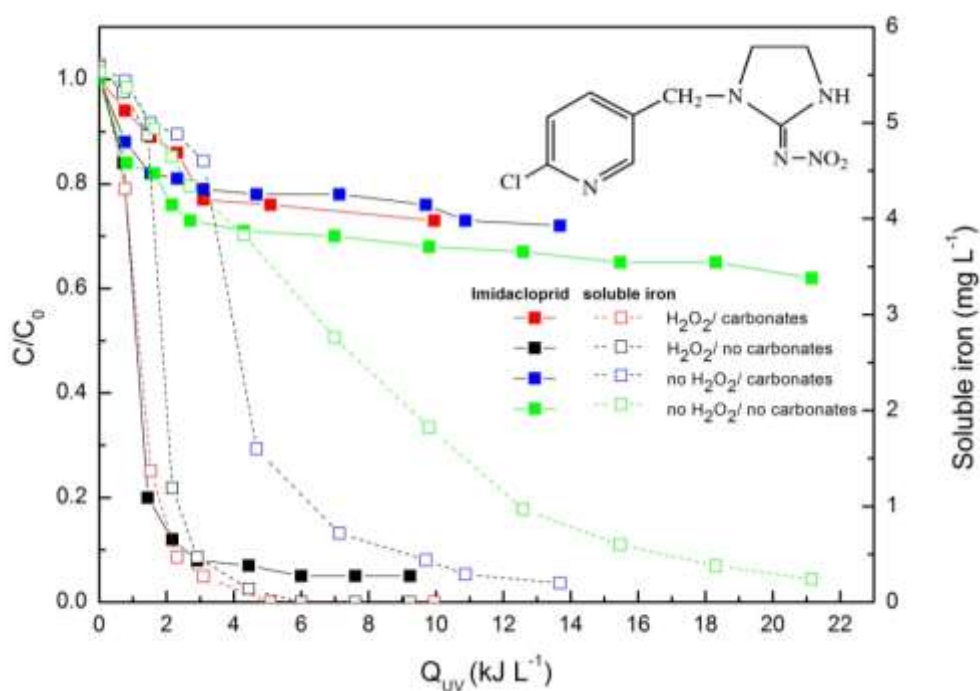
Fig.3.5. Degradation of 60 mg L^{-1} Imidacloprid and evolution of iron in solution in natural water with and without HCO_3^-/CO_3^{2-} at pH 6.8 and with 0.1:0.2 mM of Fe:EDDS in CPC reactor. The structure of Imidacloprid can be seen in the upper-right corner.

3.3.3.2. EFFECT OF OXYGEN SATURATION AND DEPRIVATION

As demonstrated above, the presence of carbonates inhibits the Fenton-like process, so any degradation most likely occurs only through the action of $EDDS^{\bullet}$, $O_2^{\bullet-}$ and $HO_2^{\bullet}$ (the latter contributing mainly at lower pH). As the pathways leading to the generation of $HO_2\cdot/O_2\cdot^-$ radicals (React 3.11 and 3.12) are dependent on the presence of oxygen, it is of interest to evaluate the influence of different aeration conditions. A series of experiments have been conducted with the purpose of comparing oxygen saturated (bubbling pure oxygen to keep dissolved oxygen > 15 mg L^{-1}) and deprived (bubbling N_2 to keep dissolved oxygen < 1 mg L^{-1}) variants of the Fe(III)-EDDS treatment in the presence and absence of H_2O_2. Experiments were also done in distilled water to compare reaction rates and to avoid complications due to natural water constituents and carbonates affecting reactions 3.10-3.12.
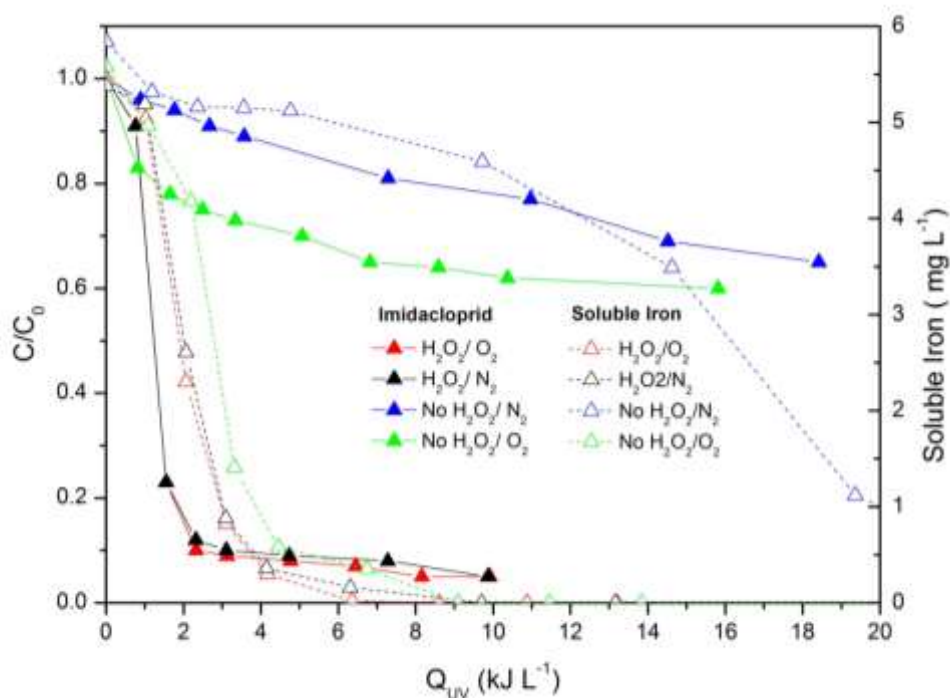
Fig.3.6. Degradation of 60 mg L^{-1} of Imidacloprid in distilled water and evolution of soluble iron at pH 6.8 in presence and absence of O_2 and/ or H_2O_2.

As seen in figure 3.6., the behavior of the Fenton-like processes (presence of H_2O_2) under both aeration conditions are identical. More than 90% degradation was achieved, requiring only about 2 kJ L^{-1} of UV energy. The loss of soluble iron is similarly unaffected, with complete precipitation occurring shortly after the removal of the contaminants.

In the absence of H_2O_2, a degradation percentage of around 40% was achieved in both cases, but with the initial rate clearly faster in conditions of oxygen abundance. This

highlights the importance of reactions React. 3.11 and 3.12 in the presence of oxygen (30% degradation at around 5 kJ L^{-1}). The degradation stops once most of the Fe precipitates. In oxygen deprived conditions (via nitrogen bubbling) the reaction rate was clearly slower (10% degradation at around 5 kJ L^{-1}). However, as Fe was kept in solution longer (most likely due to the slower oxidation of Fe^{2+} to Fe^{3+}), degradation of Imidacloprid continued (at a slower rate), eventually reaching a similar degradation percentage of around 40%.

The degradation percentage in the presence of oxygen eventually reaches a plateau at around 40%, a 10% increase from the one observed in natural water. As $O_2^{\bullet-}$/$HO_2^{\bullet}$ can also promote the production of H_2O_2 via reactions with Fe^{2+} (React. 3.13 and 3.14), it can consequently lead to a mild Fenton/photo-Fenton reaction. This 10% difference could then be attributed to the action of HO$^{\bullet}$, observed only in the absence of scavenging species in demineralized water.

$$Fe^{2+} + O_2^{\bullet-} + 2H_2O \rightarrow Fe^{3+} + H_2O_2 + 2OH^- \qquad k=1\times10^7 \text{ M}^{-1}\text{ s}^{-1} \qquad \text{React. 3.13}$$

$$Fe^{2+} + HO_2^{\bullet} + H^+ \rightarrow Fe^{3+} + H_2O_2 + OH^- \qquad k=1.2\times10^6 \text{ M}^{-1}\text{ s}^{-1} \qquad \text{React. 3.14}$$

The photochemical efficiency of 0.1 mM Fe(III)-EDDS(at 1:1 ratio) has also been evaluated for the treatment of 7.5 mg L^{-1} of 4 tert butylphenol at pH 4.0 [44].The deprivation of oxygen in that case appeared to have a much stronger detrimental effect, with a difference of about 25% in the final degradation percentage between the two treatments. Given that the pKa of React 3.12 is 4.86 [120] the $HO_2^{\bullet}$/$O_2^{\bullet-}$ equilibrium in the experimental conditions of Wu et al should be in favor of $HO_2^{\bullet}$, favoring the oxidation and consequent precipitation of iron, as $k_{Fe(II),HO2\bullet}/k_{Fe(III),HO2\bullet}>1.2\times10^3$ (comparing React. 3.15 and React. 3.16). At the pH of this work (6.8), the dominance of $O_2^{\bullet-}$ contributes to maintaining iron in solution by promoting Fe^{3+} reduction at a rate 5 times faster than its oxidation (comparing React. 3.13 and React. 3.15)

$$Fe^{3+} + O_2^{\bullet-} \rightarrow Fe^{2+} + O_2 \qquad k=5\times10^7 \text{ M}^{-1}\text{ s}^{-1} \qquad \text{React. 3.15}$$

$$Fe^{3+} + HO_2^{\bullet} \rightarrow Fe^{2+} + O_2 + H^+ \qquad k<1\times10^3 \text{ M}^{-1}\text{ s}^{-1} \qquad \text{React. 3.16}$$

Near-neutral pH values are therefore expected, in the absence of H_2O_2, to aid iron to remain in solution for longer due to the presence of $O_2^{\bullet-}$. Additionally, the use of excess EDDS in the current work (at 1:2 ratio), means that re-complexation of liberated iron is possible, leading to increased efficiency (explained in further detail in section 3.3.3.3) These results suggest that species other than HO•, generated during the photodegradation of Fe(III)-EDDS, can have an important effect in natural water, provided it is sufficiently aerated. The complex constituents of natural water and the presence of carbonates do not adversely affect the action of these species permitting some limited treatment of contaminants at neutral pH

without the need for carbonate removal. It is however clear that treating large concentrations is not possible using Fe(III)-EDDS, as continuous addition of EDDS would be necessary, significantly increasing the total organic carbon content of the water.

3.3.3.3. EFFECT OF TEMPERATURE

One of the advantages of the classical photo-Fenton process is that it can function without significant drawbacks at temperatures between 35-45°C, which are common in solar-driven processes. It has been previously shown [64] that the performance of the photo-Fenton process increases at higher temperatures, until a maximum of 42°C, above which loss of iron was observed. This could be attributed mainly to the accelerated formation kinetics of ferric hydroxides (React. 3.17- React. 3.19).

$$Fe^{3+} + H_2O \longleftrightarrow FeOH^{2+} + H^+ \qquad\qquad\qquad \text{React. 3.17}$$

$$FeOH^{2+} + H_2O \longleftrightarrow Fe(OH)^{2+} + H^+ \qquad\qquad\qquad \text{React. 3.18}$$

$$Fe(OH)^{2+} + H_2O \longleftrightarrow Fe(OH)_3 \downarrow + H^+ \qquad\qquad\qquad \text{React. 3.19}$$
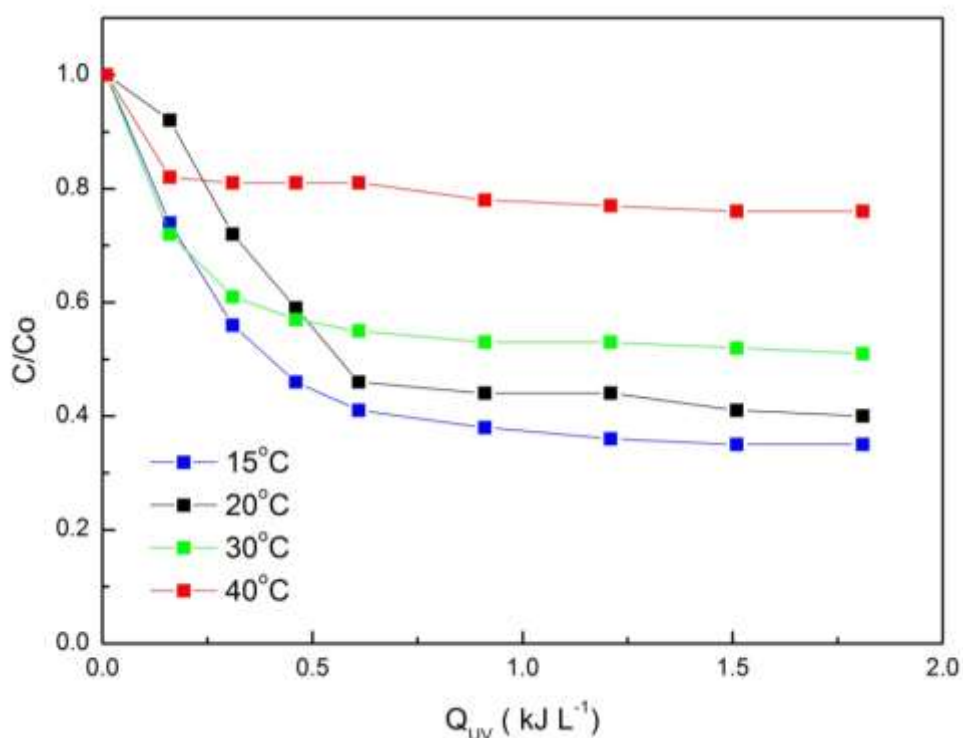

Fig.3.7. Effect of temperature on the degradation of 60 mg L^{-1} of Imidacloprid in natural water containing CO_3^{2-}/HCO_3^- at pH 6.8 with 0.1:0.2 mM of Fe:EDDS.
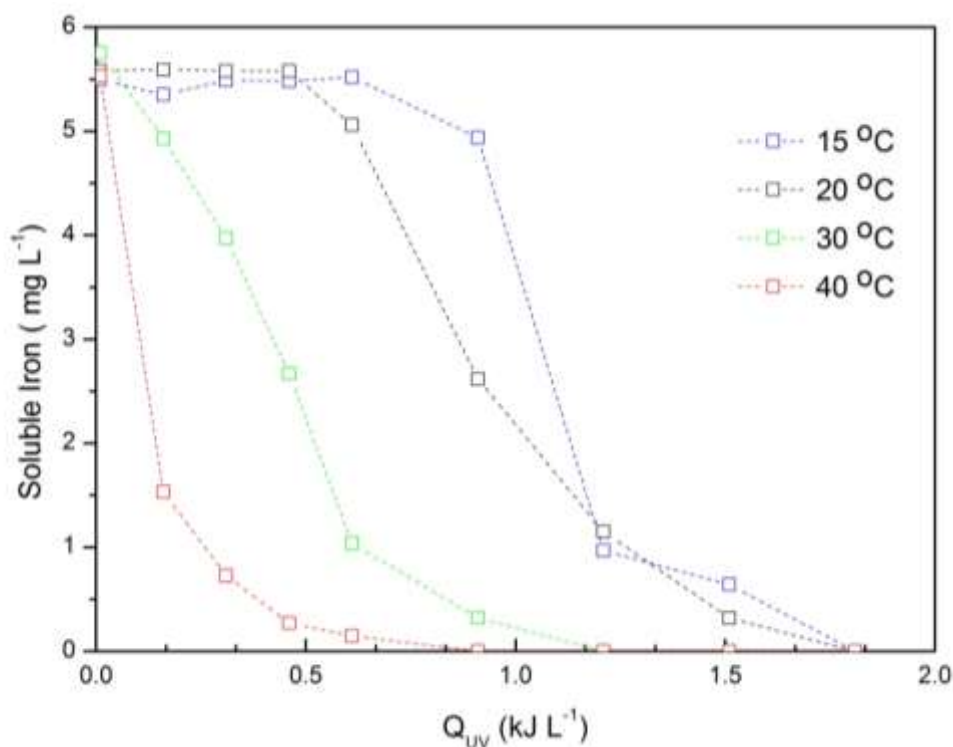
Fig. 3.8. Effect of temperature on the stability of soluble iron in solution during the treatment of 60 mg L^{-1} of Imidacloprid in natural water containing CO_3^{2-}/HCO_3^- at pH 6.8 with 0.1:0.2 mM of Fe:EDDS

A series of experiments in natural water were done in order to observe what is the effect of temperature in the alternative Fe(III)-EDDS system. As temperature control is not easily achieved in a CPC reactor, the experiments were conducted in a 1.5 L pyrex vessel placed within a solar simulator. Imidacloprid solutions were kept at different initial temperatures of 15°C (under refrigeration), 20°C, 30°C and 40°C (in a small incubator with a temperature controller). The solutions were rapidly transferred to the simulator where Fe(III)-EDDS, H_2O_2 were added. The solutions were then illuminated with simulated sunlight with a corresponding UVA irradiance of 30 W m^{-2}. Initial pH of all solutions was 6.8. As can be seen in figures 3.7 and 3.8, increasing temperatures led to faster iron precipitation and lower efficiencies. Although the difference between 15°C and 20°C was minimal, starting from a temperature of around 30°C the loss of efficiency becomes significant. As such temperatures are very common during solar-driven treatments, this temperature dependence presents an important limitation. The changes in pH were also followed during the process, decreasing to 6.4 at 30°C and 40°C and to 6.1 for the 15°C and 20°C experiments. As mentioned before, the same FeL$^-$ form [44] of the Fe:EDDS complex is predominant at the 5-8 pH range. As the pH remained within this range, one can assume that it didn't affect the process in any significant way. According to figures 3.7 and 3.8, degradation efficiency and iron availability

appear to be correlated. In the experiments at T=15°C and 20°C, no loss of iron was observed until the accumulated UV radiation in the system reached 1 kJ L^{-1}. The degradation process however began almost immediately, suggesting that the breakup of the Fe:EDDS complex (and therefore the liberation of iron) had already started. As the predominant Fe:EDDS complex at pH 6.8 is FeL$^-$ (Fe:EDDS ratio is 1:1) [44] and EDDS is always present in an excess of 2:1 in relation to iron, it can be expected that almost the entirety of the excess EDDS remains free in solution. The fact that iron does not start precipitating immediately despite the pH of 6.8 is suggestive that no insoluble oxyhydroxy complexes are formed initially. This can be possible if the Fe^{3+} released from the Fe(III)-EDDS photolysis is preferentially re-complexed with the excess EDDS forming Fe(III)-EDDS, thus kept soluble and able to participate in a homogeneous photo-Fenton like process as per React. 3.20- React. 3.22

Fe(III)-EDDS + hv → Fe^{2+} + EDDS•   React. 3.20

Fe^{2+} + H_2O_2 → Fe^{3+} + HO• + HO$^-$ React. 3.21

Fe^{3+} + EDDS → Fe(III)-EDDS   React. 3.22
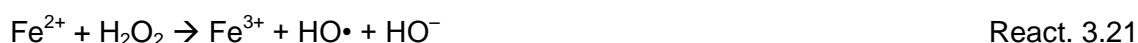
Iron precipitation begins once all of the excess EDDS is depleted. The accelerated precipitation of iron at higher temperatures may be caused by either of the following two reasons (or a combination of both): 1) Increased kinetics of $Fe(OH)_3$ formation (React. 3.17 3.19) at increased temperatures, possibly overcoming the re-complexation kinetics of Fe^{3+} via React. 3.22) Increased kinetics of Fe(III)-EDDS photolysis (React. 3.20), leading to faster depletion of EDDS and faster accumulation of Fe^{3+} in solution. Higher Fe^{3+} concentrations may then contribute to the faster formation of insoluble species. In any case, the excess EDDS is not efficiently utilized. Therefore, use of Fe(III)-EDDS is not recommended for long solar treatments in which there may be significant temperature increase.

3.3.3.4. COMPARISON BETWEEN CONVENTIONAL PHOTO-FENTON AT PH 2.8 AND FE:EDDS ASSISTED TREATMENT AT NEAR NEUTRAL PH.

The use of Fe(III)-EDDS at near-neutral pH has been compared with photo-Fenton at pH 2.8. The comparison has been made in natural water stripped of carbonates, as efficient treatment of high contaminant concentrations with either of the two processes has been demonstrated to be impossible in their presence
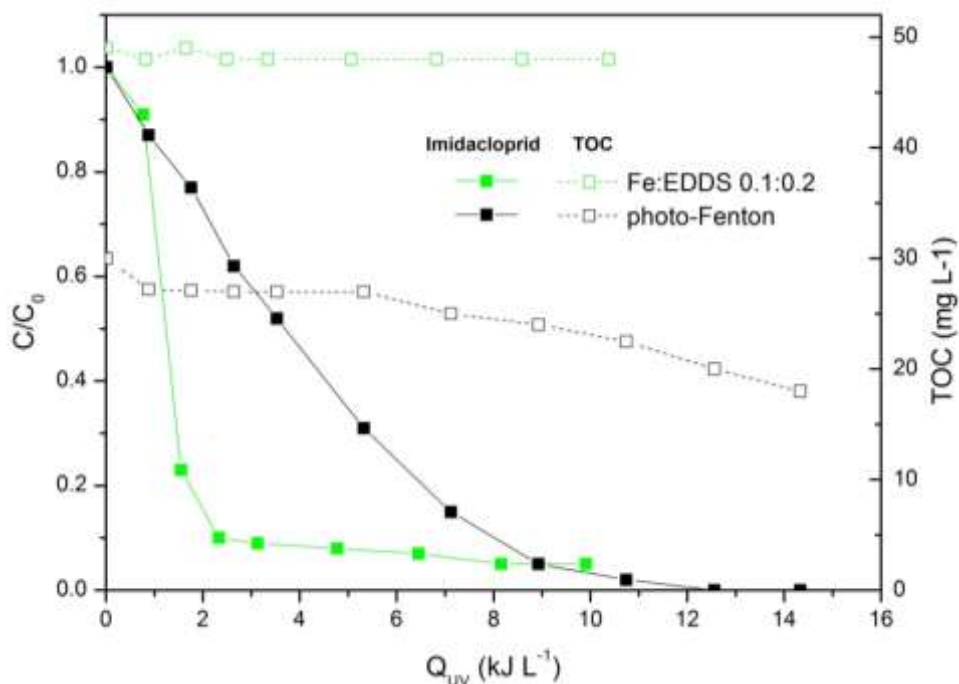
Fig.3.9. Comparison of degradation of 60 mg L^{-1} of Imidacloprid treated with conventional photo-Fenton (0.1 mM of Fe, TOC 25 mg L^{-1}, pH 2.8) and Fe:EDDS (0.1:0.2/TOC 50 mg L^{-1}, pH 6.8) in natural water stripped of carbonates.

As seen in figure 3.9, the initial degradation of Imidacloprid is very fast with Fe(III)-EDDS at near-neutral pH, with more than 90% of it removed with an accumulated UV radiation of about 1 kJ L^{-1}. 90% removal with conventional photo-Fenton at pH 2.8 required about 9 kJ L^{-1} of UV radiation. This difference could be attributed to the higher photoactivity of Fe(III)-EDDS compared to that of the aqua complexes (mainly [Fe(H$_2$O)$_5$(OH)]$^{2+}$) that usually participate in photo-Fenton. Fe^{2+} is more rapidly released and becomes available for reacting with H$_2$O$_2$. However, after the complex is photodegraded and the excess EDDS depleted, iron rapidly precipitates and the process stops. TOC degradation was negligible. Note that by using conventional photo-Fenton the initial TOC was lower and a substantial percentage (30%) was mineralized after receiving 14 kJ L^{-1} of UV radiation). .Photo-Fenton proves more robust as Fe(III)-EDDS was unable to lead to any TOC mineralization. EDDS degradation led to the process stopping, while conventional photo-Fenton was able to continue for as long as H$_2$O$_2$ was available.

3.3.3.5. TOXICITY CONCERNS

The two processes have also been evaluated in terms of changes in toxicity. The toxicity of Fe(III)-EDDS alone (without imidacloprid and without hydrogen peroxide) at a ratio of 0.1:0.2

mM has also been followed under solar illumination. Neither mineralization nor toxicity was observed.
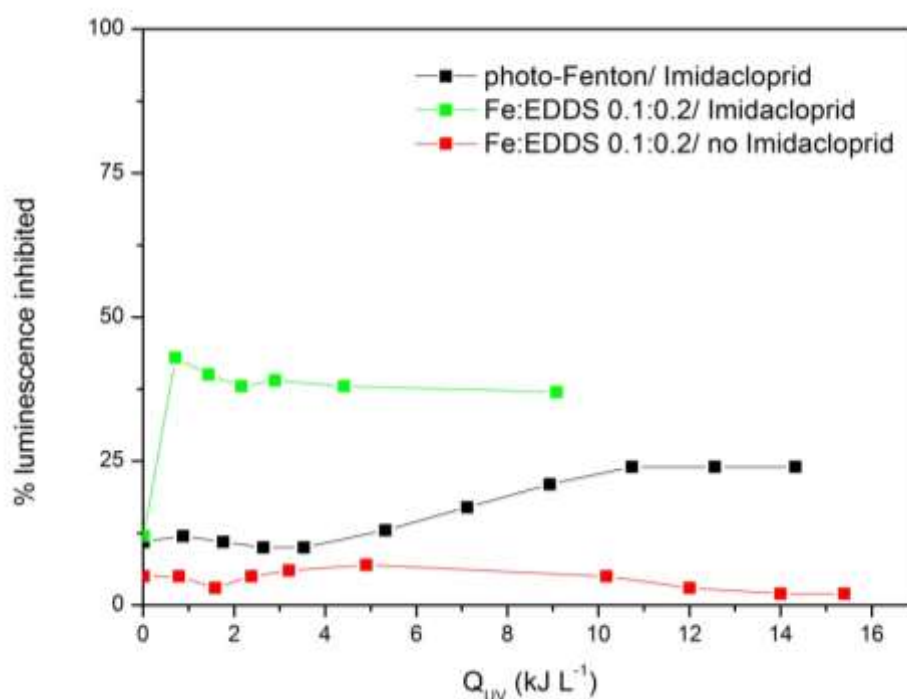
Fig.3.10. Percentage of *V.fischeri* luminescence inhibited following 30 minutes of incubation with each of the samples.

It should be clarified that this test does not have predictive value and is used for comparative purposes only. Within this context, it can be seen in figure 3.10 that Fe:EDDS treatment of Imidacloprid leads to a faster rise in toxicity levels than conventional photo-Fenton. As Fe(III)-EDDS and its photolysis transformation products have been demonstrated as non-toxic, this behavior could possibly be attributed to the faster accumulation of toxic Imidacloprid intermediates. When conventional photo-Fenton was applied, the rise in toxicity was gradual. Accumulation of toxic intermediates should be slower due to both slower reaction rates and, partly, due to simultaneous mineralization (as seen in fig. 3.9). Lack of control over mineralization (due to EDDS/contaminant TOC being impossible to distinguish) and the uncontrolled photodegradation of the complex can lead to the process stopping when potentially dangerous intermediates are still present in significant concentrations. As seen in this case, this can be a problem even when photo-Fenton with Fe(III)-EDDS is unhindered by the presence of carbonates.

While definitely not conclusive, these results are indicative of the dangers associated with the lack of mineralization control when using Fe(III)-EDDS. This is not necessarily

detrimental when treating emerging contaminants, but the accumulated intermediates of high TOC effluents could introduce significant toxicity concerns.

3.3.4. CONCLUSIONS

Some of the benefits and limitations of the use of the Fe (III)-EDDS complex have been studied:

Benefits

- Photolysis of Fe(III)-EDDS generates radical species that are able to act independently of carbonate scavengers that are often present in natural waters. This is clearly of interest in cases where radical species different to $HO^{\bullet}$ could be sufficient (e.g for some classes of microcontaminants)

- The generation of the $HO_2 \cdot /O_2 \cdot /EDDS \cdot$ species involved is dependent on aeration but not on the presence of H_2O_2. They are produced even in low aeration conditions, although at a slower rate.

- Emerging contaminants in the concentration range of ng L^{-1} to a few mg L^{-1} (as found in municipal wastewater) could be treated via the photolysis of the complex in the water´s natural pH with minimal pre-treatment.

- The toxicity of the initial complex as well as of the intermediates generated via its photolysis is nil.

Limitations

- The reactive oxygen species formed due to the Fe(III)-EDDS photolysis ($O_2 \cdot^-/HO_2 \cdot$) do not have the high oxidation potential of the hydroxyl radical so not all compounds are fully treatable. Immediate application of the process in natural water should be evaluated on a case-by-case basis.

- Treatment of high concentrations of contaminants or achieving mineralization is difficult as continuing treatment requires adding more and more EDDS. This leads to a non-sustainable process with increasing TOC instead.

- The decreased performance observed at elevated temperatures can present a problem when considering solar applications. Conventional photo-fenton on the other hand is comparatively robust in terms of temperature stability.

In conclusion, Fe:EDDS should only be considered for relatively mild treatment of emerging contaminants, provided that some temperature control is also in place. Photo-Fenton remains a more robust solution for highly contaminated water streams.

CHAPTER 4:

ENHANCEMENT OF THE FENTON AND PHOTO-FENTON PROCESSES BY COMPONENTS FOUND IN WASTEWATER FROM THE INDUSTRIAL PROCESSING OF NATURAL PRODUCTS; THE POSSIBILITIES OF CORK BOILING WASTEWATER REUSE.

4.1. INTRODUCTION

In chapter 3 we saw how the iron-complexing agent EDDS can affect the photo-Fenton process. Apart from artificial ligands such as EDDS, efforts have also been made to estimate how components present in natural waters (lakes, rivers) can also stabilize and promote these processes at near-neutral pH [121]. Most of these components are likely products of natural vegetative or animal decay (e.g. humic acids, tannic acids, gallic acids, pyrogallol). Theis and Singer [122] have mentioned that iron complexes with these types of compounds can retard oxidation of Fe^{2+} to Fe^{3+} while Fe^{3+} to Fe^{2+} reduction is concurrently taking place.

Such type of phenolic/polyphenolic components however can also form a significant fraction of industrial wastewaters originating from the processing of natural products. Cork production industry [54] olive mills [55]**,** wineries [56]**,** tea manufacturing industry [57]. Polyphenols such as gallic acid and tannins have been studied as model pollutants present in these types of water [123]**.** Such studies however ignore the capacity of these compounds to form stable complexes with iron at a wide pH range [124], thus contributing to its availability for application of photo-Fenton. At the same time, as polyphenolic compounds are gradually oxidized, quinone derivatives may begin to accumulate. These have been described as key to Fe^{3+} reduction in the dark [22], leading to autocatalytic behaviour within the system. The reduction rates of Fe^{3+} species through dark pathways depend on the ambient redox potential of the reaction mixture. Aromatic compounds in particular are hydroxylated and yield hydroquinone-like intermediates. Irradiation of aromatic carboxylate complexes has also been linked to an enhancement of the photo-Fenton process[125].

The purpose of this work is to demonstrate that some wastewaters containing phenolic or tannin components can also actively participate in and even enhance Fenton and photo-Fenton reactions both by increasing iron availability at higher pH and by contributing to the reduction of Fe^{3+}, facilitating treatment or even enhancing, in some specific cases, the treatment of other types of wastewater by an appropriate mixing. Instead of using artificial iron-complexing ligands to enhance photo-Fenton (such as oxalate or EDDS), this work could open up the possibilities of industrial wastewater reuse for this type of applications.

Cork Boiling Wastewater (CBW) has been selected as a representative wastewater of this type, as it contains a large fraction of polyphenolic components and has not been studied extensively. It is mainly the result of boiling the bark of the Quercus suber tree in water in order to refine some of its properties. Although the boiling time is approximately one hour, the same water is reused multiple times (typically 20-30), eventually becoming highly concentrated in corkwood extracts (phenolic acids, tannins, 2,4,6-trichloroanisol, pentachlorophenol) [126]. As the generated volumes of CBW are high (more than 400 L per ton of cork produced), there are also significant economic and technical constraints concerning its treatment. So very often, despite the recalcitrance of the extracts to conventional biological treatment, this water is frequently discharged directly to water streams, leading to serious environmental impacts. As the Quercus suber tree is native to countries of southwest Europe and northwest Africa, the world's cork production industry is exclusively based in there, with more than 80% being in Portugal and Spain, and the rest in Morocco, Algeria, Tunisia, Italy and France. As they are all regions of ample sunlight, encouraging wastewater reuse for the enhancement of solar photo-Fenton can contribute to its already higher regional feasibility.

This work is focused on the following objectives:

1) Observe how CBW and some of the components present in it affect the stability of iron at a near- neutral pH range.

2) Determine what is the beneficial effect of CBW on the degradation/ mineralization of model compound imidacloprid (DOC = 30 mg L^{-1}) by Fenton and photo-Fenton processes at acidic and near-neutral pH values.

3) Verify if CBW and some of its polyphenolic components (gallic and tannic acid) can lead to a similar beneficial effect in a more complex contaminant mixture (phenol/ methomyl/ imidacloprid) at the same (30 mg L^{-1}) or higher (300 mg L^{-1}) DOC values.

4.2. MATERIALS AND METHODS

4.2.1. REAGENTS

Iron (III) sulfate   (Fe$_2$(SO$_4$)$_3$*H$_2$O, 75% purity) provided by Sigma-Aldrich was used as a source of iron. Reagent grade hydrogen peroxide (30% w/v) was provided by Pancreac. sulphuric acid and sodium hydroxide (for pH adjustment) were provided by J.T. Baker. Gallic acid (97% purity) was provided by Sigma-Aldrich, Tannic acid and phenol were provided by Merck. Methomyl (99.5% purity) was provided by Aragonesas Agro SA. Acetonitrile (ACN) for the HPLC mobile phase was HPLC-grade and provided by Sigma-Aldrich. Millipore Nylon

0.20 µm filters were used for the preparation of the samples for HPLC, TOC, soluble iron and H_2O_2 analyses.

4.2.2. ANALYTICAL METHODS

Pollutant concentrations were monitored with an Agilent 1100 series High Pressure Liquid Chromatography (HPLC) equipped with a C18 column (Supelcosil LC-18, 5 µm particle size, length 15 cm, i.d. 3 mm). For Imidacloprid, a mobile phase of 25 mM formic acid/acetonitrile was used at 80/20 ratio. Flow rate was 0.5 ml min^{-1}. The UV signal was recorded at 270 nm. For the phenol/ methomyl/imidacloprid mixture a mobile phase of H_2O/acetonitrile was used at a 80/20 ratio. Flow rate was 0.5 ml min^{-1}. UV signals were recorded at 210, 210 and 234 nm. All samples were prepared by diluting 8 ml of sample with 2 ml of acetonitrile.and filtered through a 0.2 µm syringe-driven filter prior to analysis. The introduced acetonitrile was sufficient to interrupt any Fenton or Fenton-like reactions (checked against a standard). The injected volume for all samples was 20 µL.Total Organic Carbon (TOC), H_2O_2 and total iron concentrations were measured with the protocols described in section 2.2.

4.2.3. COMPOSITION OF NATURAL WATER AND CBW.

Parameter	CBW	Natural water (stripped of CO_3^{2+}/HCO_3^-)
pH	7.4	6.9
Conductivity (mS cm^{-1})	1.9	1.0
Turbidity (NTU)	213	
TSS	249	
Chemical Oxygen Demand (COD)	1243	
Dissolved Organic Carbon (DOC)	748	1.7
Ions (mg L^{-1})		
Total Iron	3.4	
Na^+	60.6	165
NH_4	17.3	
K^+	254.7	7
Mg^{2+}	22.8	17
Ca^{2+}	113.6	21
Cl-	143	109
SO_4^{2-}	4.8	289

Table 4.1. Some characteristics of CBW and the natural water used in the experiments.

Cork Boiling Wastewater was collected from a cork processing plant located in San Vicente de Alcántara (Extremadura, Spain). All tests were performed at the Plataforma Solar de Almeria (Tabernas, Spain). No pre-treatment was effectuated in order to maintain the concentration of phenolic components intact. Natural water (groundwater) was acquired from the well of the Plataforma Solar de Almeria. CO_3^{2-}/HCO_3^- were stripped with H_2SO_4 prior to the experiments. Their characteristics are presented in Table 4.1.

4.2.4. EXPERIMENTAL SET-UP AND PROCEDURE

All experiments were conducted in a cylindrical Pyrex glass vessel (height 8.5 cm, diameter 19 cm, wall thickness 3.2 mm) placed on a magnetic stirrer. For the experiments with CBW, contaminant solution in natural water was mixed with the corresponding volume of CBW to a final volume of 1.5 L. pH was adjusted to the required value and the iron was added. pH was adjusted again following iron addition and the reaction was initiated with H_2O_2.

For Fenton experiments, the vessel was completely covered with aluminium foil to avoid penetration of light. Photo-Fenton experiments were conducted in an Atlas XLS Suntest solar simulator under constant illumination from a Xenon lamp with a constant UV irradiance of 30 W m^{-2} (typical solar UV power during a sunny day. The UV radiation was monitored throughout the a process with a SOLARLIGHT PMA2100 radiometer placed within the simulator.

4.3. RESULTS AND DISCUSSION

4.3.1. IRON AVAILABILITY IN CORK BOILING WASTEWATER

4 different dilutions of CBW with water were prepared (1:20, 1:50 and 1:100) and the pH set to values between 3 and 9. 10 mg L^{-1} of Fe^{3+} were added, the pH was readjusted and the solutions were left for one hour in order to reach equilibrium. Soluble iron was then measured for each solution. As seen in figure 4.1, at the lower dilution ratio (1:20) soluble iron even at pH 3 (optimal for classical Fenton) is limited. This suggests the presence of species in CBW that tend to form insoluble complexes with iron. At high dilution ratios (1:50 and 1:100), some iron is still lost at pH 3 (2.5 and 1.5 mg L^{-1} ,respectively) as fewer insoluble complexes are formed. 1:20 dilution aprovides higher robustness at higher pH values, while at 1:50 and 1:100, almost all iron is lost from pH 6 upwards. However, lower dilution ratios also introduce much greater organic carbon content, so a compromise is necessary.
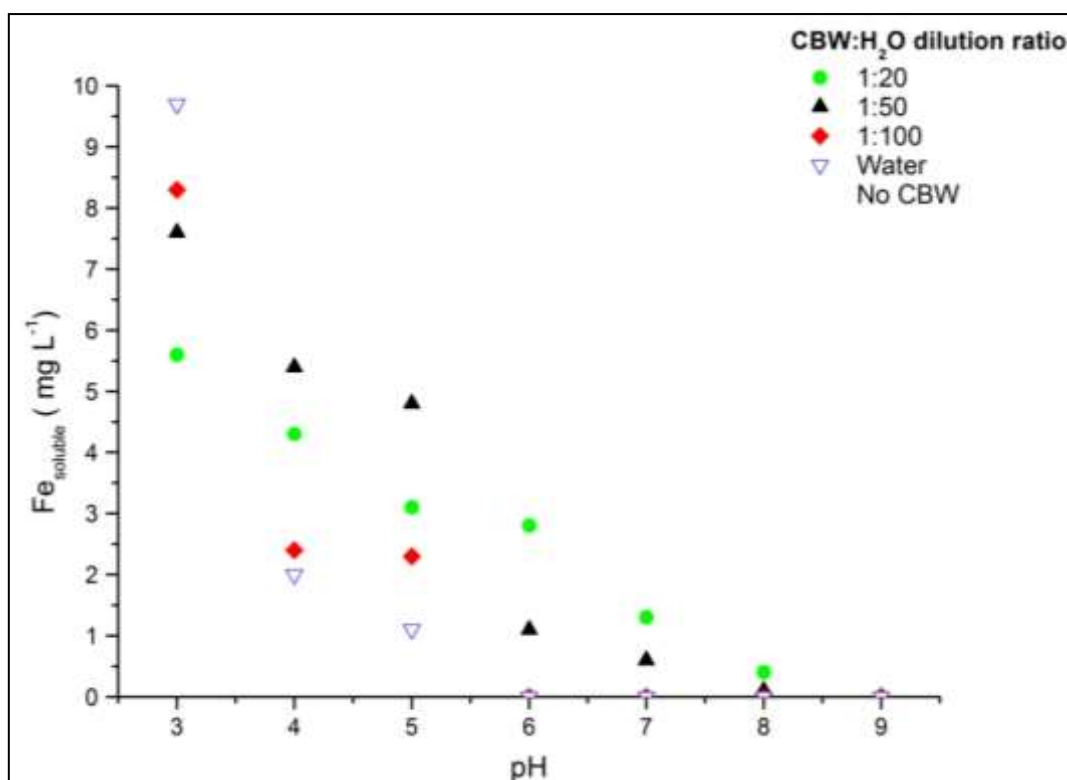
Fig. 4.1. Soluble iron in natural water containing CBW at different dilution ratios at the 3-9 pH range after 1 hour. Initial $[Fe^{3+}]$ added was 10 mg L^{-1}.

4.3.2. INFLUENCE OF CBW ON THE FENTON AND PHOTO-FENTON PROCESSES.

As the organic load of CBW is very high (DOC > 700 mg L^{-1}), evaluating the degradation of a relatively small quantity of contaminant (e.g. 70 mg L^{-1} of Imidacloprid) in undiluted CBW would be difficult due to the high competition for the generated radicals. In order to make a compromise between increased iron stability and modest DOC increase, some preliminary experiments with different dilution ratios were tested at pH 5 (highest pH with significant iron stability for the different dilution ratios) in the dark (Fenton). At lower dilution ratios (1:20), imidacloprid degradation rate was low due to a significant competition with the organic components of CBW for the radical species generated by the Fenton reaction. At high dilution ratios (e.g. 1:100), imidacloprid degradation rate was also low as the concentration of phenolic/polyphenolic components was too low in order to enhance Fenton reactions either by increasing iron availability or by contributing to the reduction of Fe^{3+}. A dilution ratio of 1:50 was chosen for subsequent experiments (15 mg L^{-1} increase of DOC) as imidacloprid degradation rate was the highest.
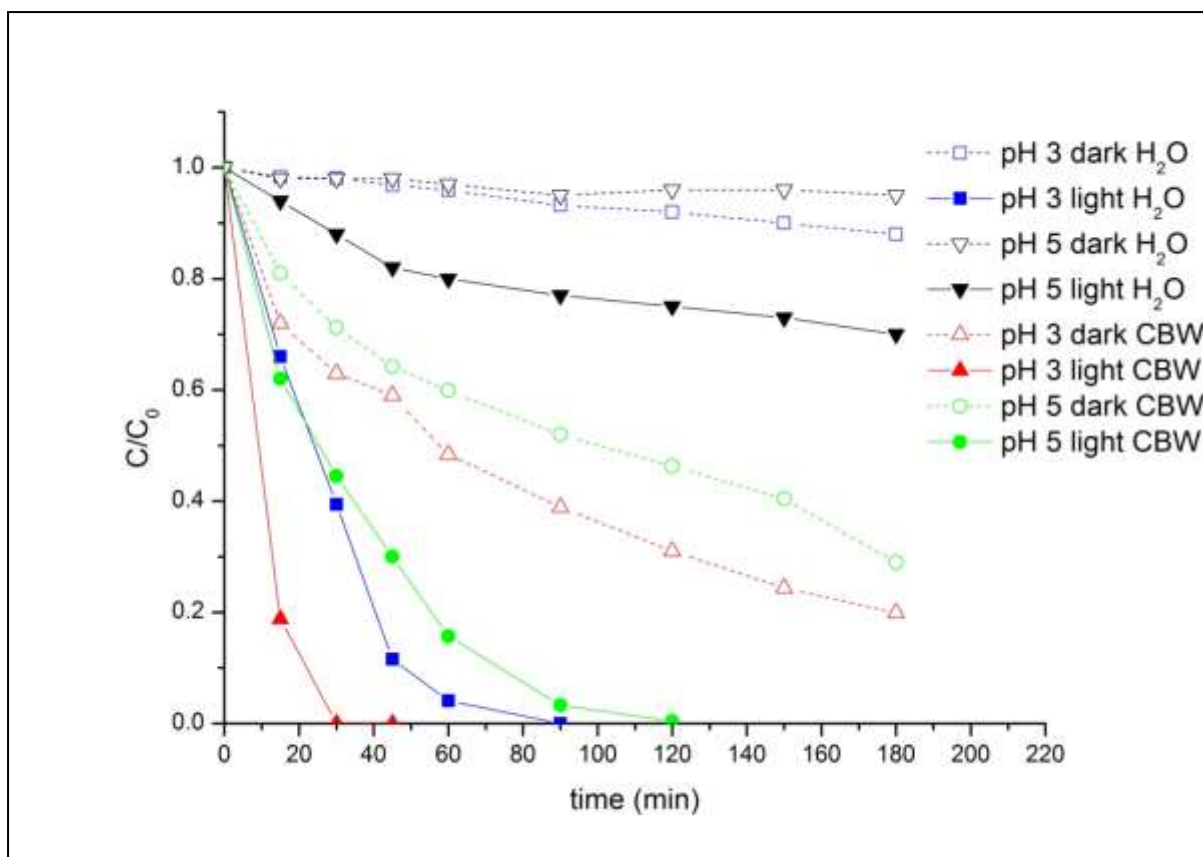
Fig. 4.2. Degradation of 70 mg L^{-1} of Imidacloprid in cork boiling wastewater (CBW) diluted 1:50 with natural water (H$_2$O) by Fenton and photo-Fenton. [Fe^{3+}]= 10 mg L^{-1}

Experiments were conducted both in darkness and under simulated light at 1:50 ratio (figure 4.2). In darkness (Fenton), Imidacloprid degradation at pH 3 exhibits an initial burst in which about 30% is degraded within the first 20 minutes of treatment. Subsequent degradation is slower, as the gradual degradation of the iron-reductive components in CBW slow down the reduction of Fe^{3+}. At pH 5, only about 20% of Imidacloprid is degraded during the initial burst, with subsequent degradation following very similar kinetics as at pH 3. This behavior suggests that the reduction of Fe^{3+} to Fe^{2+} at both pH values follow similar kinetics and dominates the process. Without CBW, less than 15% of Imidacloprid is degraded after 3 hours.

Under illumination (photo-Fenton), the presence of CBW leads to faster Imidacloprid degradation (despite the higher TOC), with more than 95% removal after 30 minutes at pH 3 and a little after 90 minutes at pH 5; This large difference in kinetics between pH 5 and pH 3 could suggest the presence of different types of complexes at pH 5 which are less photosensitive than the ones present at pH 3. Less available soluble iron could also be responsible for the slower kinetics. For comparison, in the absence of CBW, 95% removal

was reached at 60 minutes at pH 3, while at pH 5 no more than 25% could be removed, even after 3 hours of treatment.
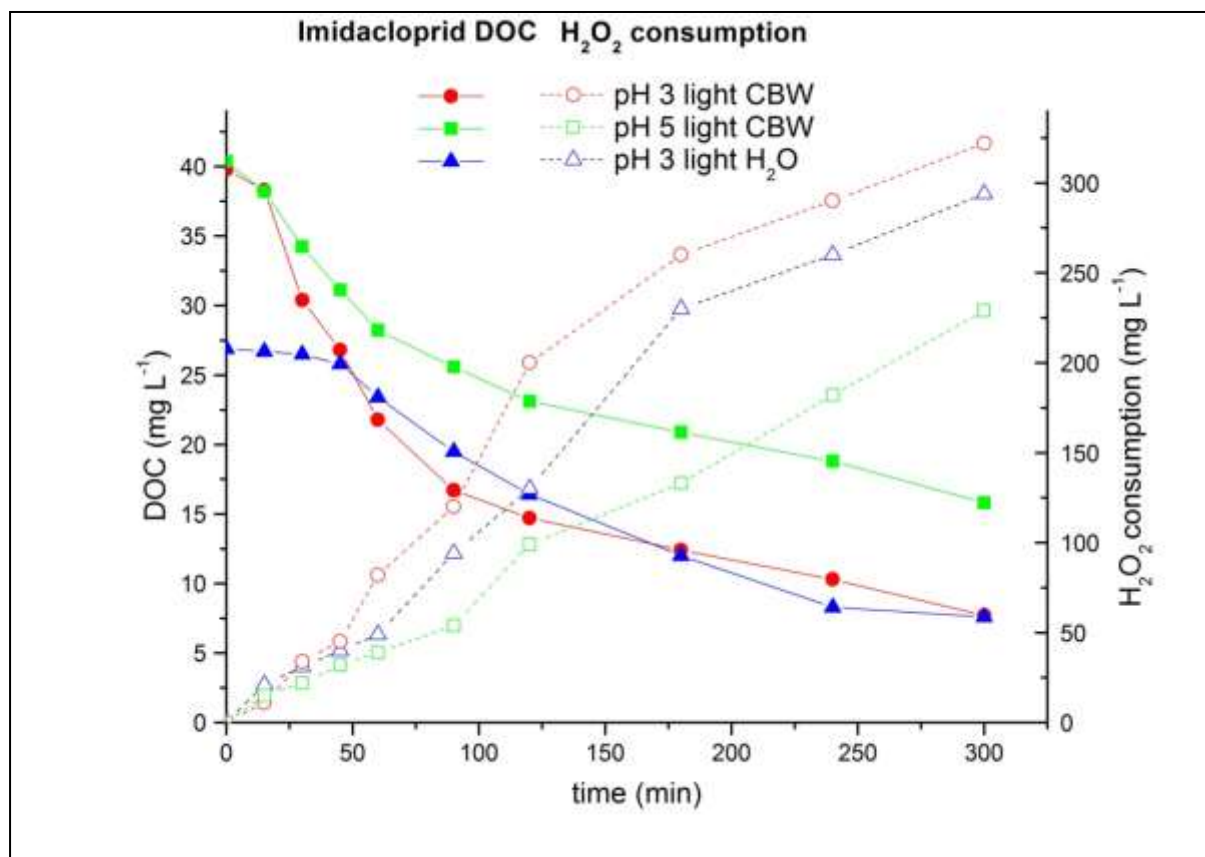

Fig. 4.3. DOC elimination and H_2O_2 consumption during treatment of 70 mg L^{-1} of Imidacloprid in CBW diluted 1:50 in natural water by photo-Fenton, $[Fe^{3+}]$= 10 mg L^{-1}

Comparing the removal of DOC between the different processes is interesting. As can be seen in figure 4.3, initial DOC of Imidacloprid in natural water is 28 mg L^{-1}, while the presence of CBW components raises DOC to a value of around 40 mg L^{-1}. When performing photo-Fenton in natural water, there is an initial lag of around 50 minutes before DOC starts decreasing. In CBW solutions, the decrease of DOC begins almost instantaneously. Also the mineralization rate, apart from differences in the initial burst, was almost exactly the same between pH 3/light/CBW and pH 3/light/H_2O despite the higher initial DOC of the former. With addition of CBW, DOC drops from 40 to 10 in 240 minutes. Without CBW, DOC drops from 25 to 10 at roughly the same time. This is important because it suggests that CBW can be used as an efficient photo-Fenton enhancer for degrading contaminants without any detrimental effect due to the extra DOC (provided a proper dose is selected). At pH 5, no mineralization was observed in absence of CBW (not shown), while in its presence, mineralization is slower, dropping from 40 to 19 in 240 minutes. It should be noted that EDDS assisted treatment of Imidacloprid at near-neutral pH, as seen in chapter 4, could not

102

lead to any mineralization. Fenton experiments are not shown, as no mineralization was observed in any of the tested conditions.

These promising results regarding mineralization of a contaminant in the presence of low quantities of CBW are also followed by only modest differences in H_2O_2 consumption. Photo-Fenton in natural water and in CBW at pH 3 show similar consumption patterns, consuming 270 mg L^{-1} in natural water and 320 mg L^{-1} in CBW.

The above results demonstrate that CBW has the potential to be reused for enhancing the remediation of other wastewaters. This effect is possibly achieved due the contribution of CBW polyphenolic components in the autocatalytic reduction of Fe^{3+} and by increasing iron stability at higher pH.

Due to the very high complexity of CBW however, specific polyphenol or tannin concentrations are not easy to determine quantitatively. Most studies express total polyphenolic content only in the form of an equivalent to a reference polyphenol (usually gallic or caffeic acids). Total polyphenolic content (as gallic acid equivalents) can typically vary from 1 up to more than 3.5 kg m^{-3} of CBW, with tannins (as tannic acid equivalents) typically accounting for 0.85 to 1.70 kg m^{-3} of it [127; 128; 129]. Some studies however have identified ellagic acid, gallic acid and protocatechuic acid as some the most abundant phenolic compounds present in CBW [130]. Ellagic acid, despite being present in higher concentrations, has been known to act as a metal precipitant, removing both Fe^{2+} and Fe^{3+} almost exclusively from solution via chelation [131; 132]. Gallic acid however is capable of forming complexes with Fe^{3+} that are capable of participating in its reduction [48].

4.3.3. INFLUENCE OF GALLIC ACID AND TANNINS ON THE PHOTO-FENTON PROCESS

As demonstrated in section 4.3.2, a small quantity of CBW was able to enhance the degradation of 70 mg L^{-1} of Imidacloprid both at pH 3 and 5. It is of interest to see whether some of the isolated compounds found abundantly in CBW are capable of enhancing the treatment of contaminated water of higher DOC values. Gallic acid and tannic acid were chosen as representative compounds [130] in order to test this hypothesis.

For this purpose, a mixture of 3 different contaminants was prepared with a total DOC value of 300 mg L^{-1}. Of the total DOC, 135 mg L^{-1} were due to phenol ([phenol]=178 mg L^{-1}), 135 mg L^{-1} due to methomyl ([methomyl] =364 mg L^{-1}), and 30 mg L^{-1} due to imidacloprid ([imidacloprid]= 70 mg L^{-1}). This mixture was chosen so to be able to see the behaviour of

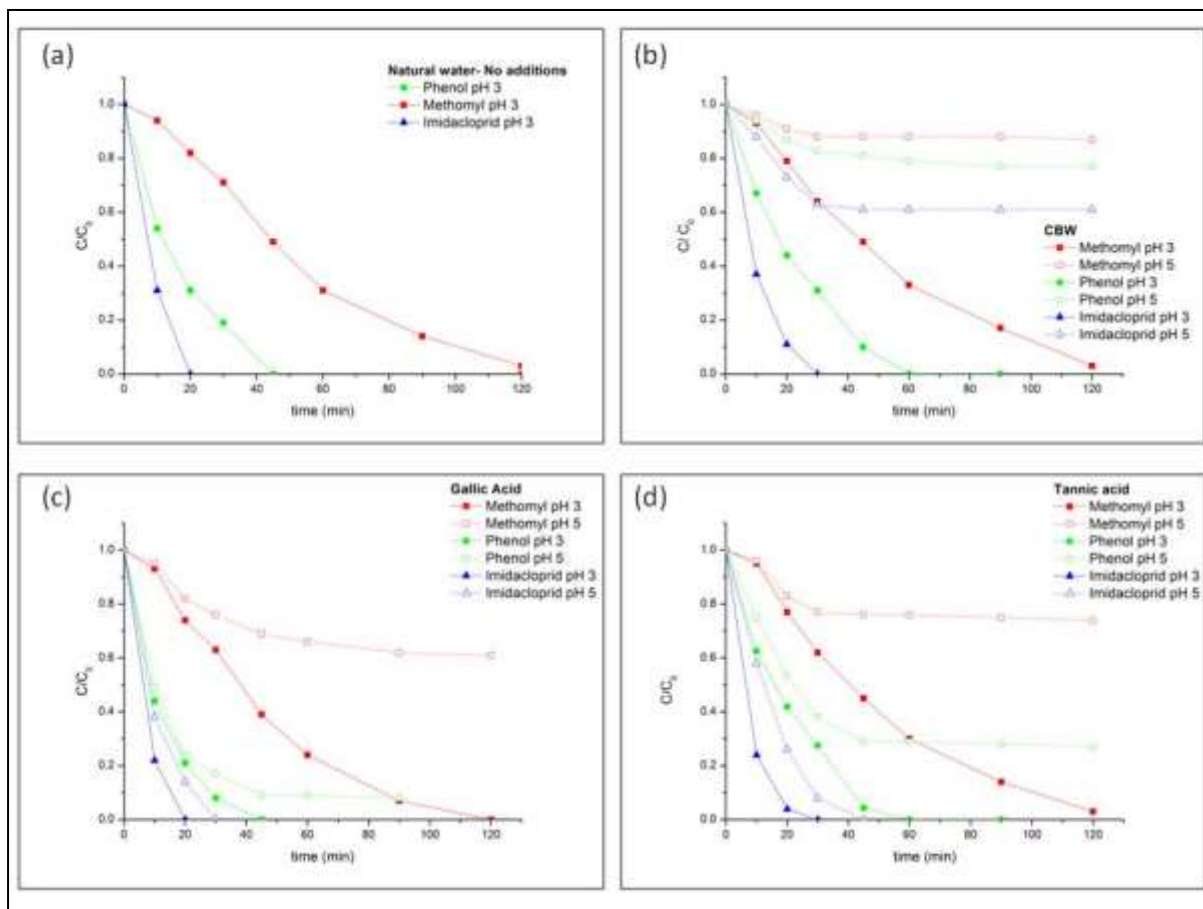aromatic (phenol), non-aromatic highly substituted rings (imidacloprid) and aliphatic (methomyl) contaminants.

Fig. 4.4. Photo-Fenton treatment of a methomyl/phenol/imidacloprid mixture with a DOC value of 300 mg L^{-1} in (a) natural water, (b) CBW diluted 1:50 in natural water, (c) Gallic acid (DOC= 15 mg L^{-1})and (d) Tannic acid (DOC= 15 mg L^{-1}). [Fe^{3+}]=10 mg L^{-1}.

The mixture was first treated in natural water at pH 3 in the solar simulator (figure 4.4a). As seen in figure 4.2, treatment at pH 5 is not possible so no experiment was done at that pH. Under illumination, complete degradation of imidacloprid, phenol and methomyl was achieved after 20, 40 and 120 minutes, respectively. Compared with figure 4.2, it can be seen that despite the much higher DOC of the mixture solution degradation occurs much faster. The increased degradation kinetics of the mixture compared to imidacloprid alone can possibly be attributed to the high concentration of phenol, whose degradation intermediates autocatalyse the process. Accumulation of quinones from the gradual degradation of aromatic rings has been reported by Chen and Pignatello [133] to lead to increased Fe^{2+} production by promoting Fe^{3+} reduction. Similarly, Aguiar et al [134] have observed that systems containing phenol derivatives behaved similarly whether the source of iron was Fe^{3+} or Fe^{2+}.

104

Experiments were also done in the presence of gallic acid (GA) and tannic acid (TA) , at concentrations corresponding to a DOC value of 15 (GA= 30.6 mg L^{-1}, TA= 27.8 mg L^{-1}), equal to the CBW tested in sections 6.3.1 and 6.3.2. Concentrations of iron and initial H_2O_2 were respectively, 10 mg L^{-1} and 200 mg L^{-1}. H_2O_2 was added as needed whenever it fell beneath 100 mg L^{-1}.

As seen in figures 4.4c and 4.4d, the differences between TA and GA at pH 3 are minimal. Complete imidacloprid removal occurs at near-identical times, around 30 minutes of treatment. Phenol at pH 3 is similarly removed around 50 minutes, while methomyl is completely degraded after 2 hours of treatment. At pH 5, the difference is more pronounced, with GA exhibiting better degradation rates than TA. Imidacloprid was completely removed at 30 and 45 minutes with GA and TA, respectively. However, only 90% and 70% of phenol could be removed in presence of, respectively, GA and TA. For methomyl, 40% is degraded in presence of GA and around 25% in presence of TA. It is evident that neither gallic nor tannic acid can sufficiently enhance the degradation of so high contaminant concentrations at higher pH values. It has, however, been verified that gallic acid is the more efficient of the two.

For comparison purposes, the degradation was also tested in diluted CBW (figure 4.4b). Although similar at pH 3, the degradation percentage was evidently worse at pH 5, with around 60% of Imidacloprid, 20 % of phenol and 10% of methomyl degraded by the end of a 2 hour treatment.

No mineralization was observed in any of the above experiments. However, as mineralization was shown to be possible in 1:50 diluted CBW for 70 mg L^{-1} of Imidacloprid (figure 4.3), it would be interesting to see if it is also possible in the contaminant mixture of similar DOC. A diluted mixture of methomyl/phenol/imidacloprid containing 30 mg L^{-1} DOC content was prepared and treated in absence and presence of CBW and GA.

As seen in figure 4.5, more than 75% mineralization (DOC from 45 to 13 mg L^{-1}) was achieved in the presence of GA and CBW at pH 5 after 2 hours of photo-Fenton treatment In comparison, in water without any additions, a decrease of only 15% was observed (from 30 to 25 mg L^{-1}). These results are very encouraging, as they verify that CBW can function successfully when the appropriate dosage in relation to DOC is chosen. Additionally, they verify that there must be some correlation between the efficiency of CBW and its polyphenolic content, as the behaviour in presence of GA and CBW was very similar.

At pH 3, the behaviour was similar regardless of the added components, with a slightly better performance when GA was used instead.
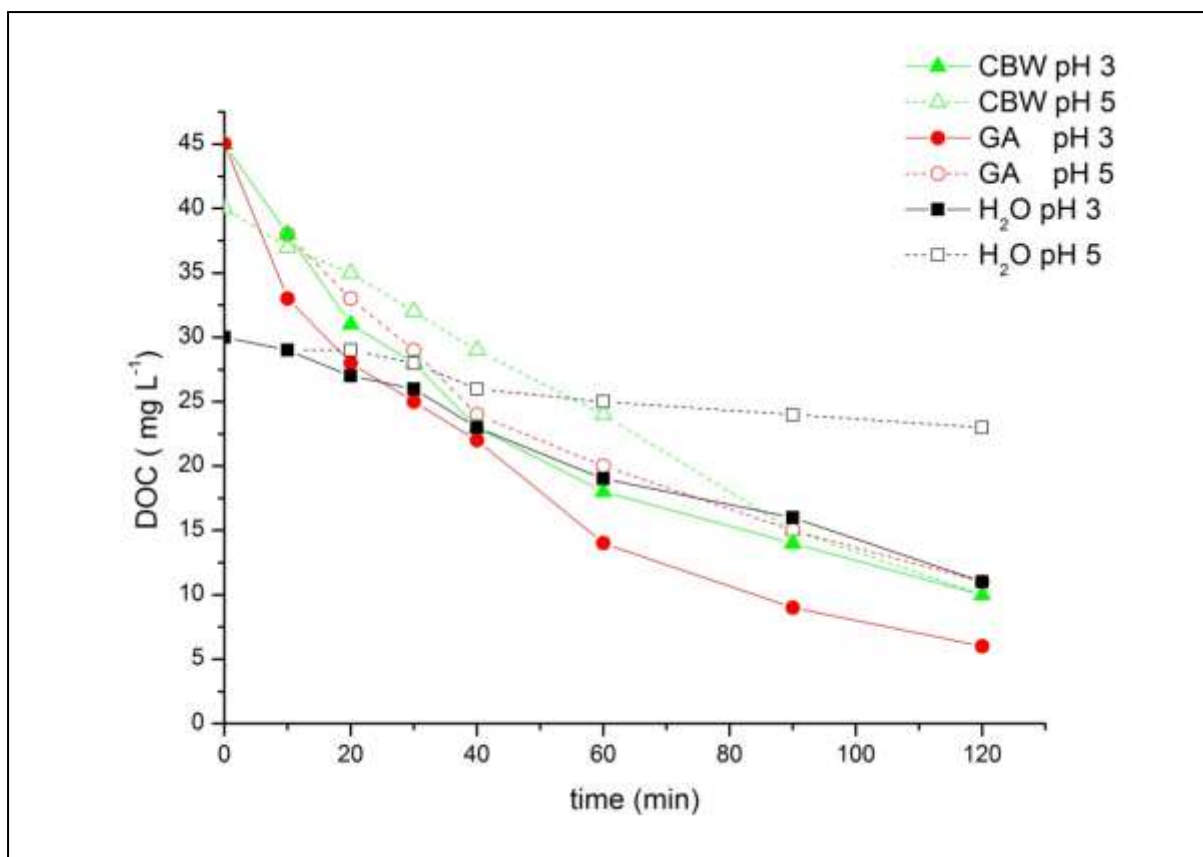
Fig. 4.5. Mineralization of a methomyl/phenol/imidacloprid mixture with a DOC content of 30 mg L^{-1} in natural water at pH 3 and 5 in absence and presence of 1:50 diluted CBW and gallic acid at pH 3 and 5. $[Fe^{3+}]$=10 mg L^{-1}

4.3.4. COMPLEXES OF GALLIC ACID WITH IRON AT DIFFERENT PH VALUES

As polyphenols such as gallic acid and tannins seem to be mainly responsible for the positive effect of CBW on photo-Fenton, it is interesting to try and gain a practical understanding of the type of iron complexes that are most likely to form. As gallic acid proved the most efficient, the stability of iron in its presence was studied. As mentioned in the literature, gallic acid is known to form several different types of complexes with iron, dependent on the pH. While highly stable complexes are known to be formed at the whole pH range between 3 and 9, the degree of chelation differs depending on the pH. While a 1:1 iron gallate complex is said to be initially formed (starting at pH 2.5), there is evidence of 1:2 [124] and even 1:3 [135] complexes formed at higher pH values(from 5.5 upwards). In order to verify the effect of the pH on the formation of the different complexes and, subsequently, the availability of soluble iron, different iron to gallic acid ratios have been mixed in distilled water. The soluble iron was measured at pH values between 3 and 9.
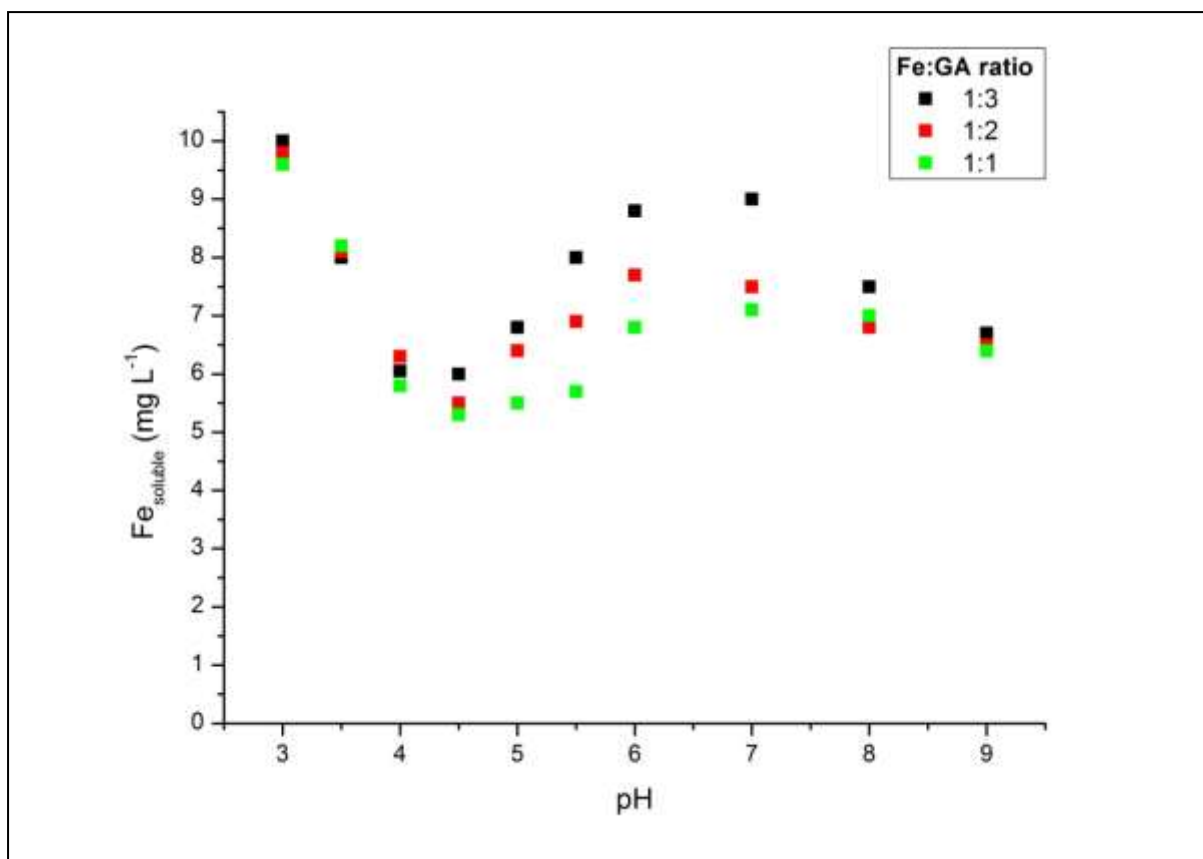
106

Fig.4.6. Effect of different iron: gallic acid ratios on soluble iron at the 3-9 pH range, $[Fe^{3+}]=$ 10 mg L^{-1}

As seen in figure 4.6, between pH 3 and 4.5, there is little difference regardless of the Fe:GA ratio used. From pH 5 upwards however, 1:2 and 1:3 ratios allow a higher amount of iron to remain in solution. This is indicative of the different degrees of Fe:GA chelation happening at the higher pH values. These results appear consistent with the observations of Knockaert et al [136] who have noted a strong increase in complexation of Fe^{3+} with GA from pH 5.4 upwards This is of interest if GA alone is to be considered as an alternative iron-chelating agent. However, as no soluble iron was measured in real CBW (figure 4.1) at pH values higher than 6, it suggests that the other compounds present in CBW (e.g ellagic acid) are capable of preferentially sequestering the iron, binding it to a non-soluble form instead.

4.4. CONCLUSIONS

This work has verified that cork boiling wastewater has some properties that can be beneficial when considering its reuse as an additive for enhancing Fenton and photo-Fenton treatment of other types of wastewater. It can contribute both to maintaining iron in solution at higher pH via the generation of stable ferric complexes and to the reduction of Fe^{3+}. The Fenton process (absence of light) is improved, as alternative mechanisms for iron

regeneration are introduced. This contributes to the enhancement of photo-Fenton, as the dark and photocatalytic iron regeneration mechanisms act concurrently. While treatment of contaminant solutions with very high DOC values (300 mg L^{-1}) is still not very efficient at higher pH values, lower contaminant concentrations (DOC around 30 mg L^{-1}) can be mineralized to a significant degree. In the latter case any additional DOC introduced from the CBW does not present a significant problem, as it can be removed at almost the same time as the model contaminants. In any case, a cross-linked study between contaminant load in wastewater and dose of CBW should be performed in a case by case basis.

Considering this success, cork boiling wastewater and possibly other types of wastewater from the industrial processing of natural products could be used as an additive in photo-Fenton treatment processes with a similar effect as other commercial iron-complexing ligands such as EDDS.

As more than 80% of the world's cork industry is based in Spain and Portugal, both countries with ample sunlight, any insight that can enhance the application of solar photo-Fenton can be highly beneficial. Logistics costs would be limited, as the reused CBW could be used locally at municipal wastewater treatment plants or local industries within a short radius of the cork production plants.

CHAPTER 5:

GENERAL CONCLUSIONS AND PERSPECTIVES

Different strategies were investigated for the improvement of the photo-Fenton treatment of several types of wastewater effluents:

The work conducted with ultrasound has demonstrated the potential presence of synergistic effects, even though they are highly dependent on the properties of the water matrix as well as of the treated contaminants. Significant synergy was observed for the partially solubilized BPA and diuron (both hydrophobic), suggesting that the combined process could be more useful for highly concentrated effluents, with contaminant concentrations above their saturation point. Favorable H_2O_2 consumption rates were also obtained for most of the combined treatments. Application of ultrasound for the treatment of Iohexol in municipal wastewater effluent and in urine however, did not however confer any advantages. Any efforts to develop an economically viable ultrasound/photo-Fenton system will probably not be easy and would have to be evaluated on a case-by-case basis, carefully considering the properties of the treated effluent.

Addition of EDDS has proven to be effective for the treatment of micro-contaminants in real wastewater effluent at a pH range between 5 and 8. Complete degradation can be achieved in the entire pH range, even though degradation rate decreases at higher pH values. The fact that the contaminants are eliminated in the presence of relatively high DOC values (about 2 orders of magnitude greater) is especially promising. Complete contaminant removal was achieved at pilot-scale within just a few minutes.

A more in-depth analysis of the action of Fe(III)-EDDS revealed that its photolysis generates radical species that are able to act independently of the carbonate scavengers often present in natural waters. No H_2O_2 addition is necessary for their generation. These species (most likely $HO_2\cdot/O_2\cdot/EDDS\cdot$) do not have the high oxidation potential of the hydroxyl radical so not all compounds are fully treatable. Their generation rate is dependent on aeration, increasing under good aeration conditions. Treatment of high concentrations of contaminants or achieving mineralization is nevertheless difficult as the rapid photolysis of EDDS does not permit long treatment times. The decreased performance observed at elevated temperatures can present a problem when considering solar applications, with conventional photo-fenton being more robust in terms of temperature stability. In summary, application of the EDDS-assisted process does have some advantages that could be useful for real-world applications but at the same time is subject to significant constraints that limit its general

applicability. Fe:EDDS should only be considered for relatively mild treatment of emerging contaminants, provided that some temperature control is also in place. Photo-Fenton remains a more robust solution for highly contaminated water streams.

The discovery with the highest potential for future applications is that components present in some types of wastewater (mainly polyphenolic compounds) can also act as iron-complexing agents, providing both an alternative Fe^{3+} reduction pathway while at the same time maintaining iron in solution at higher pH via the generation of stable ferric complexes. Using Cork Boiling Wastewater as a model wastewater with high polyphenolic content, mineralization of moderate contaminant concentrations (DOC around 30 mg L^{-1}) could be achieved to a significant degree. DOC introduced from the CBW itself did not present a problem, as it was removed along with the model contaminants. Considering this success, cork boiling wastewater and possibly other types of wastewater from the industrial processing of natural products (e.g wastewater from olive mills, wineries, breweries) could be investigated for being reused as potential additives in photo-Fenton treatment processes with a similar effect as other commercial ligands like EDDS. Future investigative efforts should also evaluate whether these benefits are also present when treating microcontaminants in MWTP effluents. Especially for the cork and olive oil industry, both prominent in Mediterranean countries with ample sunlight, promising results in this direction have the potential to greatly improve their current wastewater management practices. Logistics costs would be limited, as the reused wastewater could be used locally at municipal wastewater treatment plants or local industries within a short radius of the source industries.

REFERENCES

[1] A.R. Ribeiro, O.C. Nunes, M.F.R. Pereira, and A.M.T. Silva, An overview on the advanced oxidation processes applied for the treatment of water pollutants defined in the recently launched Directive 2013/39/EU. Environment International 75 (2015) 33-51.

[2] Y. Luo, W. Guo, H.H. Ngo, L.D. Nghiem, F.I. Hai, J. Zhang, S. Liang, and X.C. Wang, A review on the occurrence of micropollutants in the aquatic environment and their fate and removal during wastewater treatment. Science of the Total Environment 473–474 (2014) 619-641.

[3] W.L. Kruczynski, and P.J. Fletcher, Tropical Connections: South Florida's Marine Environment, Ian Press, 2012.

[4] C. Ort, J. Hollender, M. Schaerer, and H. Siegrist, Model-Based Evaluation of Reduction Strategies for Micropollutants from Wastewater Treatment Plants in Complex River Networks. Environ Sci Technol 43 (2009) 3214-3220.

[5] R.I.L. Eggen, J. Hollender, A. Joss, M. Schärer, and C. Stamm, Reducing the Discharge of Micropollutants in the Aquatic Environment: The Benefits of Upgrading Wastewater Treatment Plants. Environ Sci Technol 48 (2014) 7683-7689.

[6] A. Joss, M. Schaerer, and C. Abegglen, Micropollutants: the Swiss Strategy, Federal Office of the Environment (FOEN).

[7] W.H. Glaze, J.-W. Kang, and D.H. Chapin, CHEMISTRY OF WATER TREATMENT PROCESSES INVOLVING OZONE, HYDROGEN PEROXIDE AND ULTRAVIOLET RADIATION, Ozone: Science and Engineering, 1987, pp. 335-352.

[8] J. Hollender, S.G. Zimmermann, S. Koepke, M. Krauss, C.S. McArdell, C. Ort, H. Singer, U. von Gunten, and H. Siegrist, Elimination of Organic Micropollutants in a Municipal Wastewater Treatment Plant Upgraded with a Full-Scale Post-Ozonation Followed by Sand Filtration. Environ Sci Technol 43 (2009) 7862-7869.

[9] I. Oller, S. Malato, and J.A. Sanchez-Perez, Combination of Advanced Oxidation Processes and biological treatment for wastewater decontamination - A review. Science of the Total Environment 409 (2011) 4141-4166.

[10] S. Malato, P. Fernandez-Ibanez, M.I. Maldonado, J. Blanco, and W. Gernjak, Decontamination and disinfection of water by solar photocatalysis: Recent overview and trends. Catalysis Today 147 (2009) 1-59.

[11] H.J.H. Fenton, LXXIII.-Oxidation of tartaric acid in presence of iron. Journal of the Chemical Society, Transactions 65 (1894) 899-910.

[12] W.G. Barb, J.H. Baxendale, P. George, and K.R. Hargrave, Reactions of ferrous and ferric ions with hydrogen peroxide. Nature 163 (1949) 692-694.

[13] C.M. Flynn, Hydrolysis of inorganic iron(III) salts. Chemical Reviews 84 (1984) 31-41.

[14] J. De Laat, G. Truong Le, and B. Legube, A comparative study of the effects of chloride, sulfate and nitrate ions on the rates of decomposition of H2O2 and organic compounds by Fe(II)/H2O2 and Fe(III)/H2O2. Chemosphere 55 (2004) 715-723.

[15] P.L. Huston, and J.J. Pignatello, Degradation of selected pesticide active ingredients and commercial formulations in water by the photo-assisted Fenton reaction. Water Research 33 (1999) 1238-1246.

[16] G. Ruppert, R. Bauer, and G. Heisler, The photo-Fenton reaction — an effective photochemical wastewater treatment process. Journal of Photochemistry and Photobiology A: Chemistry 73 (1993) 75-78.

[17] D. Prato- Garcia, R. Vasquez-Medrano, and M. Hernandez- Esparza, Solar photoassisted advanced oxidation of synthetic phenolic wastewaters using ferrioxalate complexes. Solar Energy (2009) 306-315.

[18] J.V.D. Zee, B.B.H. Krootjes, C.F. Chignell, T.M.A.R. Dubbelman, and J.V. Steveninck, Hydroxyl radical generation by a light-dependent fenton reaction. Free Radical Biology and Medicine 14 (1993) 105-113.

[19] J. Bandara, C. Morrison, J. Kiwi, C. Pulgarin, and P. Peringer, Degradation/decoloration of concentrated solutions of Orange II. Kinetics and quantum yield for sunlight induced reactions via Fenton type reagents. Journal of Photochemistry and Photobiology A: Chemistry 99 (1996) 57-66.

[20] S. Andrianirinaharivelo, G. Mailhot, and M. Bolte, Photodegradation of organic pollutants induced by complexation with transition metals (Fe3+ and Cu2+) present in natural waters. Solar Energy Materials and Solar Cells 38 (1995) 459-474.

[21] P. Cieśla, P. Kocot, P. Mytych, and Z. Stasicka, Homogeneous photocatalysis by transition metal complexes in the environment. Journal of Molecular Catalysis A: Chemical 224 (2004) 17-33.

[22] J.J. Pignatello, E. Oliveros, and A. MacKay, Advanced oxidation processes for organic contaminant destruction based on the Fenton reaction and related chemistry. Critical reviews in environmental science and technology 36 (2006) 1-84.

[23] S. Giannakis, F.A. Gamarra Vives, D. Grandjean, A. Magnet, L.F. De Alencastro, and C. Pulgarin, Effect of advanced oxidation processes on the micropollutants and the effluent organic matter contained in municipal wastewater previously treated by three different secondary methods. Water Research 84 (2015) 295-306.

[24] J. Beltran-Heredia, J. Torregrosa, J.R. Dominguez, and J.A. Peres, Comparison of the degradation of p-hydroxybenzoic acid in aqueous solution by several oxidation processes. Chemosphere 42 (2001) 351-359.

[25] J. Marugán, J. Aguado, W. Gernjak, and S. Malato, Solar photocatalytic degradation of dichloroacetic acid with silica-supported titania at pilot-plant scale. Catalysis Today 129 (2007) 59-68.

[26] F. Mazille, T. Schoettl, A. Lopez, and C. Pulgarin, Physico-chemical properties and photo-reactivity relationship for para-substituted phenols in photo-assisted Fenton system. Journal of Photochemistry and Photobiology A: Chemistry 210 (2010) 193-199.

[27] L. Rayleigh, VIII. On the pressure developed in a liquid during the collapse of a spherical cavity. Philosophical Magazine Series 6 34 (1917) 94-98.

[28] W.T. Richards, and A.L. Loomis, THE CHEMICAL EFFECTS OF HIGH FREQUENCY SOUND WAVES I. A PRELIMINARY SURVEY. Journal of the American Chemical Society 49 (1927) 3086-3100.

[29] H.G. Flynn, Physics of acoustic cavitation in liquids. in: W.P. Mason, (Ed.), Physical Acoustics, Academic Press, New York, 1964, pp. 57-172.

[30] K.S. Suslick, S.J. Doktycz, and E.B. Flint, On the origin of sonoluminescence and sonochemistry. Ultrasonics 28 (1990) 280-290.

[31] Handbook on applications of ultrasound :Sonochemistry for sustainability, CRC Press, 2012.

[32] P. Riesz, D. Berdahl, and C.L. Christman, Free radical generation by Ultrasound in aqueous and Nonaqueous solutions. Environmental Health Perspectives 64 (1985) 233-252.

[33] G.V. Buxton, C.L. Greenstock, W.P. Helman, and A.B. Ross, Critical review of rate constants for reactions of hydrated electrons, hydrogen atoms and hydroxyl radicals in aqueous solution. J Phys Chem Ref. Data 17 (1988).

[34] Y.G. Adewuyi, Sonochemistry: Environmental science and engineering applications. Industrial and Engineering Chemistry Research 40 (2001) 4681-4715.

[35] M.M. van Iersel, J.P.A.J. van den Manacker, N.E. Benes, and J.T.F. Keurentjes, Pressure-induced reduction of shielding for improving sonochemical activity. The Journal of Physical Chemistry B 111 (2007) 3081-3084.

[36] H.M. Hung, and M.R. Hoffmann, Kinetics and mechanism of the sonolytic degradation of chlorinated hydrocarbons: Frequency effects. The Journal of Physical Chemistry A (1999) 2374-2739.

[37] R.A. Torres, F. Abdelmalek, E. Combet, C. Pètrier, and C. Pulgarin, A comparative study of ultrasonic cavitation and Fenton's reagent for bisphenol A degradation in deionised and natural waters. Journal of Hazardous Materials 146 (2007) 546-551.

[38] C. Minero, P. Pellizzari, V. Maurino, E. Pelizzetti, and D. Vione, Enhancement of dye sonochemical degradation by some inorganic anions present in natural waters. Applied Catalysis B: Environmental 77 (2008) 308-316.

[39] C. Pétrier, R.A. Torres-Palma, E. Combet, G. Sarantakos, S. Baup, and C. Pulgarin, Enhanced sonochemical degradation of bisphenol-A by bicarbonate ions. Ultrasonics Sonochemistry 17 (2010) 111-115.

[40] N.N. Mahamuni, and Y.G. Adewuyi, Advanced oxidation processes (AOPs) involving ultrasound for waste water treatment: A review with emphasis on cost estimation. Ultrasonics Sonochemistry 17 (2010) 990-1003.

[41] R.A. Torres, P. C, E. Combet, M. Carrier, and C. Pulgarin, Ultrasonic cavitation applied to the treatment of bisphenol A. Effect of sonochemical parameters and analysis of BPA by-products. Ultrasonics Sonochemistry 15 (2008) 605-611.

[42] G. Liu, S. Zheng, X. Xing, Y. Li, D. Yin, Y. Ding, and W. Pang, Fe(III)-oxalate complexes mediated photolysis of aqueous alkylphenol ethoxylates under simulated sunlight conditions. Chemosphere 78 (2010) 402-8.

[43] Y. Chen, Z. Liu, Z. Wang, M. Xue, X. Zhu, and T. Tao, Photodegradation of propranolol by Fe(III)-citrate complexes: kinetics, mechanism and effect of environmental media. Journal of Hazardous Materials 194 (2011) 202-8.

[44] Y. Wu, M. Brigante, W. Dong, P. de Sainte-Claire, and G. Mailhot, Toward a better understanding of Fe(III)-EDDS photochemistry: theoretical stability calculation and experimental investigation of 4-tert-butylphenol degradation. J Phys Chem A 118 (2014) 396-403.

[45] N. Klamerth, S. Malato Rodríguez, A. Aguera, and A. Fernández-Alba, Photo-Fenton and modified photo-Fenton at neutral pH for the treatment of emerging contaminants in wastewater treatment plant effluents: a comparison. Water Research (2013) 833-840.

[46] N.R. Perron, and J.L. Brumaghim, A review of the antioxidant mechanisms of polyphenol compounds related to iron binding. Cell Biochem Biophys 53 (2009) 75-100.

[47] R.C. Hider, Z.D. Liu, and H.H. Khodr, Metal chelation of polyphenols, Methods in Enzymology, Academic Press, 2001, pp. 190-203.

[48] M.J. Hynes, and M.n. Ó Coinceanainn, The kinetics and mechanisms of the reaction of iron(III) with gallic acid, gallic acid methyl ester and catechin. Journal of Inorganic Biochemistry 85 (2001) 131-142.

[49] P. Ryan, and M.J. Hynes, The kinetics and mechanisms of the complex formation and antioxidant behaviour of the polyphenols EGCg and ECG with iron(III). Journal of Inorganic Biochemistry 101 (2007) 585-593.

[50] G.N.L. Jameson, and W. Linert, The oxidation of 6-hydroxydopamine in aqueous solution. Part 3: Kinetics and mechanism of the oxidation with iron(III). Journal of the Chemical Society, Perkin Transactions (2001) 569-575.

[51] J.F. Moran, R.V. Klucas, R.J. Grayer, J. Abian, and M. Becana, Complexes of Iron with Phenolic Compounds from Soybean Nodules and Other Legume Tissues: Prooxidant and Antioxidant Properties. Free Radical Biology and Medicine 22 (1997) 861-870.

[52] K. Hiramoto, N. Ojima, K. Sako, and K. Kikugawa, Effect of plant phenolics on the formation of spin-adduct of hydroxyl radical and the DNA strand breaking of hydroxyl radical. Biological and Pharmaceutical Bulletin (1996) 558-563.

[53] A. Puppo, Effect of flavonoids on hydroxyl radical formation by fenton-type reactions; influence of the iron chelator. Phytochemistry 31 (1992) 85-88.

[54] M. Dias-Machado, L.M. Madeira, B. Nogales, O.C. Nunes, and C.M. Manaia, Treatment of cork boiling wastewater using chemical oxidation and biodegradation. Chemosphere 64 (2006) 455-461.

[55] L. Bertin, F. Ferri, A. Scoma, L. Marchetti, and F. Fava, Recovery of high added value natural polyphenols from actual olive mill wastewater through solid phase extraction. Chemical Engineering Journal 171 (2011) 1287-1293.

[56] L.A. Ioannou, G.L. Puma, and D. Fatta-Kassinos, Treatment of winery wastewater by physicochemical, biological and advanced processes: A review. Journal of Hazardous Materials 286 (2015) 343-368.

[57] W. Sabaikai, M. Sekine, M. Tokumura, and Y. Kawase, UV light photo-Fenton degradation of polyphenols in oolong tea manufacturing wastewater. Journal of Environmental Science and Health, Part A 49 (2013) 193-202.

[58] R.A. Torres, G. Sarantakos, E. Combet, C. Pètrier, and C. Pulgarin, Sequential helio photo-Fenton and sonication processes for the treatment of bisphenol A. Journal of Photochemistry and Photobiology A: Chemistry 199 (2008) 197-203.

[59] Y. Li, W.-P. Hsieh, R. Mahmudov, X. Wei, and C.P. Huang, Combined ultrasound and Fenton (US-Fenton) process for the treatment of ammunition wastewater. Journal of Hazardous Materials 244–245 (2013) 403-411.

[60] X.-a. Ning, H. Chen, J. Wu, Y. Wang, J. Liu, and M. Lin, Effects of ultrasound assisted Fenton treatment on textile dyeing sludge structure and dewaterability. Chemical Engineering Journal 242 (2014) 102-108.

[61] M.A. Beckett, and I. Hua, Impact of ultrasonic frequency on aqueous sonoluminescence and sonochemistry. Journal of physical Chemistry A (2001) 3796-3802.

[62] B. David, Sonochemical degradation of PAH in aqueous solution.Part I: monocomponent PAH solution. Ultrasonics Sonochemistry 16 (2009) 260-265.

[63] P. Villegas-Guzman, J. Silva-Agredo, A.L. Giraldo-Aguirre, O. Flórez-Acosta, C. Petrier, and R.A. Torres-Palma, Enhancement and inhibition effects of water matrices during the sonochemical degradation of the antibiotic dicloxacillin. Ultrasonics Sonochemistry 22 (2015) 211-219.

[64] A. Zapata, I. Oller, L. Rizzo, S. Hilgert, M.I. Maldonado, J.A. Sanchez-Perez, and S. Malato, Evaluation of operating parameters involved in solar photo-Fenton treatment of wastewater : Interdependence of initial pollutant concentration, temperature and iron concentration. Applied Catalysis B: Environmental 97 (2010) 292-298.

[65] P.S. Bapat, P.R. Gogate, and A.B. Pandit, Theoretical analysis of sonochemical degradation of phenol and its chloro-derivatives. Ultrasonics Sonochemistry 14 (2008) 564-570.

[66] T. Tuziuti, K. Yasui, Y. Iida, H. Taoda, and S. Koda, Effect of particle addition on sonochemical reaction. Ultrasonics 42 (2004) 597-601.

[67] S. Pérez, and D. Barceló, Fate and occurrence of X-ray contrast media in the environment. Analytical and Bioanalytical Chemistry 387 (2007) 1235-1246.

[68] T.A. Ternes, and R. Hirsch, Occurrence and Behavior of X-ray Contrast Media in Sewage Facilities and the Aquatic Environment. Environ Sci Technol 34 (2000) 2741-2748.

[69] A. Putschew, S. Schittko, and M. Jekel, Quantification of triiodinated benzene derivatives and X-ray contrast media in water samples by liquid chromatography–electrospray tandem mass spectrometry. Journal of Chromatography A 930 (2001) 127-134.

[70] L.J. Fono, and D.L. Sedlak, A simple method for the measurement of organic iodine in wastewater and surface water. Water Research 41 (2007) 1580-1586.

[71] W. Kalsch, Biodegradation of the iodinated X-ray contrast media diatrizoate and iopromide. Science of the Total Environment 225 (1999) 143-153.

[72] M. Carballa, F. Omil, J.M. Lema, M.a. Llompart, C. García-Jares, I. Rodríguez, M. Gómez, and T. Ternes, Behavior of pharmaceuticals, cosmetics and hormones in a sewage treatment plant. Water Research 38 (2004) 2918-2926.

[73] S.E. Duirk, C. Lindell, C.C. Cornelison, J. Kormos, T.A. Ternes, M. Attene-Ramos, J. Osiol, E.D. Wagner, M.J. Plewa, and S.D. Richardson, Formation of toxic iodinated disinfection by-products from compounds used in medical imaging. Environ Sci Technol 45 (2011) 6845-6854.

[74] F. Herrera, C. Pulgarin, V. Nadtochenko, and J. Kiwi, Accelerated photo-oxidation of concentrated p-coumaric acid in homogeneous solution. Mechanistic studies, intermediates and precursors formed in the dark. Applied Catalysis B: Environmental 17 (1998) 141-156.

[75] P. Ribordy, C. Pulgarin, J. Kiwi, and P. Péringer, Electrochemical versus photochemical pretreatment of industrial wastewaters. Water Science and Technology 35 (1997) 293-302.

[76] J. Jeong, J. Jung, W.J. Cooper, and W. Song, Degradation mechanisms and kinetic studies for the treatment of X-ray contrast media compounds by advanced oxidation/reduction processes. Water Research 44 (2010) 4391-4398.

[77] W. Seitz, J.-Q. Jiang, W. Schulz, W.H. Weber, D. Maier, and M. Maier, Formation of oxidation by-products of the iodinated X-ray contrast medium iomeprol during ozonation. Chemosphere 70 (2008) 1238-1246.

[78] T.E. Doll, and F.H. Frimmel, Kinetic study of photocatalytic degradation of carbamazepine, clofibric acid, iomeprol and iopromide assisted by different TiO2 materials—determination of intermediates and reaction pathways. Water Research 38 (2004) 955-964.

[79] M.N. Sugihara, D. Moeller, T. Paul, and T.J. Strathmann, TiO2-photocatalyzed transformation of the recalcitrant X-ray contrast agent diatrizoate. Applied Catalysis B: Environmental 129 (2013) 114-122.

[80] V.J. Pereira, H.S. Weinberg, K.G. Linden, and P.C. Singer, UV Degradation Kinetics and Modeling of Pharmaceutical Compounds in Laboratory Grade and Surface Water via Direct and Indirect Photolysis at 254 nm. Environ Sci Technol 41 (2007) 1682-1688.

[81] B. Ning, N.J. Graham, and P.D. Lickiss, A comparison of ultrasound-based advanced oxidation processes for the removal of X-ray contrast media. Water Sci Technol 60 (2009) 2383-90.

[82] M. Stieber, A. Putschew, M. Jekel, and K. Wasserreinhaltung, Treatment of urine with zero-valent iron to minimize the aquatic pollution with compounds emitted by hospitals PharmaTreat. (2011).

[83] G.B. Tissot, A. Anglada, P. Dimitriou-Christidis, L. Rossi, J.S. Arey, and C. Comninellis, Kinetic experiments of electrochemical oxidation of iohexol on BDD electrodes for wastewater treatment. Electrochemistry Communications 23 (2012) 48-51.

[84] A. Ohara, and S. Miyamoto, Oxygen radicals and related species. in: K. Pantopoulos, and H.M. Schipper, (Eds.), Principles of Free Radical Biomedicine, Nova Science Publishers, 2011.

[85] S. Goldstein, G. Czapski, J. Lind, and G. Merényi, Carbonate Radical Ion Is the Only Observable Intermediate in the Reaction of Peroxynitrite with CO2. Chemical Research in Toxicology 14 (2001) 1273-1276.

[86] D.F. Putnam, Composition and concentrative properties of human urine. in: M.D.A.c.-W. Division, (Ed.), National Aeronautics and Space Administration, Washington D.C, 1971.

[87] D.L. Perry, Handbook of Inorganic Compounds, CRC Press, 2011.

[88] B. Davis, P. Saltman, and S. Benson, The stability constants of the iron-transferrin complex. Biochemical and Biophysical Research Communications 8 (1962) 56-60.

[89] L.E. Bang, J. Holm, and T.L. Svendsen, Retinol-Binding Protein and Transferrin in Urine: New Markers of Renal Function in Essential Hypertension and White Coat Hypertension? American Journal of Hypertension 9 (1996) 1024-1028.

[90] D.R. Manenti, P.A. Soares, A.N. Módenes, F.R. Espinoza-Quiñones, R.A.R. Boaventura, R. Bergamasco, and V.J.P. Vilar, Insights into solar photo-Fenton process using iron(III)–organic ligand complexes applied to real textile wastewater treatment. Chemical Engineering Journal 266 (2015) 203-212.

[91] H. Nakagawa, and E. Yamaguchi, Influence of oxalic acid formed on the degradation of phenol by Fenton reagent. Chemosphere 88 (2012) 183-187.

[92] H.B. Abrahamson, A.B. Rezvani, and J.G. Brushmiller, Photochemical and spectroscopic studies of complexes, of iron(III) with citric acid and other carboxylic acids. Inorganica Chimica Acta 226 (1994) 117-127.

[93] J. Guo, Y. Du, Y. Lan, and J. Mao, Photodegradation mechanism and kinetics of methyl orange catalyzed by Fe(III) and citric acid. Journal of Hazardous Materials 186 (2011) 2083-2088.

[94] M.J. Farré, X. Doménech, and J. Peral, Combined photo-Fenton and biological treatment for Diuron and Linuron removal from water containing humic acid. Journal of Hazardous Materials 147 (2007) 167-174.

[95] M. Kępczyński, A. Czosnyka, and M. Nowakowska, Photooxidation of phenol in aqueous nanodispersion of humic acid. Journal of Photochemistry and Photobiology A: Chemistry 185 (2007) 198-205.

[96] E. Lipczynska-Kochany, and J. Kochany, Effect of humic substances on the Fenton treatment of wastewater at acidic and neutral pH. Chemosphere 73 (2008) 745-750.

[97] N. Klamerth, S. Malato, M.I. Maldonado, A. Agüera, and A. Fernández-Alba, Modified photo-Fenton for degradation of emerging contaminants in municipal wastewater effluents. Catalysis Today 161 (2011) 241-246.

[98] Z. Yuan, and J. Van Briesen, Formation of Intermediates in EDTA and NTA Biodegradation. Environmental Engineering Science (2006) 533-544.

[99] C.K. Schmidt, M. Fleig, F. Sacher, and H.J. Brauch, Occurrence of aminopolycarboxylates in the aquatic environment of Germany. Environ Pollut 131 (2004) 107-24.

[100] A. Rastogi, S.R. Al-Abed, and D.D. Dionysiou, Effect of inorganic, synthetic and naturally occurring chelating agents on Fe(II) mediated advanced oxidation of chlorophenols. Water Res 43 (2009) 684-94.

[101] N.J. Velupula, G.J. Tedros, and M.C. Andrew, Determination of copper and iron using [S,S]-Ethylenediaminedisuccinic acid as a chelating agent in wood pulp by capillary electrophoresis. Analytical Science 23 (2007) 493-496.

[102] Y. Wu, M. Passananti, M. Brigante, W. Dong, and G. Mailhot, Fe(III)-EDDS complex in Fenton and photo-Fenton processes: from the radical formation to the degradation of a target compound. Environ Sci Pollut Res Int (2014).

[103] W. Huang, M. Brigante, F. Wu, C. Mousty, K. Hanna, and G. Mailhot, Assessment of the Fe(III)-EDDS complex in Fenton-like processes: from the radical formation to the degradation of bisphenol A. Environ Sci Technol 47 (2013) 1952-9.

[104] J. Li, G. Mailhot, F. Wu, and N. Deng, Photochemical efficiency of Fe(III)-EDDS complex: OH radical production and 17β-estradiol degradation. Journal of Photochemistry and Photobiology A: Chemistry (2010) 1-7.

[105] S. Miralles-Cuevas, I. Oller, J.A.S. Pérez, and S. Malato, Removal of pharmaceuticals from MWTP effluent by nanofiltration and solar photo-Fenton using two different iron complexes at neutral pH. Water Research (2014).

[106] N. Klamerth, S. Malato, A. Aguera, A. Fernandez-Alba, and G. Mailhot, Treatment of municipal wastewater treatment plant effluents with modified photo-Fenton as a tertiary treatment for the degradation of micro pollutants and disinfection. Environ Sci Technol 46 (2012) 2885-92.

[107] P.J. Whitcomb, and M.J. Anderson, RSM Simplified: Optimizing Processes Using Response Surface Methods for Design of Experiments, Productivity Press, 2004.

[108] W. Huang, M. Brigante, F. Wu, K. Hanna, and G. Mailhot, Development of a new homogenous photo-Fenton process using Fe(III)-EDDS complexes. Journal of Photochemistry and Photobiology A: Chemistry (2012) 17-23.

[109] S. Metsarinne, T. Tuhkanen, and R. Aksela, Photodegradation of ethylenediaminetetraacetic acid (EDTA) and ethylenediamine disuccinic acid (EDDS) within natural UV radiation range. Chemosphere (2001) 949-955.

[110] N.R. Costa, J. Lourenço, and Z.L. Pereira, Desirability function approach: A review and performance evaluation in adverse conditions. Chemometrics and Intelligent Laboratory Systems 107 (2011) 234-244.

[111] S. Malato, J. Blanco, J. Cáceres, A.R. Fernández-Alba, A. Agüera, and A. Rodríguez, Photocatalytic treatment of water-soluble pesticides by photo-Fenton and TiO2 using solar energy. Catalysis Today 76 (2002) 209-220.

[112] B.H.J. Bielski, and H.W. Richter, A study of the superoxide radical chemistry by stopped-flow radiolysis and radiation induced oxygen consumption. Journal of American Chemical Society (1977) 3019-3023.

[113] S. Miralles-Cuevas, F. Audino, I. Oller, R. Sánchez-Moreno, J.A. Sánchez Pérez, and S. Malato, Pharmaceuticals removal from natural water by nanofiltration combined with advanced tertiary treatments (solar photo-Fenton, photo-Fenton-like Fe(III)–EDDS complex and ozonation). Separation and Purification Technology 122 (2014) 515-522.

[114] O. Augusto, and S. Miyamoto, Principles of Free Radical Biomedicine, Nova Science Publishers Inc.

[115] S.J. Blanskby, and G.B. Ellison, Bond dissociation energies of organic molecules. Acc. Chem. Res. (2003) 255-263.

[116] J. Li, A quantitative relationship for the shock sensitivities of energetic compounds based on X–NO2 (X = C, N, O) bond dissociation energy. Journal of Hazardous Materials 180 (2010) 768-772.

[117] S. Malato, J. Caceres, A. Agüera, M. Mezcua, D. Hernando, J. Vial, and A.R. Fernández-Alba, Degradation of Imidacloprid in Water by Photo-Fenton and TiO2 Photocatalysis at a Solar Pilot Plant: A Comparative Study. Environ Sci Technol 35 (2001) 4359-4366.

[118] Y. Li, J. Niu, L. Yin, W. Wang, Y. Bao, J. Chen, and Y. Duan, Photocatalytic degradation kinetics and mechanism of pentachlorophenol based on Superoxide radicals. Journal of Environmental Sciences 23 (2011) 1911-1918.

[119] H. Che, and W. Lee, Selective redox degradation of chlorinated aliphatic compounds by Fenton reaction in pyrite suspension. Chemosphere 82 (2011) 1103-8.

[120] W.H. Glaze, Y. Lay, and J.W. Kang, Advanced oxidation processes: A kinetic model for the oxidation of 1,2-dibromo-3-chloropropane in water by the combination of hydrogen peroxide and UV radiation. Ind. Eng. Chem. Res 34 (1995) 2314-2323.

[121] J. Ndounla, S. Kenfack, J. Wéthé, and C. Pulgarin, Relevant impact of irradiance (vs. dose) and evolution of pH and mineral nitrogen compounds during natural water disinfection by photo-Fenton in a solar CPC reactor. Applied Catalysis B: Environmental 148–149 (2014) 144-153.

[122] T.L. Theis, and P.C. Singer, Complexation of iron(II) by organic matter and its effect on iron(II) oxygenation. Environ Sci Technol 8 (1974) 569-573.

[123] F.J. Benitez, F.J. Real, J.L. Acero, A.I. Leal, and C. Garcia, Gallic acid degradation in aqueous solutions by UV/H2O2 treatment, Fenton's reagent and the photo-Fenton system. Journal of Hazardous Materials 126 (2005) 31-39.

[124] M.S. Masoud, A.E. Ali, S.S. Haggag, and N.M. Nasr, Spectroscopic studies on gallic acid and its azo derivatives and their iron(III) complexes. Spectrochim Acta A Mol Biomol Spectrosc 120 (2014) 505-11.

[125] D.A. Nichela, J.A. Donadelli, B.F. Caram, M. Haddou, F.J. Rodriguez Nieto, E. Oliveros, and F.S. García Einschlag, Iron cycling during the autocatalytic decomposition of benzoic acid derivatives by Fenton-like and photo-Fenton techniques. Applied Catalysis B: Environmental 170–171 (2015) 312-321.

[126] V. Mazzoleni, L. Dallagiovanna, M. Trevisan, and M. Nicelli, Persistent organic pollutants in cork used for production of wine stoppers. Chemosphere 58 (2005) 1547-1552.

[127] F.J. Benitez, J.L. Acero, J. Garcia, and A.I. Leal, Purification of cork processing wastewaters by ozone, by activated sludge, and by their two sequential applications. Water Research 37 (2003) 4081-4090.

[128] E. Mendonça, A. Picado, L. Silva, and A.M. Anselmo, Ecotoxicological evaluation of cork-boiling wastewaters. Ecotoxicology and Environmental Safety 66 (2007) 384-390.

[129] M. Bernardo, A. Santos, P. Cantinho, and M. Minhalma, Cork industry wastewater partition by ultra/nanofiltration: A biodegradation and valorisation study. Water Research 45 (2011) 904-912.

[130] I.P. Marques, L. Gil, and F. La Cara, Energetic and biochemical valorization of cork boiling wastewater by anaerobic digestion. Biotechnol Biofuels 7 (2014) 67.

[131] S.R. Przewloka, and B.J. Shearer, The further chemistry of ellagic acid II. Ellagic acid and water-soluble ellagates as metal precipitants. Holzforschung 56 (2002) 13-19.

[132] P.E. Bock, K.R. Srinivasan, and J.D. Shore, Activation of intrinsic blood coagulation by ellagic acid: insoluble ellagic acid-metal ion complexes are the activating species. Biochemistry 20 (1981) 7258-66.

[133] R. Chen, and J.J. Pignatello, Role of quinone intermediates as electron shuttles in Fenton and photoassisted Fenton oxidations of aromatic compounds. Environmental Science and Technology 31 (1997) 2399-2406.

[134] A. Aguiar, and A. Ferraz, Fe3+- and Cu2+-reduction by phenol derivatives associated with Azure B degradation in Fenton-like reactions. Chemosphere 66 (2007) 947-954.

[135] S. Arif Kazmi, M. Saqib Qureshi, and Z. Maqsood, Reactivity of an iron(III) complex of gallic acid. Inorganica Chimica Acta 137 (1987) 151-154.

[136] D. Knockaert, K. Raes, K. Struijs, C. Wille, and J. Van Camp, Influence of microbial conversion and change in pH on iron–gallic acid complexation during lactobacillus fermentation. LWT - Food Science and Technology 55 (2014) 335-340.

Curriculum Vitae

Stefanos Papoutsakis

PERSONAL DETAILS

Born: 20 August 1981, Athens, Greece

Address: Karvela 15, Agia Paraskevi, 15342, Athens, Greece

Email: stefpap@gmail.com

WORK EXPERIENCE

- Doctoral assistant at the laboratory of Advanced Oxidation Processes, Federal Polytechnic School of Lausanne (EPFL), Lausanne, Switzerland
  May 2011-present
  Contact: Prof. Cesar Pulgarin   email: *cesar.pulgarin@epfl.ch*
                    tel: (+41)216934720

- Private tutoring on science and English language for high school students
  March 2009- May 2011

- Part time research and teaching associate at the laboratory of food chemistry and technology, National Technical University of Athens, Greece
  March 2009- March 2010
  Contact: Prof. Contantina Tzia   email: *tzia@chemeng.ntua.gr*
                    tel: (+30)2107723165

- Assistant at an analytical medical laboratory, Artemis Medical Centre, Artemis, Greece
  November 2005- July 2006
  Contact: Krampovitis Spyridon   email: *krampoerg@yahoo.com*
                    tel: (+30)2106669090

- Guest researcher (Erasmus program) at the industrial crystallization research group, Department of Chemical Engineering and Technology, KTH Royal Institute of Technology, Stockholm, Sweden
  November 2004- May 2005

EDUCATION

- ***MSc in Cybernetics (Merit)***
  School of Systems Engineering, University of Reading, UK
  2007-2008

  Thesis :Multiresolution wavelet decomposition analysis of transient neuromuscular events relating to Parkinson's disease tremor onset

  Supervisors: *Dr. Victor M. Becerra   email: v.m.becerra@reading.ac.uk*
  tel: (+44)1183786703
  Prof. Kevin Warwick   email: k.warwick@reading.ac.uk
  tel: (+44)1183788210

- **MSc in Biotechnology (Distinction)**
  School of Biomedical Sciences, University of Ulster, Coleraine, Northern Ireland, UK
  2006-2007

  Thesis: Development of a DNA quadruplex aptamer exhibiting binding affinity for Nucleolin

  Supervisor: *Dr. Mateus Webba da Silva   email: mm.webba-da-silva@ulster.ac.uk*
  tel:(+44)2870324009

- **Diploma of Chemical Engineering (Grade: 7.06/10)**
  Department of Chemical Engineering, University of Patras, Greece
  1999-2005

  Thesis: Study of the inhibition of struvite precipitation in the presence of phytic acid

  Supervisor: *Prof. Petros Koutsoukos   email: pgk@chemeng.upatras.gr*
  tel: (+30)2610997265

BOOK CHAPTERS

- C. Chranioti, S. Papoutsakis, A. Nikoloudaki, C. Tzia ' Study of flavor volatile profile in microencapsulated Greek Saffron products' *Nutrition, functional and sensory properties of foods, RSC publishing, 2013*
- S. Papoutsakis, C. Tzia ' Flavor and aroma evaluation of foods, the role of the flavorist in food product development' , *Recent advances in food and flavor chemistry, RSC publishing,2009*

SCIENTIFIC ARTICLES

- S. Papoutsakis, S. Miralles-Cuevas, N.Gondrexon, S. Baup, S. Malato, C. Pulgarin Coupling between high frequency ultrasound and solar photo-Fenton at pilot scale for the treatment of selected contaminants: An initial approach.
  Ultrasonics Sonochemistry, 22 (2015) 527-534

- S. Papoutsakis, Z. Afshari, S. Malato, C. Pulgarin
Elimination of the iodinated contrast agent iohexol in water, wastewater and urine matrices by application of photo-Fenton and ultrasound advanced oxidation processes.
Journal of Environmental Chemical Engineering, 3 (2015) 2002-2009

- S. Papoutsakis, S. Miralles-Cuevas, I.Oller, J.L. Garcia Sanchez, C. Pulgarin, S. Malato
Microcontaminant degradation in municipal wastewater treatment plant secondary effluent by EDDS assisted photo-Fenton at near-neutral pH: An experimental design approach.
Catalysis Today, 252 (2015) 61-69

- S. Papoutsakis, F.F. Brites- Nobrega, C. Pulgarin, S. Malato.
Benefits ad limitations of using Fe(III)-EDDS for the treatment of highly contaminated water at near-neutral pH.
Journal of Photochemistry and Photobiology A: Chemistry, 15 (2015) 1-7

- S. Papoutsakis, C. Pulgarin, S. Malato
Enhancement of the Fenton and photo-Fenton processes by components found in wastewater from the industrial processing of natural products: The possibilities of Cork Boiling Wastewater reuse.
(Review Pending)

PARTICIPATION IN CONFERENCES

- 11th SOLLAB doctoral colloquium, Melchsee-Frutt, Switzerland, March 2-4 2015
- 8th European meeting on solar chemistry and photocatalysis: Environmental applications - SPEA 8, Thessaloniki, Greece, June 25-28 2014
- 2eme Journées Sonochimie Ultasons et Procédés, Chàmbery, France, June 11-12 2013
- 12th international flavor conference, Skiathos, Greece, May 25-29, 2009

ACQUIRED SCHOLARSHIPS

- SFERA program scholarship for conducting research at the Solar Platform of Almeria (Spain) within the framework of the doctoral research in EPFL
- Engineering and Physical Sciences Research Council (EPSRC) scholarship for the MSc in Cybernetics
- European Social Fund (ESF) scholarship for the MSc in Biotechnology

LANGUAGES

- Greek: Native Language
- English: Full professional Proficiency
- Spanish: Full professional Proficiency
- French: Moderate professional Proficiency